2017

A Flexible Physics-Based Lifing Method for Metals Under Creep and Thermomechanical Fatigue

Firat Irmak
University of Central Florida

A FLEXIBLE PHYSICS-BASED LIFING METHOD FOR METALS UNDER CREEP AND THERMOMECHANICAL FATIGUE

by

FIRAT IRMAK

B.S. University of Central Florida, 2016

A thesis submitted in partial fulfillment of the requirements
for the degree of Master of Science
in the Department of Mechanical and Aerospace Engineering
in the College of Engineering and Computer Science
at the University of Central Florida
Orlando, Florida

Fall Term
2017

Major Professor: Ali P. Gordon

ABSTRACT

This thesis focuses on the development of a flexible, physics-based life prediction approach for steels under complex conditions. Low alloy steels continue to be the materials of choice for large turbomachinery structures experiencing high temperatures for long durations. There has been significant advancement in the research of modern alloys; furthermore, these materials are continue to be utilized in boilers, heat exchanger tubes, and throttle valve bodies in both turbomachinery and pressure-vessel/piping applications. The material 2.25Cr-1Mo is studied in the present work. The resistance of this alloy to deformation and damage under creep and/or fatigue at elevated temperatures make it appropriate for structures required to endure decades of service. Also, this material displays an excellent balance of ductility, corrosion resistance, and creep strength under aggressive operating conditions. Both creep-fatigue (CF) and thermomechanical fatigue (TMF) have been the limiting factor for most turbine components fabricated from various alloys; therefore, a life prediction approach is constructed for simulating fatigue life for cases where the material is experiencing mechanical loading with thermal cycling. Flexibility is imparted to the model through its ability to emphasize the dominant damage mechanism which may vary among alloys. A material database is developed to improve and compare the model with experimental data. This database contains low cycle fatigue (LCF), creep fatigue (CF), and thermomechanical fatigue (TMF) experiments. Parameters for the model are obtained with regression fits with the support of a broad experimental database. Additionally, the cumulative damage approach, better known as Miner's rule, is used in this study as the fundamental method to combine damage mechanisms. Life predictions are obtained by the usage of a non-interacting

creep-plasticity constitutive model capable of simulating not only the temperature- and rate-dependence.

ACKNOWLEDGMENTS

I would like to thank my mentor, advisor, and teacher Dr. Ali P. Gordon for his support and guidance during this research and many others. Also, I would like to thank my committee members, Dr. Necati Catbas and Dr. Seetha Raghavan for their time and helpful insights.

I wish to thank all of the members of Mechanics of Materials Research Group who helped to perform this study. Additionally, a special thanks to Mr. Thomas Bouchenot for developing the constitutive model that was used in this research.

Finally, I would like to thank my parents and sister for their support and sacrifices for my academic endeavors.

TABLE OF CONTENTS

LIST OF FIGURES

LIST OF TABLES

CHAPTER 1 INTRODUCTION

Fielding life prediction models to be employed to support durability modeling of structures subjected to combined extreme environments generally proceeds with analysis at the material length scale. Test specimens of 2.25 Cr-1Mo material are exposed to cases that the subject structure would experience during usage. Traditionally, mechanical tests are performed under high temperature low cycle fatigue (LCF), creep-fatigue (CF), thermomechanical fatigue (TMF), creep-TMF, multiaxial fatigue, as well as other conditions. Experimental data take generally includes deformation (e.g. stress-strain curves) and crack initiation responses (e.g. strain-life). Nominally, a constitutive model is tuned to match hysteresis and a lifing model is used to regress fatigue life data. The models are subsequently exercised and in some cases embedded in general-purpose finite element modeling packages. Although a number of approaches have been developed, the framework of testing, modeling, and application has not varied much since the 1980s as evidenced in recent reviews [1-3].

As newer alloys emerge as potential candidates for hot structures; however, their adaptation in designs can be decelerated due to the expansive test programs needed to develop the requisite data set mentioned earlier. A novel approach to deformation and life prediction modeling is presented here to allow for the development of accurate first approximations of durability under complex conditions with simply experiments: LCF, creep, and oxidation. Other experiments (i.e., creep-fatigue, TMF, multiaxial) are used for model verification. As a result, the modeling approach represents a viable framework that can be used to vet a candidate alloy for complex conditions

under which it has only been minimally characterized.

The goal of the present work is to develop a life prediction model without having similar limitations described previously. Many components in the turbomachinery industry experience long hold periods with thermal cycling; therefore, it is essential to be able to estimate material behavior under such conditions. Figure 1-1 demonstrates strain range against number of cycles to failure values for three different important type of conditions. Isothermal low cycle fatigue (LCF) conditions, has the longest life. Isothermal creep-fatigue conditions are displayed with the middle curve. Lastly, thermomechanical fatigue cases are shown with the line having shortest life. More detailed explanation of the effect of different type of conditions are included in Chapter 4 and Chapter 6. Review of published papers shows that most of the previous approaches can predict LCF cases accurately; however, few methods are able to simulate dwell periods. For example, the approach published by Neu and Sehitoglu cannot determine the middle curve in the figure. The most complex type of loading is having a dwell period with thermal cycling, show with the bottom curve.

The life prediction approach developed for this study can be applied for different materials by changing material constants and the flexibility function in environmental-fatigue module, which is explained in Chapter 7.

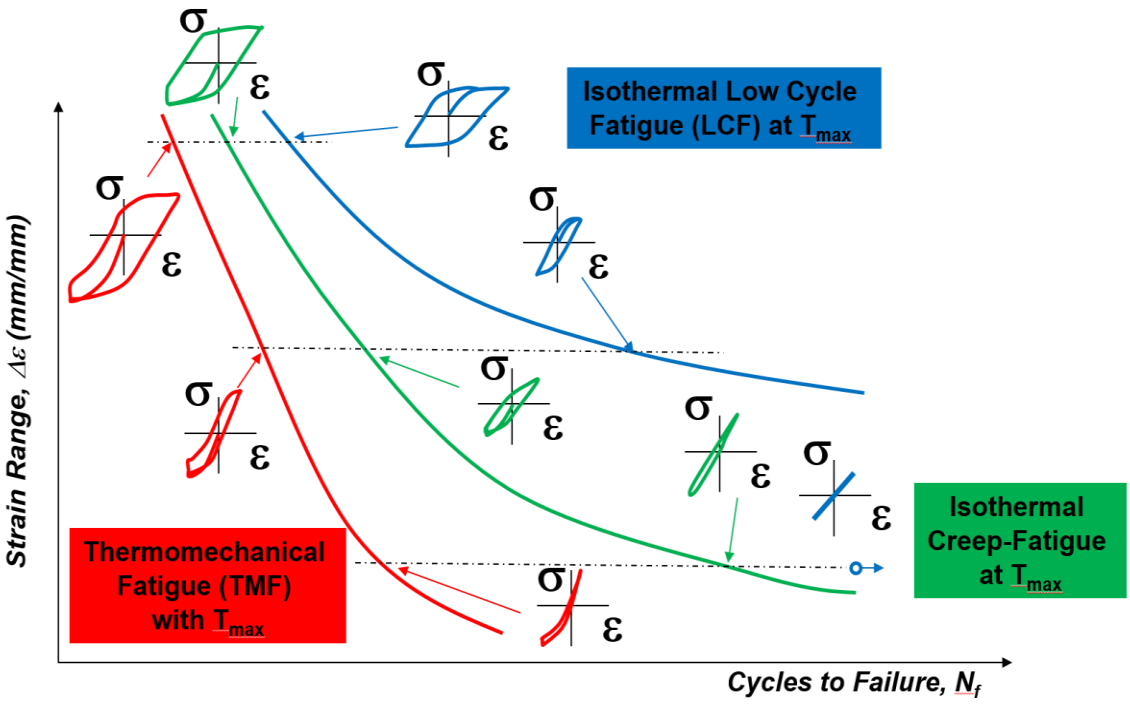

Figure 1-1: Demonstration of different loading type.

CHAPTER 2 LITERATURE REVIEW

2.1 Candidate Material

A low-alloy ferritic steel, 2.25Cr-1Mo, is the material presented in this study. It exhibits good mechanical and creep characteristics at temperatures between 450°C and 650°C; therefore, it has been heavily used in both nuclear and gas power generation and chemical processing applications. These characteristics provide long service life for structural components composed of 2.25Cr-1Mo, where non-isothermal fatigue, ratcheting, and thermally driven deformation are exist. The chemical composition of 2.25Cr-1Mo required by ASTM A542-A542M-13 is presented in Table 2-1.[4] The material displays strong corrosion resistance from alloying with Cr which also increases the ultimate tensile strength, cyclic hardening, and the elongation of the material. Addition of Mo ameliorate heat resistance; consequently, elevating the strength of the low alloy steel at high temperatures. Material 2.25Cr-1Mo has a melting temperature, T_m of 1500°C.The microstructure of the material is presented in Figure 2-1. The figure displays that the material has isotropic properties from the random grain orientation. Also, the Poisson's ratio of this material is reported to be 0.29, which is in the range for isotropic behavior. Additionally, the average grain size is approximately 40 $\mu m.$ Figure 2-2 includes graphs of the elastic modulus, monotonic yield and ultimate strength, elongation, and cyclic yield strength for different temperatures. Based on the comparison between the monotonic and cyclic strength of the material, 2.25Cr-1Mo is expected to soften over a range of temperatures.

Table 2-1: Elemental composition for 2.25Cr-1Mo required by ASTM A542-A542M-13; percent compositions listed are the maximum value unless otherwise indicated.

Element	C	Mn	P	S	Si	Cr	Mo	Cu	Ni	V	Fe
Required Composition (%)	0.18	0.25-0.66	0.025	0.025	0.50	1.88-2.62	0.85-1.15	0.43	0.43	0.04	Bal.

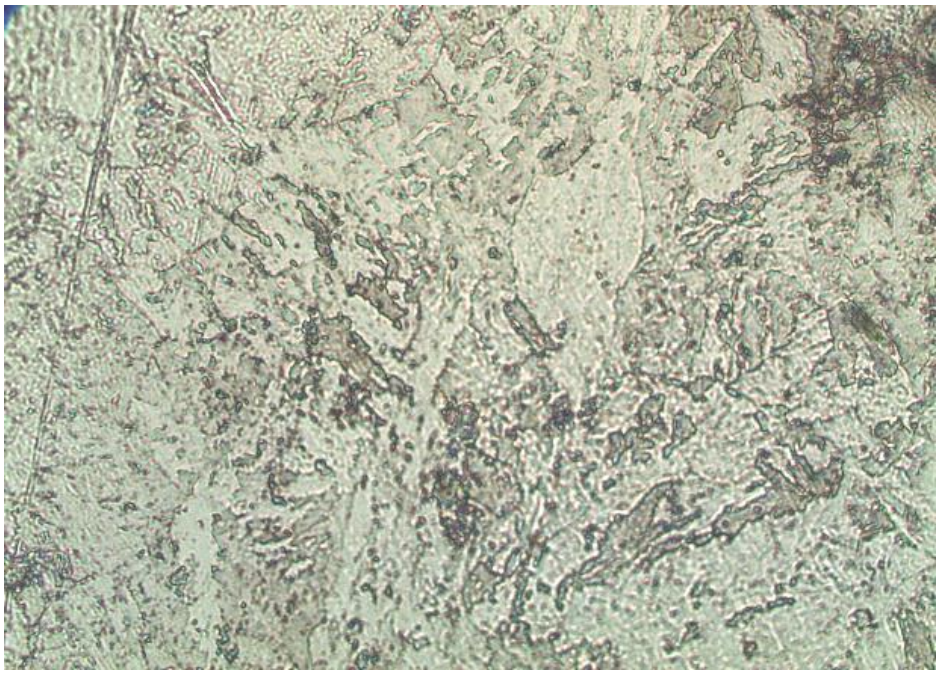

Figure 2-1: Microstructure of 2.25Cr-1Mo.

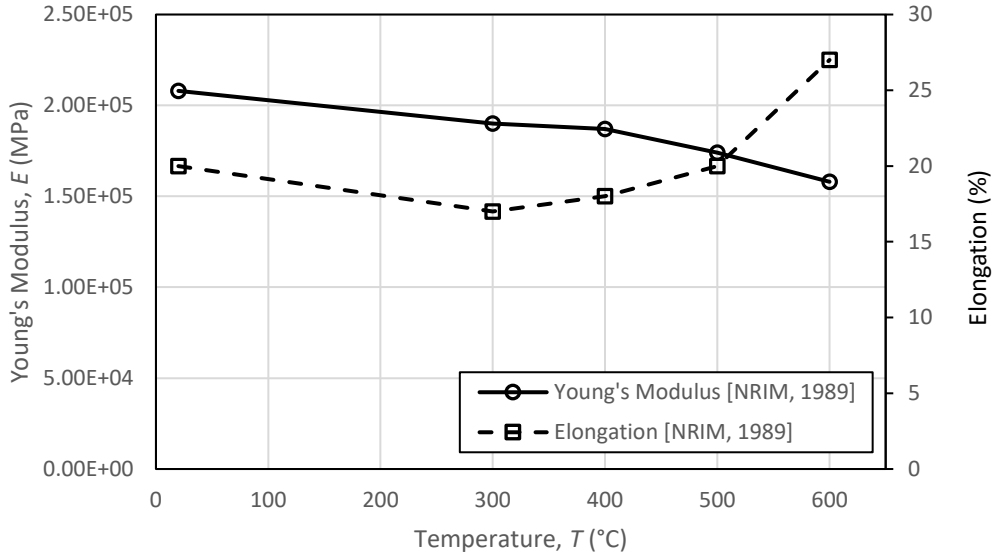

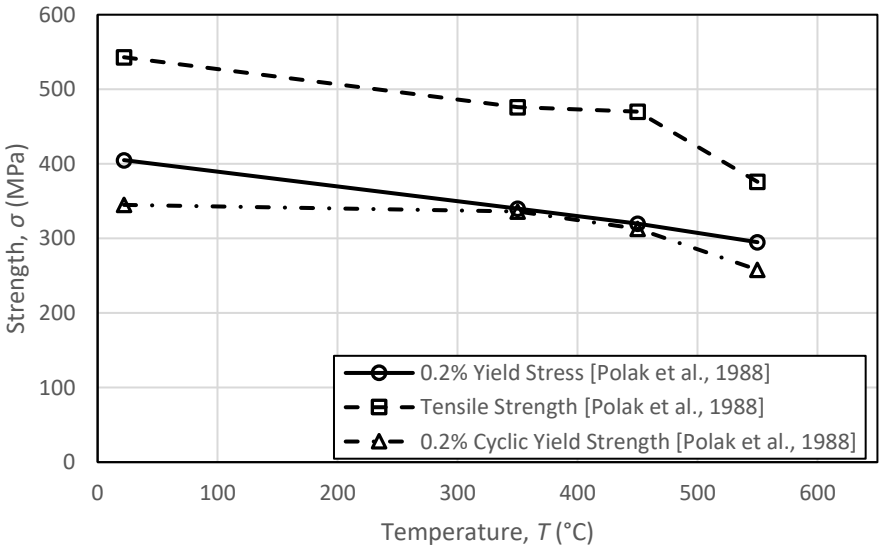

Figure 2-2: Temperature of the (a) Young's modulus, elongation, (b) yield strength, ultimate tensile strength, and cyclic yield strength for 2.25Cr-1Mo; values obtained from literature sources (Metals 1989) (Parker 1985).

2.2 Review of Literature Data

Material 2.25Cr-1Mo is a widely used material in the energy industry; thusly, a large pool of experimental data available for the alloy. Table 2-2 presents different sources for variety of experiment types. This large pool of literature-based data includes: tensile [5,6], low cycle fatigue [7-10], creep deformation and rupture [11,12], creep-fatigue [10-13], thermomechanical fatigue [14,15], and stress-free oxidation kinetics experiments [16,17] as displayed in the table. It can be seen that the material has received steady attention over the past four decades. The first column of Table 2-2 includes type of experiments on 2.25Cr-1Mo material, while the second column is showing the sources for these experiments.

Table 2-2: Synopsis of mechanical testing on 2.25Cr-1Mo

Test type	Sources
Monotonic Tensile	Polak et al., 1988; Bynum et al., 1976
Low Cycle Fatigue (LCF)	NRIM, 1989; NIMS, 2004; Tian et al., 2016
Creep	Parker et al., 1985; NIMS, 2003; Kushima et al., 2005; dos Rei Sobrihno et al., 2014
Creep-Fatigue (CF)	Tian et al., 2016; Zhang et al., 2016
Thermomechanical Fatigue (TMF)	Iwasaki et al., 1987; Saltsman and Halford, 1994
Multiaxial Fatigue	Inoue et al., 1989; Inoue et al., 1994, Blass, 1990
Oxidation Ingression	Bueno and Marino, 2001; Sumida et al., 1995

The mid-life stress and strain amplitude response under low cycle fatigue (LCF) at temperatures from 20°C to 600°C and strain rates from 1×10^{-5} s^{-1} to 5×10^{-3} s^{-1} were obtained by the National Institute for Material Science (NIMS). It is discovered that 2.25Cr-1Mo cyclically softens over a range of temperatures after comparing the monotonic and cyclic stress-strain curves. This reference also includes the elastic modulus and elongations with the monotonic Ramberg-Osgood constants *K* and *n*. Ultimate tensile and yield strength values for the material are provided by Polak and colleagues. [6] NIMS [7] and Parker [29] contributed data useful for creep modeling. Tian and colleagues [10] conducted isothermal LCF and creep-fatigue conditions at 355°C, 455°C, and 555°C with a strain rate of 2×10^{-3} s^{-1}. For verifying the deformation model performing; thermomechanical fatigue (TMF) conditions, the first loop of a TMF cycle was utilized from Iwasaki and co-authors. [14] In conclusion, the literature data used in this research generated from a variety of references.

Due to a large pool of experimental data available for 2.25Cr-1Mo material, a database was created for better analyzation of the number of cycles to failure values for range of conditions. This database was essential for improving and validating the life prediction model in this study. The database is provided in the Appendix section. After studying the literature-based data, some key knowledge gaps were discovered in the database. Figure 2-3 presents the available lifing data for various conditions. As show in the figure, there are plenty of LCF data at temperatures from 200°C to 600°C. Additionally, most of the dwell data at either at 550°C or has 3600 seconds tensile hold period; however, there are only three data points for compressive dwells. It is important to consider with compressive holds in this study for understanding the effect of this type of dwell period on 2.25Cr-1Mo material.

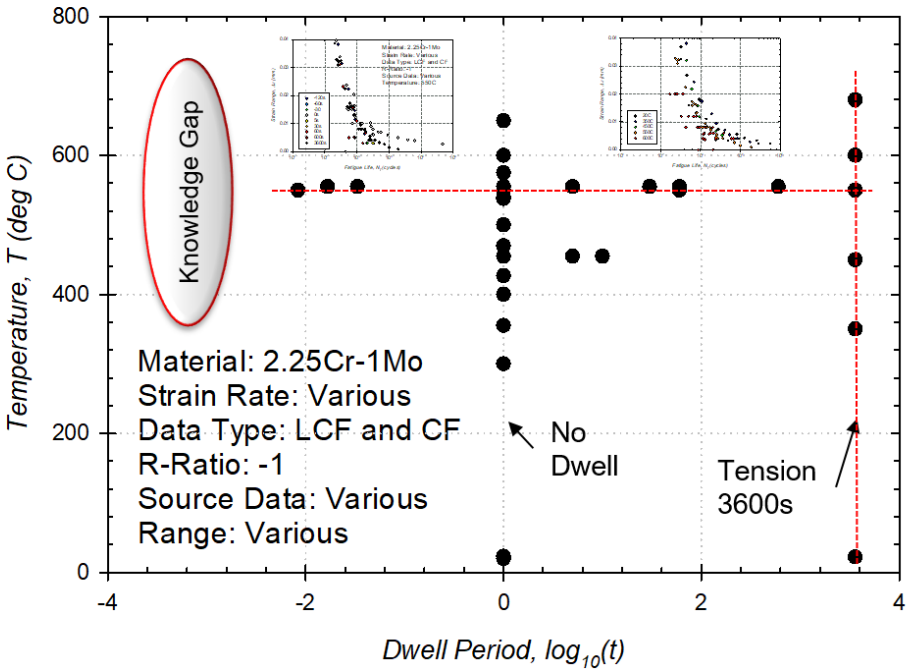

Figure 2-3: Knowledge gaps in the literature-based data presentation

In this study, a physically- based life prediction approach is presented. Metallurgical response of the material to different type of conditions is analyzed carefully. Metallurgical preparation and analysis from this work are explained in Chapter 3 and 4, respectively. Additionally, the metallurgical response of 2.25 Cr-1Mo material is available in different sources. After studying other sources, it is observed that experiencing low-cycle fatigue cases with strain rates at or above 1e-3s^{-1}, classical fatigue mechanisms are responsible for crack initiation and early propagation from the surface. This crack initiation from the surface behavior caused by fatigue mechanisms is shown in Figure 2-4. When 2.25Cr-1Mo steel is subjected to long periods of compressive dwell at high temperature, oxides form at the surface. Upon cycling, these oxides crack and expose material beneath the surface (Figure 2-5). If the dwell period is tensile instead of

compressive, the crack initiation process proceeds with the formation of subsurface micro-pores that coalesce to form microcracks (Figure 2-6). Observations from other studies were also used to support these claims [5-13].

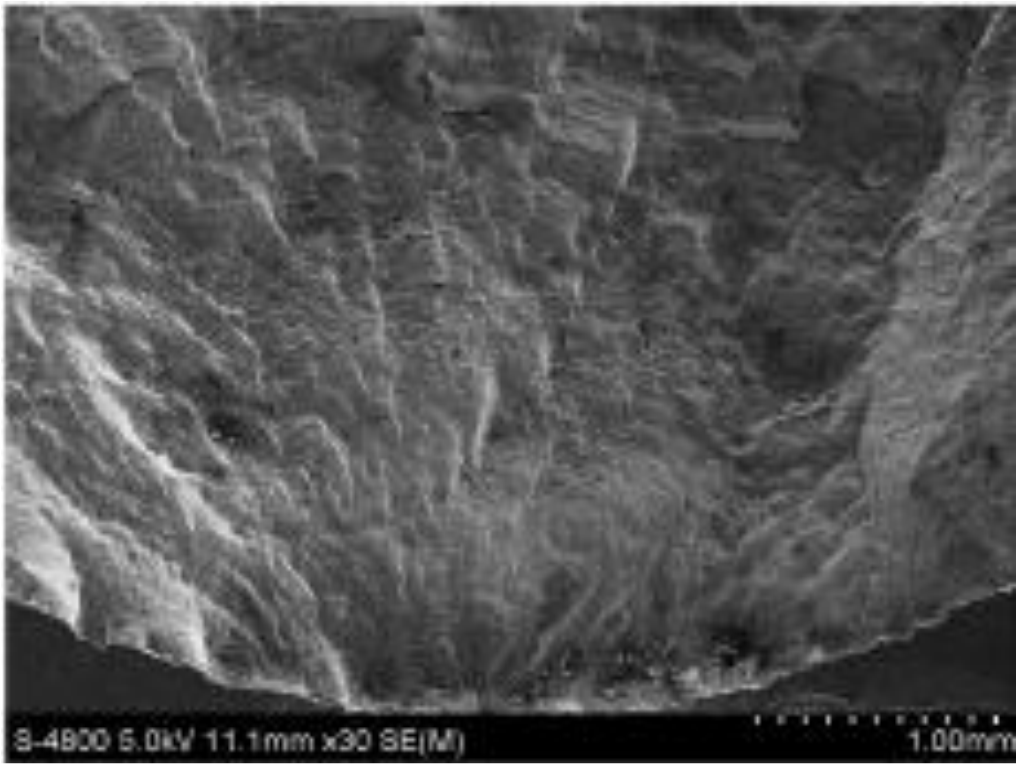

Figure 2-4: Crack initiation caused by fatigue mechanicsm. [10]

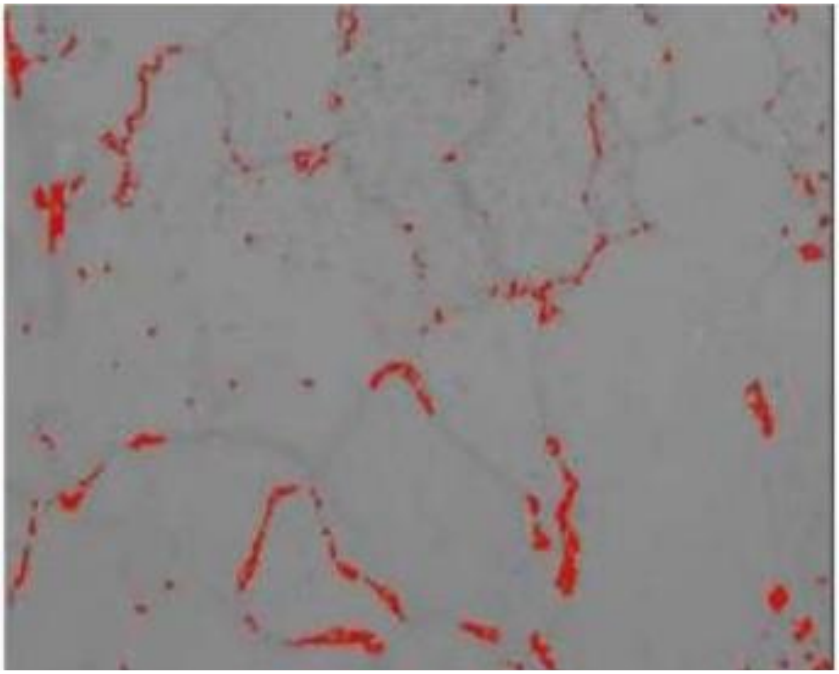

Figure 2-5: Microcracks from long dwell periods. [8]

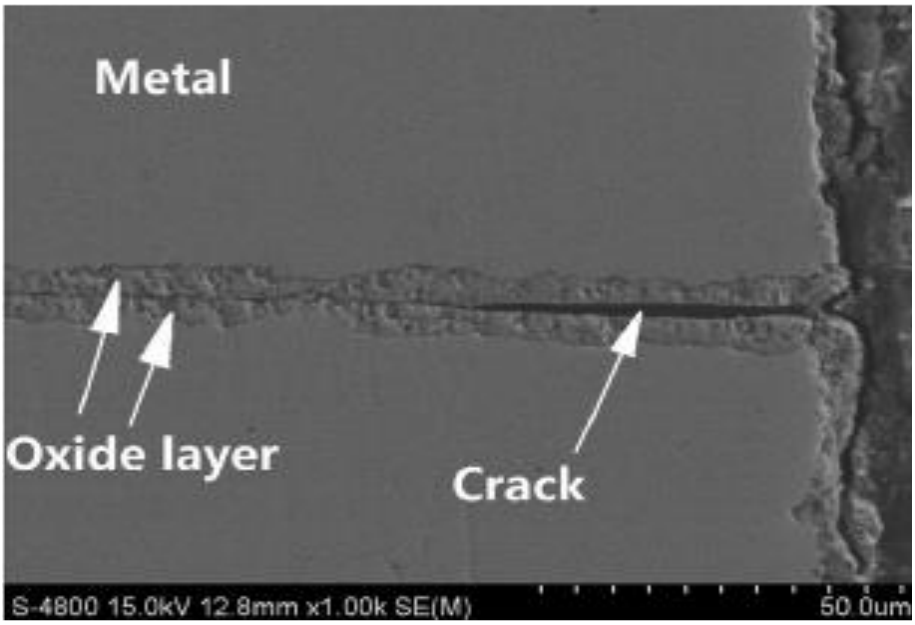

Figure 2-6: Oxide spikes formed at the surface from compressive dwells.[10]

2.3 Review of Life Prediction Approaches

A variety of approaches have been developed to predict fatigue life of materials and structures under complex conditions. It is important to accurately predict life-span of a component experiencing fatigue damage or unexpected structural failures could occur. Table 2-3 presents different life prediction approaches from past decades. Each approach was developed for different materials as shown. Additionally, limitations for each life prediction approach are available as well.

Table 2-3: Review of Life Prediction Approaches

Author(s), Year	Material	Approach	Limitations
Manson et al., 1971	Hayes 188	Creep-Fatigue Strain Range Partitioning	No insight into microstructural response of the material (e.g. phenomenologically-based)
Neu and Sehitoglu, 1989	304 Steel	Stress-strain-based; Cumulative Damage: Fatigue, Creep, Oxidation	Isotropic;Creep contribution depends on oxidation response; no dwell
McGaw, 1992	316 Steel	TMF-Strain-Range Partitioning	No insight into microstructural response of the material (e.g. phenomenologically-based)
Gordon, 2006	DS GTD-111	Stress-strain-based; Cumulative Damage: Fatigue, Creep, Oxidation	Needs lots of oxidation data
Grutzner et al., 2014	Alloy 247	Energy-based: Cumulative Damage: Fatigue, Creep, Oxidation	No insight into microstructural response of the material (e.g. phenomenologically-based)

One of the earliest life prediction approaches was introduced by Manson and colleagues in 1971. This was a creep-fatigue strain range partitioning approach using Hayes 188 material, a cobalt-based alloy. The limiting factor for this method was that the microstructural response of the material. Similar limitations were discovered with the approaches by Mcgaw, and Grutzner and colleagues. It is consequential to analyze microstructural response of the material to identify the effects of different damage mechanisms.

In 1989, Neu and Sehitoglu presented a stress-strain based life-prediction method. This approach utilizes cumulative damage methos with modules including; classical fatigue, creep rupture, and oxidation. [11] A similar cumulative damage approach is used in this study, which will be explained in Chapter 6. The method developed by Neu and Sehitoglu assumes isotropic behavior for the material, also it is limited for conditions with no dwell periods. These restrictions result in non-realistic predictions. Gordon introduced another stress-strain based approach in 2006, additionally the author used a cumulative damage method too for predicting life of directionally solidified (DS) Ni-base super alloy GTD 111. This approach required a large number of oxidation data and this type of data is not available in variety of conditions. Main difference between the approaches by Gordon, and Neu and Sehitoglu is the order taken for fitting the constants for each damage module. Gordon fitted fatigue, then creep damage, and finally environmental fatigue module; while Neu and Sehitoglu worked on environmental fatigue after the fatigue model, and creep at last. Recently, Tian and coworkers published a study on 2.25Cr1-MoV material, a slightly different alloy from this study, using a strain energy-based model. This approach was limited for only isothermal cases.

CHAPTER 3 EXPERIMENTAL APPROACH

Two types of tests were performed to validate the life prediction approach presented in this study. Tensile tests were conducted primarily for acquiring the material properties; elastic modulus, ultimate tensile strength and 0.2% yield strength. Fatigue tests were performed to determine the number of cycles to failure, N_{total}, under the specified loading conditions. Additionally, the deformed specimens were analyzed for studying the crack initiation mechanisms. Figure 3-1 shows the test sample geometry used for the experiments. All the dimensions and tolerance criteria for the specimen design are available in the drawing. This geometry satisfies the dimensions specified by ASTM E8 [34] and ISO [35] strain-controlled, low cycle fatigue and creep-fatigue standards. ASTM requires round test specimens to have diameter less than 12.5 mm. Also, the gauge length of the specimens is 15 mm. A batch of normalized and tempered 2.25Cr-1Mo bars were provided to fabricate the test specimens. After the fabrication, dimensions of specimens were measured and recorded using a digital caliper. Measuring the specimens correctly is essential for getting accurate results. Table 3-1 presents 21 fabricated specimens with their identification numbers and measured diameters. All the specimens were measured to be in the tolerance criteria of the specimen design.

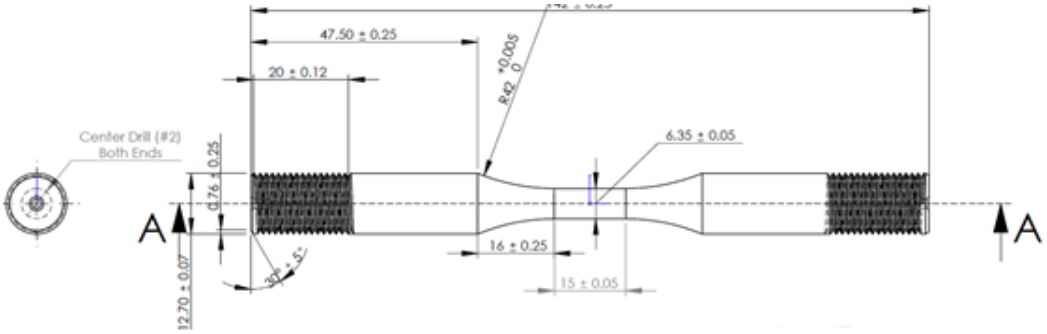

Figure 3-1: Specimen design for tensile and fatigue experiments on 2.25Cr-1Mo

Table 3-1: Fabricated 2.25Cr-1Mo specimens with the IDs and diameters

Specimen ID	Diameter(mm)
BR 15 LCF	6.36
BR 16 LCF	6.36
BR 17 LCF	6.35
BR 22 LCF	6.34
BR 26 LCF	6.36
BR 30 LCF	6.36
BR 28 LCF	6.37
BR 24 LCF	6.36
BR 27 LCF	6.37
BR 23 LCF	6.36
BR 25 LCF	6.36
BR 21 LCF	6.36
BR 32 LCF	6.36
BR 37 LCF	6.35
BR 35 LCF	6.35
BR 31 LCF	6.35
BR 29 LCF	6.35
BR 33 LCF	6.35
BR 38 LCF	6.35
BR 39 LCF	6.34
BR 36 LCF	6.33

3.1 Tensile Testing

The main purpose for conducting the tensile tests was to measure the various mechanical properties for the supplied specimens. Elastic modulus, *E*, ultimate tensile strengts, σ_{UTS}, and yield strength, σ_{YS} of the provided test specimens were obtained and compared with the literature data. These properties were used to calibrate the constitutive model used in this study. The experimental results are presented in the next chapter. Aside from material properties, the deformation response of the material was also investigated. The tensile tests were performed using the ASTM-E8 Standard Test Method for Tension Testing of Metallic Materials [4].

Figure 3-2: Experimental set-up for tensile testing.

The uniaxial tensile tests were conducted using a load-cell and a direct contact extensometer. This test set-up is shown in Figure 3-2. A computer software was utilized for running and recording of the experiments. Linear variable differential transformers, LVDTs, were used to acquire the displacement of both ends of the gauge section. These sensors are used for to convert mechanical motion into electrical voltage. All the experiments were recorded with a frequency of 1.14 points per second (Hz). Additionally, experiments were strain-controlled with isothermal conditions. After the tests were completed, the raw data was saved to Excel file for later analysis.

After carefully analyzing available data from other sources for 2.25Cr-1Mo materials, conditions for the tensile tests were chosen to provide material properties that would support constitutive and life prediction modeling. This material is heavily utilized in turbomachinery components where it experiences very high temperatures. The tensile specimens, consequently, were mostly tested at 600°C and 650°C. One specimen was tested at room temperature to analyze how the material behaves at low temperatures. Two different strain rates were used during tensile testing, 1e-3 and 1e-5 per second. These rates were strategically selected to compare with the data from other sources. The test matrix that was used for the tensile testing is provided in Table 3-2. Specimen number, temperature and strain rate of the experiments are presented in this table.

Table 3-2: Tensile test matrix for 2.25Cr-1Mo at elevated temperature.

Speciemen No.	Temperature(s), T (°C)	Strain Rate, $d\varepsilon/dt$ (mm/mm/s)
BR23	20	0.001
BR25	650	0.001
BR26	600	0.00001
BR27	650	0.00001
BR28	600	0.001
BR24	600	0.00001

3.2 Fatigue Testing

Validation of the life prediction approach in this study required fatigue testing performed on 2.25Cr-Mo material. It is essential to obtain number of cycles to failure under certain cases to optimize the constants in the approach, which will be detailed in the Chapter 6. A strain-controlled testing method was chosen for the experiments. Direct contact thermocouples and strain measurement were used to control the temperature and deformation of the gage section of the test coupon. Table 3-3 represents the test matrix that was used for the fatigue tests. This table includes: specimen number, strain range, temperature, strain rate, strain ratio, and dwell time of the experiments, respectively. These parameters strongly influence the deformation response and fatigue life.

Table 3-3: Fatigue test matrix for 2.25Cr-1Mo at elevated temperature.

Specimen No.	Total Strain Range, $\Delta\varepsilon$ (mm/mm)	Temperature(s), T (°C)	Strain Rate, $d\varepsilon/dt$ (mm/mm/s)	Strain Ratio, R_e	Dwell Time, t_h (sec) and Type
BR 15	0.007	600	0.001	-1	90s in Tens.
BR 17	0.007	600	0.001	-1	90s in Comp.
BR 35	0.005	600	0.001	-1	90s in Comp.
BR 29	0.007	600	0.001	-1	90s in Comp.
BR 32	0.005	600	0.001	-1	0s
BR 33	0.007	650	0.001	-1	90s in Comp.
BR 34	0.007	600	0.001	-1	0
BR 31	0.0035	600	0.001	-1	90s in Tens.
BR 36	0.007	600	0.001	-∞	90s in Comp.

Although a variety of temperatures and strain rates were considered, isothermal fatigue with dwells at high temperatures were emphasized in the test design. As previously mentioned, 2.25Cr-Mo material is heavily used in the energy industry in environments with very high temperatures and long dwell periods; consequentially, the test conditions were designed according to the industrial usage of the material. In literature, it was observed that the majority of creep-fatigue experiments contained tensile dwells; consequently, compressive dwell-fatigue tests were considered here. Only 90 second dwell periods were tested due to scheduling.

A servohydraulic axial fatigue machine was used for the direct-strain fatigue tests. This test device applied a uniform strain through the cross section of the test specimen. A computer software controlled the experiments. The test set-up is shown in Figure 3-3. Like the tensile testing, linear differential variable transformers are used to turn mechanical deformation to electrical signals for data recording. The data was recorded with a frequency of 31.25 per second for all the fatigue experiments.

Figure 3-3: Experimental set-up for fatigue testing.

3.3 Metallurgical Preparation and Analysis

Some of the previous life prediction models were lacking metallurgical insight of this material. After the completion of tensile and fatigue experiments, the deformed test specimens were analyzed via two types of microscopy: white light optical microscopy (LOM) and scanning electron microscopy (SEM). This type of metallurgical analysis is important to assess the crack initiation mechanisms. These mechanisms are vital for construction of a physically-based life prediction approach in this study as previously described. The specimens needed to be prepared for the visual and microscopic inspections. This metallurgical preparation included several steps; sectioning, mounting, grinding, polishing, and finally etching.

The preparation procedure started with the sectioning of the deformed specimens into a convenient size for the inspections. Figure 3-4 displays a sectioned test specimen. A Buehler, Isomet Slow (serial. No 390-IS-11613) speed saw was used to section the specimens. The blade that was used for the saw is from Pace Technologies, WB-0045HC, 104168001f9, 4-inch diamond blade. To avoid damaging or destroying the material, a water based anti-corrosion cutting fluid was used during the sectioning. This fluid is also from Pace Technologies, WL2-30000-32, Diacut 2 water based anti-corrosion cutting fluid.

Figure 3-4: Typical sectioned specimen.

After the samples were reduced to a desired size, they were mounted in an ultrathin low viscosity resin and ultrathin hardener by Pace Technologies (Figure 3-5a). The mounting of the samples in an epoxy material was to ease the handling during the next steps of the preparation. Cure time for each sample was 8 hours at room temperature. Applying a one minute of heat to each sample mount with heat gun at low setting roughly 10" above sample increased cure time and helped epoxy bond stronger. A Buehler EcoMet3000 variable speed grinding polisher was used for the grinding and polishing phase (Figure 3-5. The grinding process was necessary to remove any damaged surfaces developed on the specimen during the sectioning step. After the grinding, the samples were polished to remove the last thin layer of the deformed metal for a smooth

reflective surface.

Figure 3-5: Mounted specimens (a) and Buehler EcoMet3000 polisher (b).

For the final step of the metallurgical preparation, the samples were placed in an etchant. This process was executed for making the microstructure of the test samples visible for the microscopy. Kalling's 2 Reagent, from Es Laboratory (Cat. No.151, Lot. No. 15020), was used for the etching process. The etchant was applied to each sample using a cotton swab for 30 seconds while constantly rubbing the surface of the specimen. Immediately after the etchant was applied, the samples were rinsed for 20 seconds and then air dried. Finally, the prepared samples were coated in the same lubricant that was used the sectioning process.

After the metallurgical preparation, the samples were examined and photographed with two types of microscopy. First, a light optical microscope by Excel Technologies was used for analyzing the prepared samples (Figure 3-6a). It was decided to use a scanning electron microscope to analyze the test specimens more meticulously after the examination with the light optical microscope. JEOL JSM-6480 scanning electron microscope was used for the final step of the metallurgical analysis (Figure 3-6b.). The results of the analysis and discussion are presented in the next chapter.

Figure 3-6: Microscopy equipment, a) Excel Tech MEF3 Microscope and b) Scanning Electron Microscope.

CHAPTER 4 EXPERIMENTAL RESULTS

The main purpose of this study is to develop an accurate model to estimate the number of cycles to fatigue failure for 2.25Cr-1Mo material; therefore, tensile tests were conducted on multiple specimens for constructing a more precise model. Fatigue tests were required to validate the life prediction model. Each deformed specimen was analyzed using multiple microscopic methods as previously explained. Some statistical techniques were used to calculate the essential material properties. The following sections include the summary of the test results and some selected cases. Also, experimental results from the present study are compared with data introduced in literature. It should be noted that test results and microscopic images are presented in the Appendix of this thesis.

4.1 Tensile Testing

Tensile tests were performed on six normalized and tempered (N&T) 2.25Cr-1Mo specimens. The tensile test matrix, Table 3-2, was utilized to conduct these tests. Specimens experienced different temperatures and strain rates to calculate the material properties. Those properties were used to develop the constitutive model for this study, which will be explained in the following chapter. Table 4-1 presents the summary of the tensile test results. The first three columns of the table show the specimen number and test conditions, respectively. The material properties are displayed in the last three columns. Elastic modulus, E ultimate tensile strength, $\sigma_{UTS,}$ and 0.2% yield strength, $\sigma_{YS,}$ of each case are calculated using the deformation response

obtained from the experiments. The deformation response for all the cases are displayed in Figure 4-1. Solid lines represent the experiments with 0.1% strain rate, and dotted lines are for 0.001% strain rate. Stress ranges are higher for lower temperatures as expected. Also, stress ranges are higher for slower strain rates which agrees with the literature data. Elastic modulus is calculated with fitting a line to the elastic region of stress-strain curve of each experiment. Additionally, ultimate tensile strength and 0.2% yield strength are obtained using the stress-strain curves. The maximum stress point on the curves are designated as ultimate tensile strengths of the experiments. The 0.2% yield strength is calculated using an offset method. It is obtained by drawing through the point of the horizontal axis of strain equals 0.002 mm/mm, a line parallel to the initial straight-line portion of the stress-strain diagram.

Table 4-1: Tensile test matrix for 2.25Cr-1Mo at elevated temperature

Speciemen No.	Temperature(s), T (°C)	Strain Rate, $d\varepsilon/dt$ (mm/mm/s)	Elastic Modulus, E (MPa)	Ultimate Tensile Strength (MPa)	0.2% Yield Strength (MPa)
BR23	20	0.001	1.04E+06	687	686
BR25	650	0.001	1.32E+05	393	372
BR26	600	0.00001	1.64E+05	367	355
BR27	650	0.00001	1.41E+05	258	238
BR28	600	0.001	1.94E+05	468	452
BR24	600	0.00001	1.64E+05	425	390

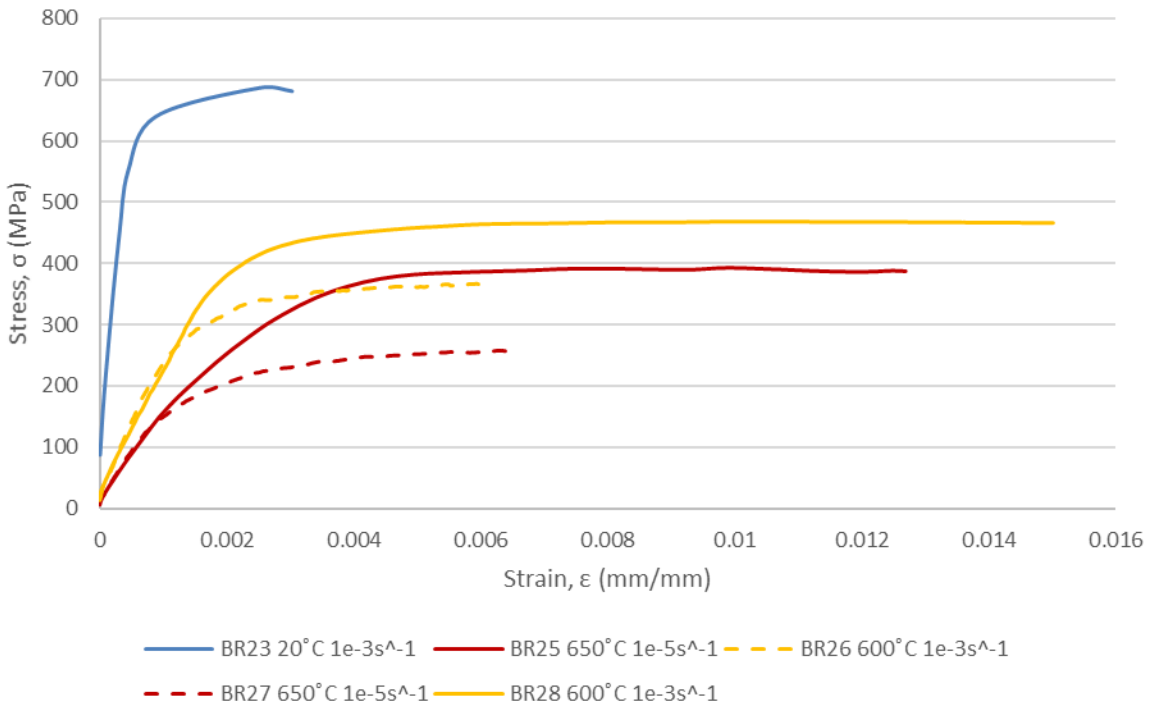

Figure 4-1: Tensile response of 2.25 Cr-1Mo.

For using the literature-based data in this study, it was necessary to compare tensile properties of provided 2.25Cr-1Mo material with the data from other sources. The material properties calculated in this study are compared with the data from other sources in Figure 4-2 and Figure 4-3. The comparison in Figure 4-2 shows that the ultimate tensile strengths from each experiment are higher than the data from literature sources. This means the N&T 2.25Cr-1Mo bars that were provided are little stronger than those reported elsewhere; therefore, it is expected to have slightly higher number of cycles to failure for these specimens than the literature-based data. Similar behavior can be seen in for the elastic modulus of the tests. The modulus of specimen BR 23 is not presented here because it was concluded that strain signal was not recorded properly.

Figure 4-1 shows the slope of elastic region for BR23 is too high for this material. This error was caused by the extensometer slipping during the testing of this specimen.

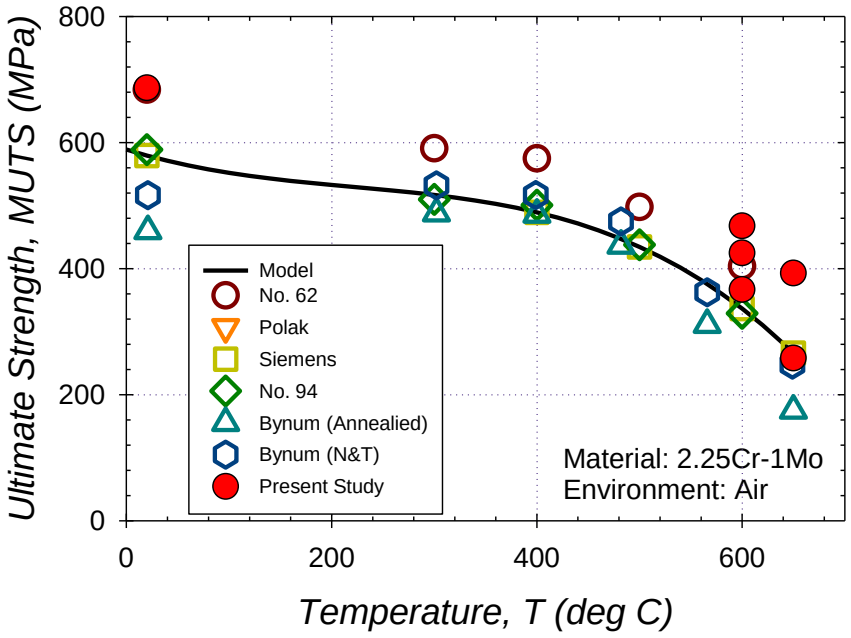

Figure 4-2: Comparison of ultimate tensile strength of experiments with the literature data.

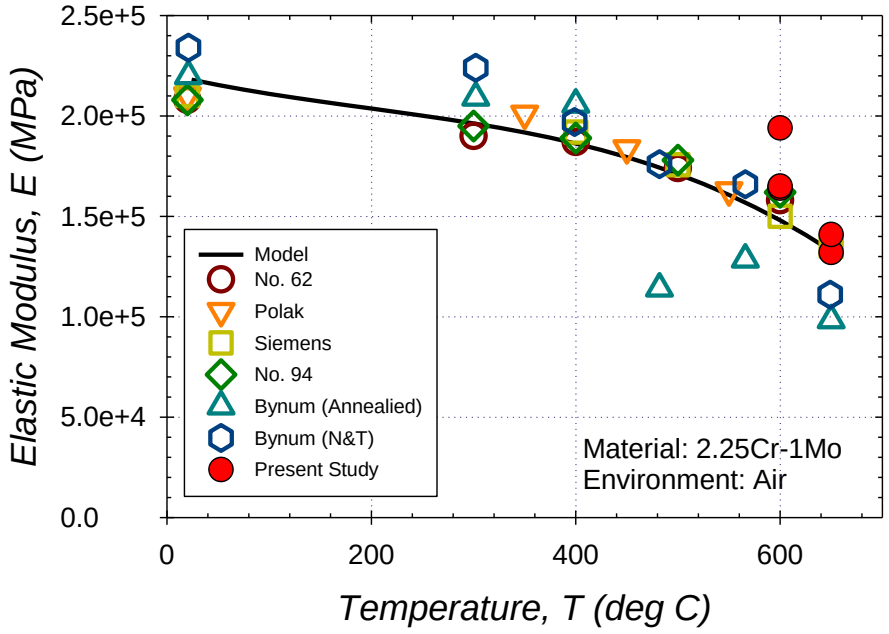

Figure 4-3: Comparison of elastic modulus of experiments with the literature data.

4.2 Fatigue Testing

There were nine fatigue experiments conducted on normalized and tempered 2.25Cr-1Mo material. These experiments are an essential part of this study because number of cycles to failure values, obtained from the tests, are used to validate, and improve the life prediction model. Also, it is important to understand the effect of temperature, strain range and different type of dwells for developing an accurate lifing model; thusly, the fatigue test matrix was constructed with different temperatures, strain ranges, and dwell types as previously shown. Stress-cycle graphs are created to better analyze the effect of these conditions on 2.25Cr-1Mo material in this section.

Table 4-2: Fatigue test matrix for 2.25Cr-1Mo at elevated temperature

Specimen No.	Total Strain Range, $\Delta\varepsilon$ (mm/mm)	Temperature(s), T (°C)	Strain Rate, $d\varepsilon/dt$ (mm/mm/s)	Strain Ratio, R_e	Dwell Time, t_h (sec) and Type	Cycles to Failure	Stress Range (MPa)	Mean Stress (MPa)
BR 15	0.007	600	0.001	-1	90s in Tens.	544	640.42	4.48
BR 17	0.007	600	0.001	-1	90s in Comp.	1051	611.81	-4.20
BR 35	0.005	600	0.001	-1	90s in Comp.	2664	595.00	9.60
BR 29	0.007	600	0.001	-1	90s in Comp.	1342	622.91	-13.03
BR 32	0.005	600	0.001	-1	0s	3242	642.74	0.46
BR 33	0.007	650	0.001	-1	90s in Comp.	797	N/A	N/A
BR 34	0.007	600	0.001	-1	0	1220	636.64	-3.72
BR 31	0.0035	600	0.001	-1	90s in Tens.	5778(Runout)	476.00	-33.00
BR 36	0.007	600	0.001	-∞	90s in Comp.	938	606.18	-3.98

After conducting fatigue tests on normalized and tempered 2.25 Cr-1Mo specimens, the results are analyzed carefully. Table 4-2 displays the fatigue test matrix with corresponding results. The first six columns represent the specimen information and experimental conditions, while the remaining columns show the results: number of cycles to failure, stress range and mean stress. Stress ranges for each experiment were recorded because it directly affects the life of the material. Only the strain rate values were held as constant during the fatigue testing since implementing slower rates could be very time consuming. Also, the different strain rate cases were in open source data for this material [8]; however, other conditions were changed to examine the effects. It was decided to repeat one case to observe the difference in the number of cycles to failure for same conditions. Specimens BR 17 and BR 29 experienced the same conditions, and it was observed the number of cycles to failure differed by 291 cycles. This behavior agrees with the data published by NRIMS [8]. Furthermore, there was a runout for the specimen BR31. The testing was stopped after cycle 5778 due to time constraints. It was estimated that this test could last around 7500

cycles from the hysteresis loops. It is important to study the relaxation of a material to understand how this material will behave over time. Figure 4-4 displays the stress relaxation response for some selected cycles of BR15 specimen. This specimen experienced 90s dwell periods at 600°C. Also, the strain range was 0.7% and strain rate at 0.001 per second for this case. It was observed that the stress values do not drop until the 500th cycle; therefore, it was concluded that evolution of stress relaxation response does not exhibit strong cycle dependence up to cycle fatigue life, N_{total} for this material.

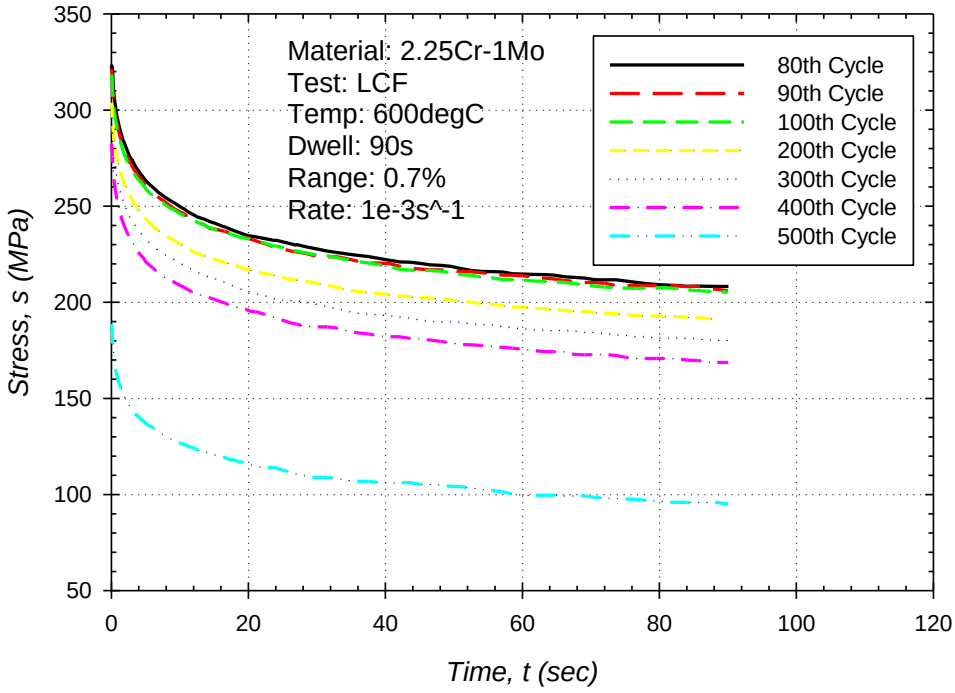

Figure 4-4: Relaxation response of 2.25 Cr-1Mo material using BR-35 specimen.

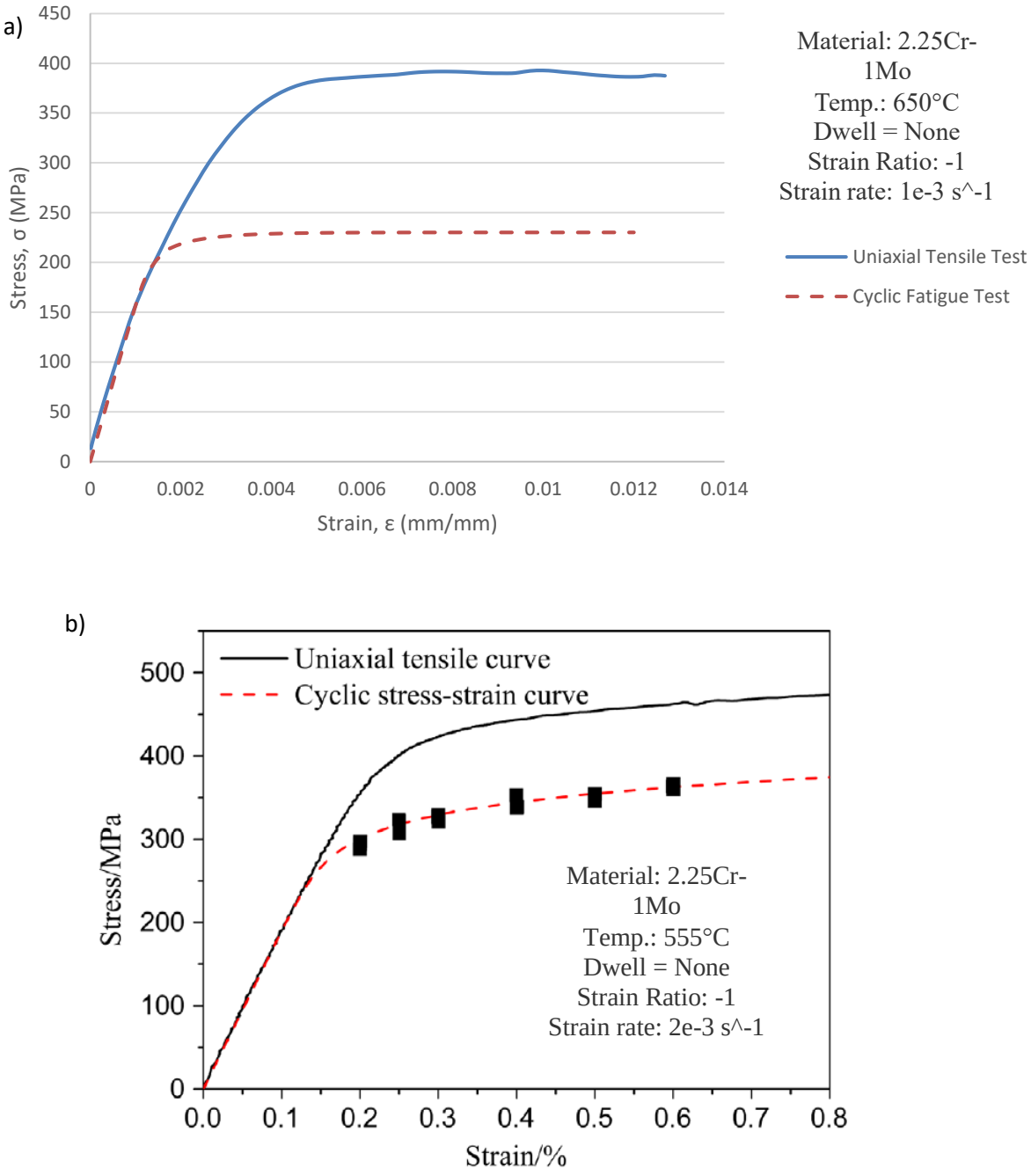

Figure 4-5: Comparison of cyclic and uniaxial deformation responses. (a) Present study and (b) Prior work. [10]

The cyclic softening is based on rearrangement of dislocations. This causes less resistance to deformation for the material; consequentially, the increased strain range makes a bigger driving force for the dislocations generation. Cyclic softening behavior is exhibited by 2.25Cr-1Mo. Comparison between uniaxial and cyclic deformation responses are shown in Figure 4-5. Figure 4-5 a presents experimental data from this study which has strain rate 1e-3 per second at 650°C. The cyclic softening behavior compares well with the data shown in literature [10]. Also, similar comparison is available in literature where cycling softening is presented at 538°C with strain rate 2e-3 per second. Thusly, normalized and tempered test specimens, fabricated in this study, have similar cyclic softening to the material presented in literature. In the present work, both experimental and literature data are used for model validation and improvement. Thusly, it is important to compare data across studies and experimental data from this study. In Section 4.1, it was shown that tensile data from this work agrees with other sources for important material properties. Figure 4-6 presents stress-strain curves for 2.25Cr-1Mo material. Figure 4-6a is from Tian and his colleagues where the material experiences; strain range 1%, strain rate 2e-3 per second at 555°C. Figure 4-6b is from experimental data using specimen BR 34. The conditions for this test are; strain range 0.7%, strain rate 1e-3 per second at 600°C. Even though these conditions are slightly different, normalized and tempered specimens in this work have similar deformation response to the data from literature, presented in the figure. Top curve shows more plasticity, as expected, because strain range is higher for that case.

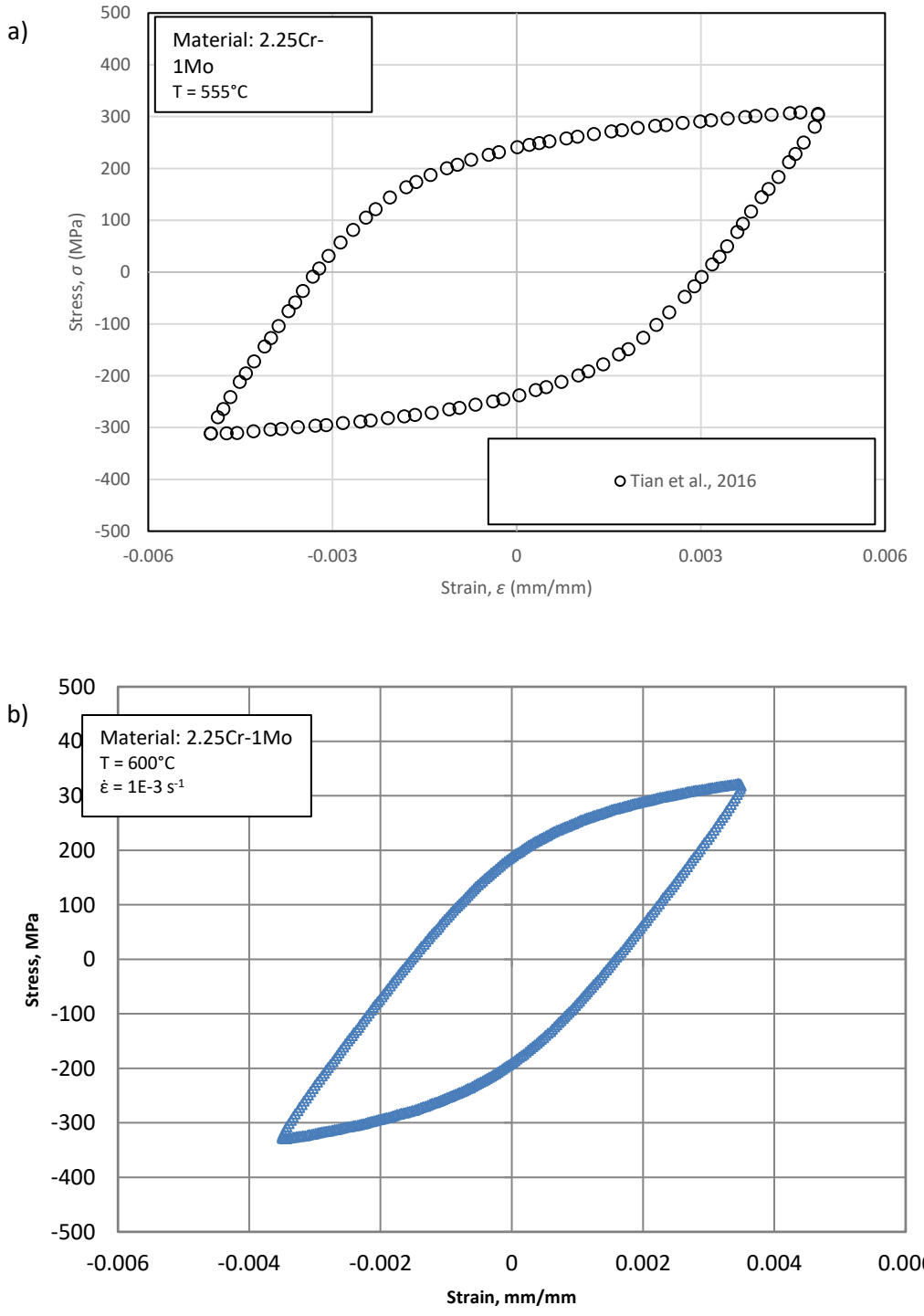

Figure 4-6: Comparison of experimental (a) and literature-based (b) stress-strain curves.

Material 2.25Cr-1Mo is heavily used in the energy industry where components experience long dwell periods. Thusly, it is important to characterize the effects of the dwell periods in this study. Only 90s dwell periods were considered during the fatigue testing because time and budget constraints. The stress history curves are shown in Figure 4-7 for multiple cases with different dwell types. Comparing no dwell case with tensile and compressive dwell cases displays that imposing a dwell period reduces the fatigue life of 2.25Cr-1Mo. At the temperature level studied, a tensile dwell is more detrimental to life compared with a compressive dwell having the same duration. This behavior can also be seen in the work of Tian and his colleagues. [10] It is important to capture this conclusion with the life prediction model too, which will be explained in Chapter 7.

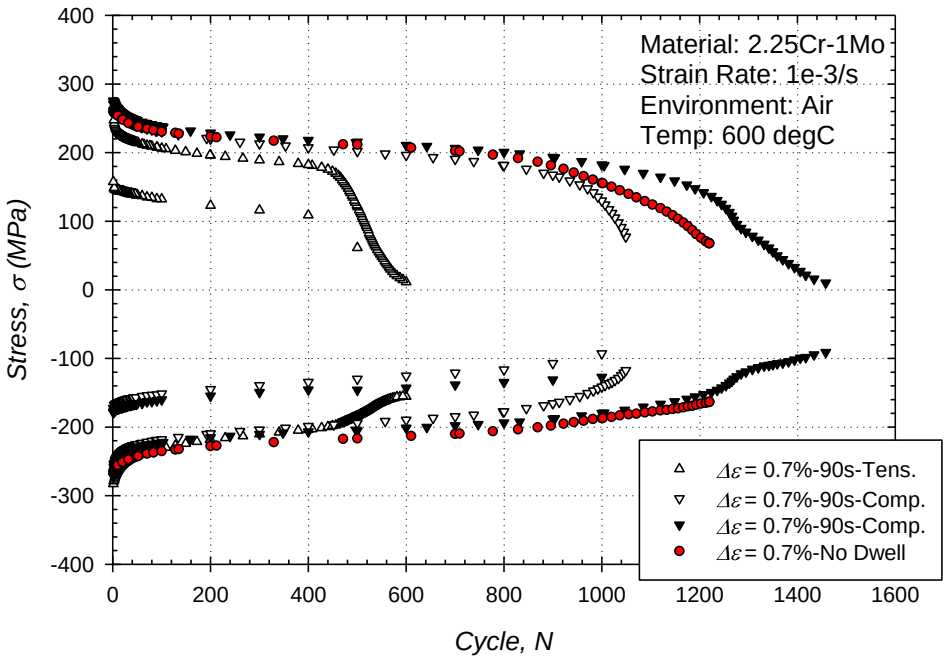

Figure 4-7: The effect of dwell type demonstrated with experimental results

The test matrix was developed to simulate the service-like conditions. Consequently, only extreme temperatures were used. Stress history curves of temperatures 600 and 650 for same dwell periods and strain ranges are presented in Figure 4-8. This figure clearly states that imposing a higher temperature decreases the life of the material as expected. Strain range is another prominent variable to affect the life of a material. The number of cycles to failure decreases with strain range increases. This behavior can be observed in Figure 4-9a and Figure 4-9b. Figure 5.7a displays the effect of strain range with compressive dwells, and Figure 5.7b with a LCF condition. Specimen BR35 has number of cycles to failure is 578 cycles less than the value for specimen BR32 with the addition of 90s compressive dwell at 0.5% strain range. Number of cycles to fatigue failure for specimen BR 34 is only 169 cycles less than specimen BR17 with the addition of 90s compressive dwell at 0.7% strain range; therefore, it is concluded that as the strain range increases, the effect of any dwell is less pronounce.

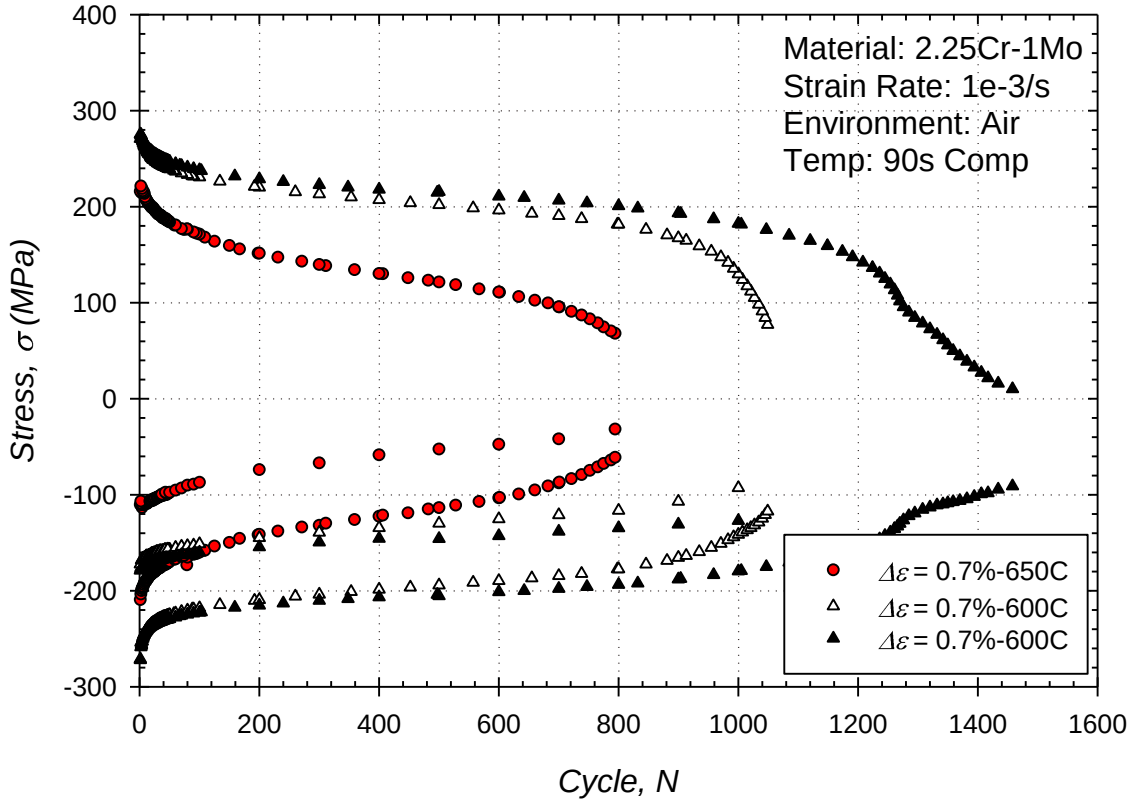

Figure 4-8: The effect of temperature demonstrated with experimental results, for all cases strain ratio, *R*, is -1.

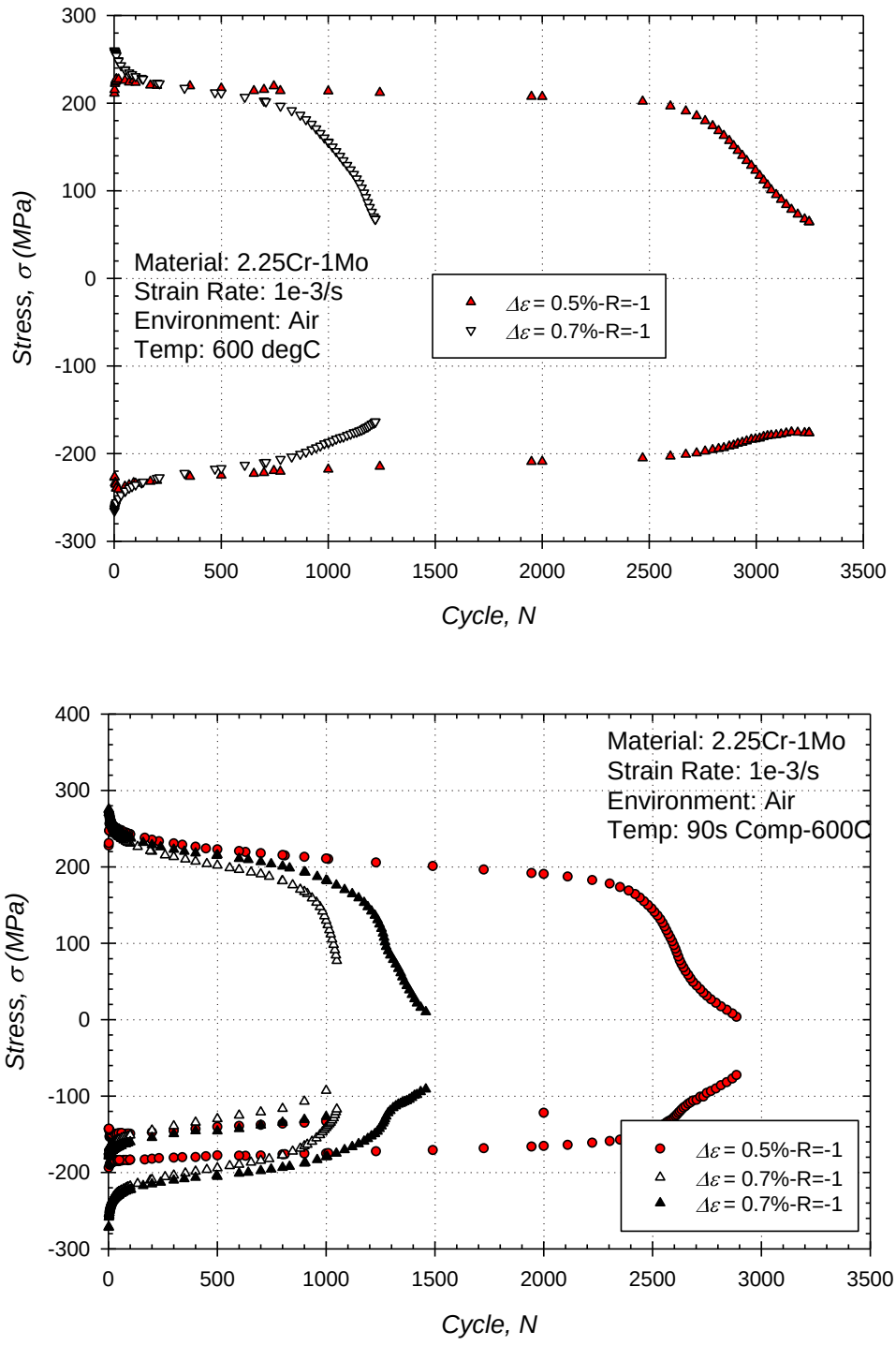

Figure 4-9: The effect of strain range for Creep-Fatigue (top) and LCF(bottom). for all cases strain ratio, *R*, is -1.

4.3 Metallurgical Analysis

Fatigue-tested specimens were analyzed visually and with two types of microscopy: white light optical (LOM) and scanning electron microscopy (SEM). The test samples were observed to display three forms dominant modes of physically-based crack initiation mechanisms. Under LCF conditions with strain rates at or above 1e-3s^{-1}, classical fatigue mechanisms are responsible for crack initiation and early propagation from the surface. Figure 4-10 displays this behavior with specimen BR34. This specimen experienced no dwell condition with 0.7% strain range at 600°C. The microscopic photography of specimen BR34 has many similarities with the demonstration of crack initiation by fatigue mechanisms.

a) b)

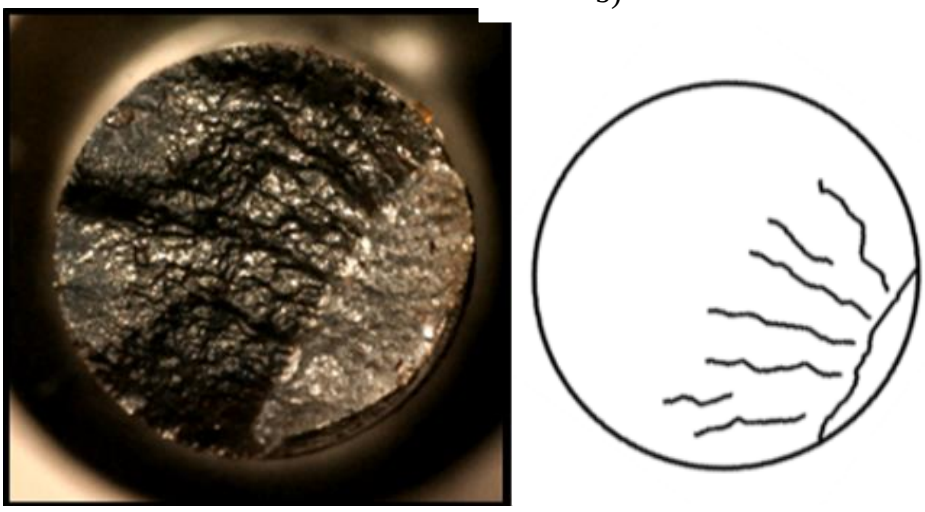

Figure 4-10: a) Microscopic image of BR34 and b) crack initiation by fatigue mechanism demonstration

When 2.25Cr-1Mo steel is subjected to long periods of compressive dwell at high temperature, oxides form at the surface. Upon cycling, these oxides crack and expose material

beneath the surface. Scanning electron microscopic image of BR17, is shown in Figure 4-10. This image was taken with a scanning electron microscope. Specimen BR17 was tested with a compressive dwell period of 90s and 0.7% strain range at 600°C. Oxide spiking is visualized in this figure. Environmental-fatigue coupled mechanism is the dominant mode of crack initiation for conditions with compressive dwell at high temperature. Additionally, this mechanism is active for thermomechanical fatigue (TMF) cases [10]. Oxide spikes starts forming upon TMF out of phase cycling.

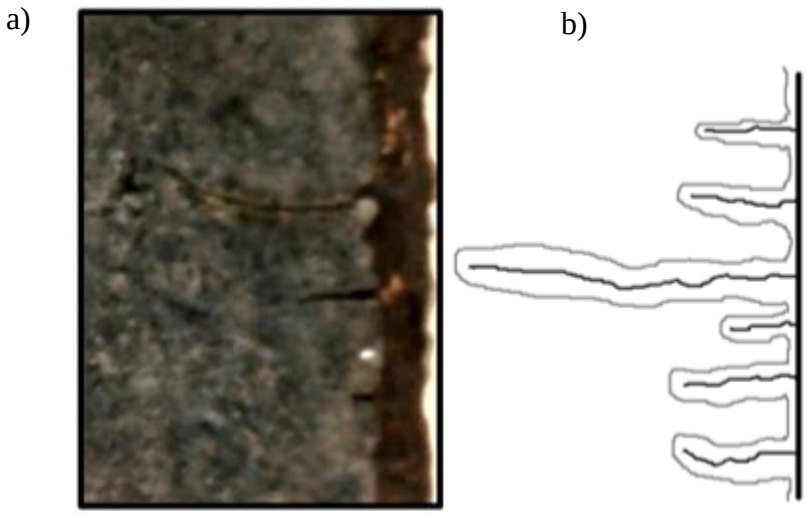

Figure 4-11: a) Microscopic image of BR17 and b) oxide spikes demonstration

If the dwell period is tensile instead of compressive, the crack initiation process proceeds with the formation of subsurface micro-pores that coalesce to form microcracks. These microcracks are shown in Figure 4-11 with the image of specimen BR15. This specimen was experimented with a tensile dwell period of 90s and 0.7% strain range at 600° C.

Microcracks are visible on the right side of the specimen, very similar to the demonstration. Observations about physically-based crack initiation mechanisms from other studies were also used to support these claims [5-13].

a) b)

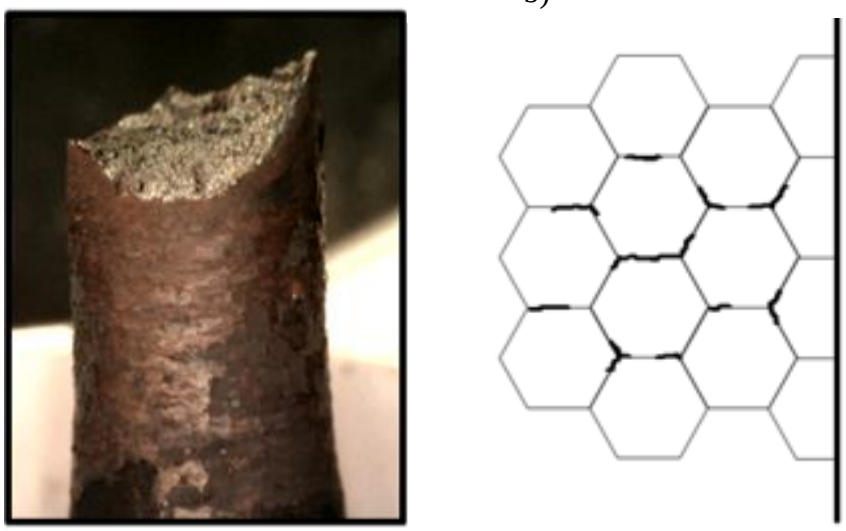

Figure 4-12: Microscopic image of BR15 and microcrack formation demonstration

CHAPTER 5 CONSTITUTIVE MODELLING

5.1 Model Review

A non-interaction (NI) method is utilized as the constitutive modeling approach for this study. The NI model decomposes inelastic strain into creep and plasticity components, such that

$$\varepsilon_{total} = \varepsilon_{el}\left(\sigma,T\right) + \varepsilon_{pl}\left(\sigma,T\right) + \varepsilon_{cr}\left(\sigma,T,t\right) \tag{5-1}$$

where ε_{total} is total strain, ε_{el} is elastic strain, ε_{pl} is time-independent plastic strain, ε_{cr} is time-dependent creep strain, σ is stress, T is temperature, and t is time. In this approach, creep and plasticity are estimated as uncoupled; however, the deformation mechanism could be connected from a microstructural perspective. Table 5-1 presents model parameters. The constitutive model is developed using a methodical progress in this study. The cyclic Ramberg-Osgood [23] model is informed by the mid-life cyclic stress-strain curves from LCF experiments.

$$\varepsilon_a = \frac{\sigma_a}{E} + \left(\frac{\sigma_a}{K'}\right)^{\frac{1}{n'}} \tag{5-2}$$

where ε_a is the strain amplitude, σ_a is the stress amplitude, E is the elastic modulus, and K' and n' are constants that shows temperature-dependence. For generating a hysteresis loop, the Masing non-linear hardening model [24] is implemented, i.e.,

$$\Delta\varepsilon = \frac{\Delta\sigma}{E} + 2\left(\frac{\Delta\sigma}{2K'}\right)^{\frac{1}{n'}} \tag{5-3}$$

for stabilized cyclic conditions, where $\Delta\varepsilon$ is the strain range, $\Delta\sigma$ is the stress range. The non-linear kinematic hardening (NLKH) model is formulated by approximating the back stress of the plastic response as a set of multiple superimposed Armstrong-Fredrick (A-F) kinematic hardening[25] models and a component for change in temperature. There are multiple A-F models that can be employed; however, two to four are common in literature [25] . The NLKH model

$$\dot{X} = \frac{2}{3}\sum_{i=1}^{3} C_i \dot{\varepsilon}^{pl} - \gamma_i X_i \dot{p} + \frac{1}{C_i}\frac{dC_i}{d\theta}\dot{\theta} X_i \tag{5-4}$$

has $\dot{X}$ is the rate of change of the back stress tensor, C_i, γ_i, and X_i are the hardening modulus, hardening modulus rate, and back stress tensor of the three superimposed A-F models, respectively, k is the initial yield stress, $\dot{\varepsilon}^{pl}$ is the plastic strain rate tensor, $\dot{p}$ is the change of the accumulated equivalent plastic strain with respect to time, θ is the temperature, and $\dot{\theta}$ is the temperature rate. In practice, the C_i terms affect the slope of the stress-strain hysteresis loop, and the γ_i terms affect the decay of the slopes, allowing for plastic memory hardening over subsequent cycles or a less rigid model.

Table 5-1: *Summary of constitutive modeling parameters*

Constant	Unit	Model	Plot Abscissa-Axis Plot Ordinate-Axis	Primary Effect
K'	MPa	Cyclic R-O	Plastic Strain (mm/mm) vs. Stress (MPa)	Height/Magnitude
n'	-			Curvature
C_i	MPa	NLKH	Plastic Strain (mm/mm) vs. Stress (MPa)	Slope of the segments
γ_i	-			Decay of the segments
k	MPa			Proportional limit
A	hr^{-1}	SSC	log Min Creep Rate (hr^{-1}) vs. log Stress (MPa)	Horizontal shift
α	MPa^{-1}			Slope
n	-			Curvature

The large number of interdependent constants required to fully characterize a material is the disadvantage of using the NLKH model; therefore, the NLKH methods makes constitutive modeling difficult and time consuming. A heuristic method is used for achieving successful optimized parameters; however, fitting techniques depend mostly on individual data sets, which may not represent the material as a whole. This is exacerbated by the flexibility of the model, where many different sets of constants can yield similar results. This shows the necessity for an automated model that is regular, repeatable, and rapid, where resulting constants derive good continuity between temperatures directly from the demonstrated mechanical response rooted in basic material models.

The permanent inelastic deformation created from thermally-driven loads is called creep. There are multiple methods for steady-state creep (SSC), including the power law model produced

by Norton [26] and the hyperbolic sine model produced by Garofalo[27]. The Garofalo method has been employed as SSC component of the NI model, as it tends to be more accurate along the model extremities where stress is very large or very small. The Garofalo model at each temperature is given by

$$\dot{\varepsilon}_{cr} = A\left[\sinh\left(\alpha\sigma\right)\right]^{n} \tag{5-5}$$

where $\dot{\varepsilon}_{cr}$ is the creep strain rate, σ is the stress, and A, α, and n are temperature-dependent material parameters. Statistical and numerical methods have been used for obtaining the constants for these creep models in literature [28]. If data are scattered, general trends with respect to temperature are used to fit the model visually. The NLKH plasticity model is integrated with this creep model to create the non-interactive constitutive model utilized in this study. A table with each material constant and the effect it produces is shown in Table 5-1. To date, observations or formulae interrelating plasticity/creep parameters to tensile properties has yet to be presented.

The constant determination process is divided into three different steps. The first step employs a slope method to find C_1, C_2, and C_3:

$$C_i = \frac{K'\left(\Delta\varepsilon_{offset,i+1}{}^{n'} - \Delta\varepsilon_{offset,i}{}^{n'}\right)}{2^{n'-1}\left(\Delta\varepsilon_{offset,i+1} - \Delta\varepsilon_{offset,i}\right)} \tag{5-6}$$

where the bounding points are defined as

$$\Delta\varepsilon_{offset,i} = \begin{bmatrix} 0.00001 & 0.0002 & 0.002 & 0.0038 \end{bmatrix} \tag{5-7}$$

The second step includes analytically approximating the *k* constant as the yield stress of the hysteresis loop where the plastic strain amplitude is very low

$$k = K'\left(0.00001\right)^{n'} \tag{5-8}$$

For approximating the linearized back stress for a set of stress range and plastic strain range points, γ_1, γ_2, and γ_3; statistical regression or analytical methods are employed in the last step, i.e.,

$$\frac{\Delta\sigma}{2} - k = \frac{C_1}{\gamma_1}\tanh(\gamma_1\frac{\Delta\varepsilon^{pl}}{2}) + \frac{C_2}{\gamma_2}\tanh(\gamma_2\frac{\Delta\varepsilon^{pl}}{2}) + \frac{C_3}{\gamma_3}\tanh(\gamma_3\frac{\Delta\varepsilon^{pl}}{2}) \tag{5-9}$$

The stress ranges are only obtained utilizing plastic strain range values of 0.05% through 0.1% in increments of 0.01%, and 0.2% though 0.5% in increments of 0.1% because excessive amount of simulated data at the lower and upper plastic strain ranges was decreasing the quality of the fit. Least squares regression is employed to fit the γ constants.

The Garofalo creep model is regressed for each temperature like the elastic and plastic parts of the NI model. Common regression methods are utilized for calculating the three Garofalo parameters using creep deformation data, where the creep rate is obtained by taking the inverse of rupture time. The creep response is strongly affected by the peak stress at slow strain rates; thusly,

it is essential to fit the plasticity constants to data tested at relatively fast strain rates

Power law relations are developed to estimate each constant as a function of temperature, after the A, α, and n constants have been obtained for each temperature. Though α is relatively fixed, the remaining two constants have a degree of flexibility that can be exploited to help produce inclusive power law relations. A full description of the approach is provided for other alloys in prior works [18-22].

5.2 Model Application and Performance

A finite-element code was constructed to estimate the deformation of the material for a unit cell under many different loading conditions using the non-interaction model. ANSYS Mechanical APDL 17.2 was utilized to execute this finite element code on a single Solid185 element. The Solid185 element is an 8-noded cubic element. For applying axial strain, a displacement control method is used on the cubic element which has side lengths of 1mm. For allowing expansion or contraction, all the faces and degrees of freedoms were unconstrained except three mutually orthogonal faces of the cube were fixed from movement normal to the face. Each load step having a peak-to-valley part of the loading was designated a transient solver. It was decided to have the software automatically choose how many sub-steps to use for each load-step, but having restrictions of a minimum of 30 sub-steps and a maximum of 100 sub-steps at each load step. Calculated axial stresses and strains along the loading direction were extracted to an Excel file for to be used in the life prediction model and analysis.

The comparison between the NLKH hardening and cyclically stable mid-life stress-strain points is represented in Figure 5-1. This figure includes variety of temperatures but only one strain rate. Open-source LCF databases were used to retrieve this data for 2.2Cr-1Mo. It is observed that both the Young's modulus and the strength of the material decrease, when temperature increases. The SSC model has been compared with published data in Figure 5-2. This data is derived from NIMS [7] and Parker [29]. The comparison shows that a well-fitting SSC model estimates the effects of creep up to 650°C. Strain rates faster than 10^{-3} s^{-1}shows a little difference between each strain rate in the figure; thusly, it was decided to run LCF testing at this rate for reducing the effects of creep when collecting the data needed to fit K' and n' for this material.

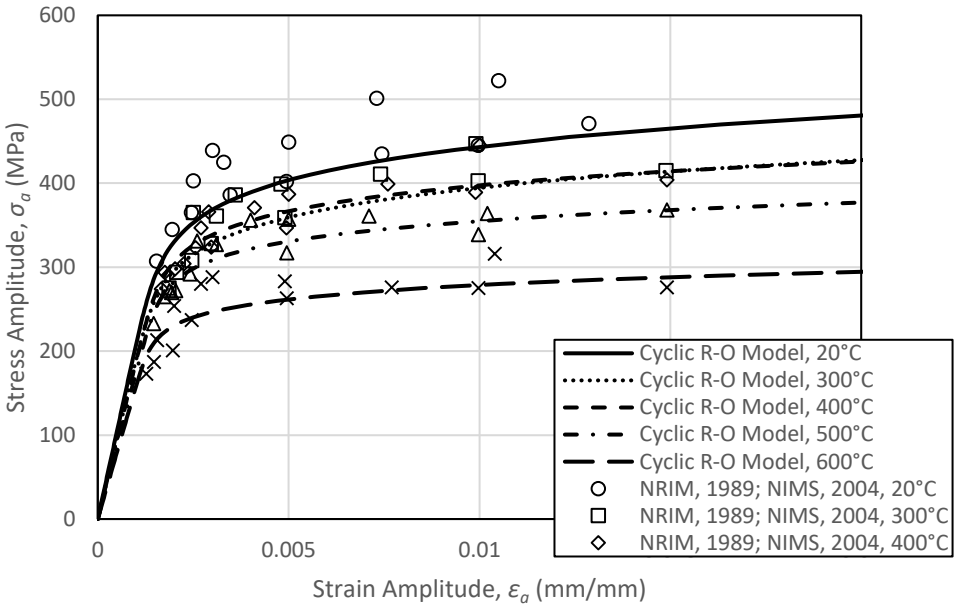

Figure 5-1. Cyclic Ramberg-Osgood models.

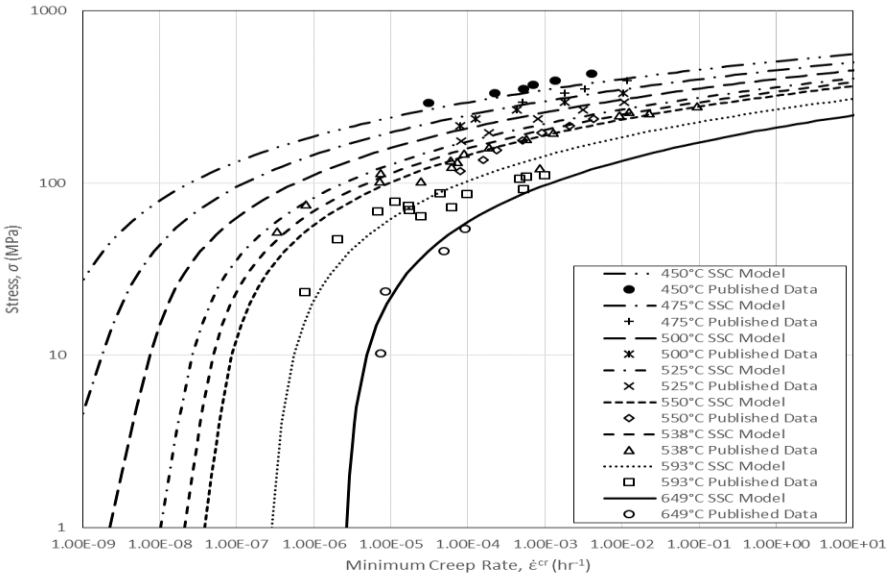

Figure 5-2. Comparison of Garofalo models.

a)

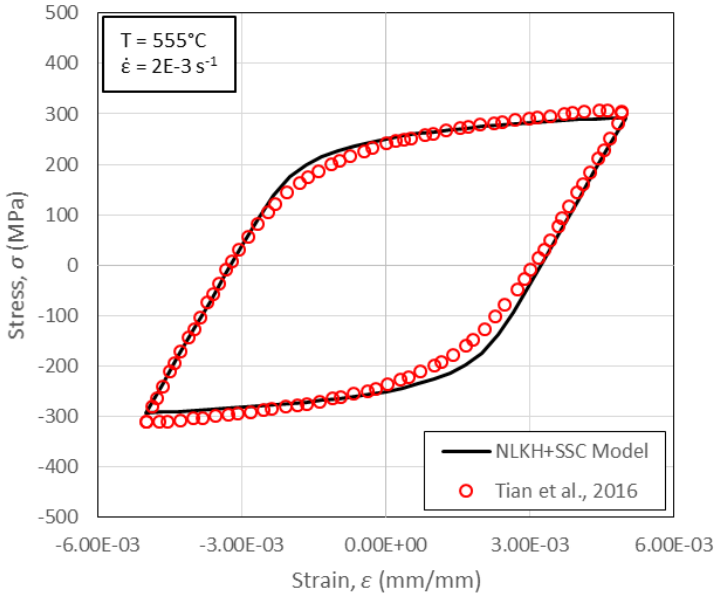

b)

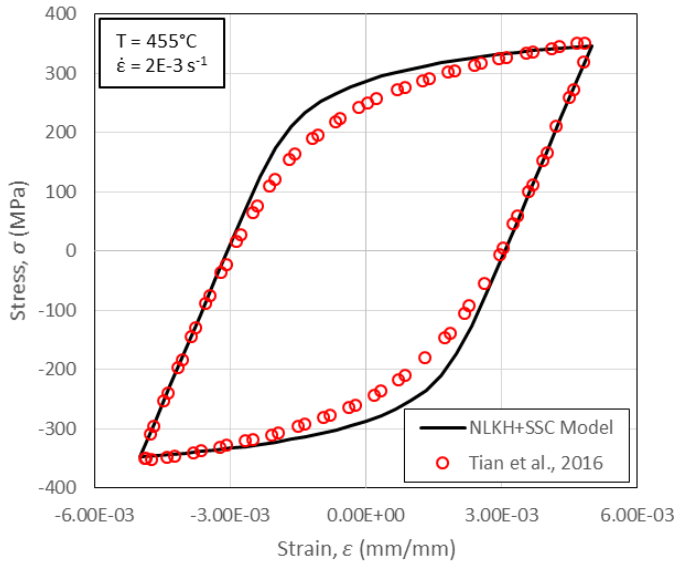

Figure 5-3. Comparison of constitutive model and experimental data for 2.25Cr-1Mo under LCF conditions at: (a) 555°C and (b) 455°C.

5.2.1 Low Cycle Fatigue

The fully-formulated NLKH+SSC NI model is compared with the low-cycle fatigue (LCF) experimental data from Tian [10]. Figure 5-3 represents the simulated hysteresis loops for 455°C and 555°C with the experimental data. The comparison displays that the NLKH+SSC model approximates a similar amount of plastic strain. When the NI model is exposed to multiple cycles, it keeps the overlapping curvature which is common for hysteresis loops. The model shows very similar hysteresis loops for both temperatures, where plasticity of the deformation is simulated well. Additionally, the loading conditions from NIMS were simulated to match the stress ranges [7]. The peak and valley stresses are accurately estimated by the model which is represented in Figure 5-4. For having better validation, the model was also subjected to a large variety of temperatures, strain ranges, and strain rates identical to accessible literature data. Figure 5-5 shows the simulated stress amplitudes compared against the experimental stress amplitudes for various temperatures and strain rates. Results display that the R^2 fitting value is 0.918 for the NLKH+SSC NI model. Coefficient of determination, R^2, is a statistical value, commonly used for to measure how close the data are to the fitted regression line.

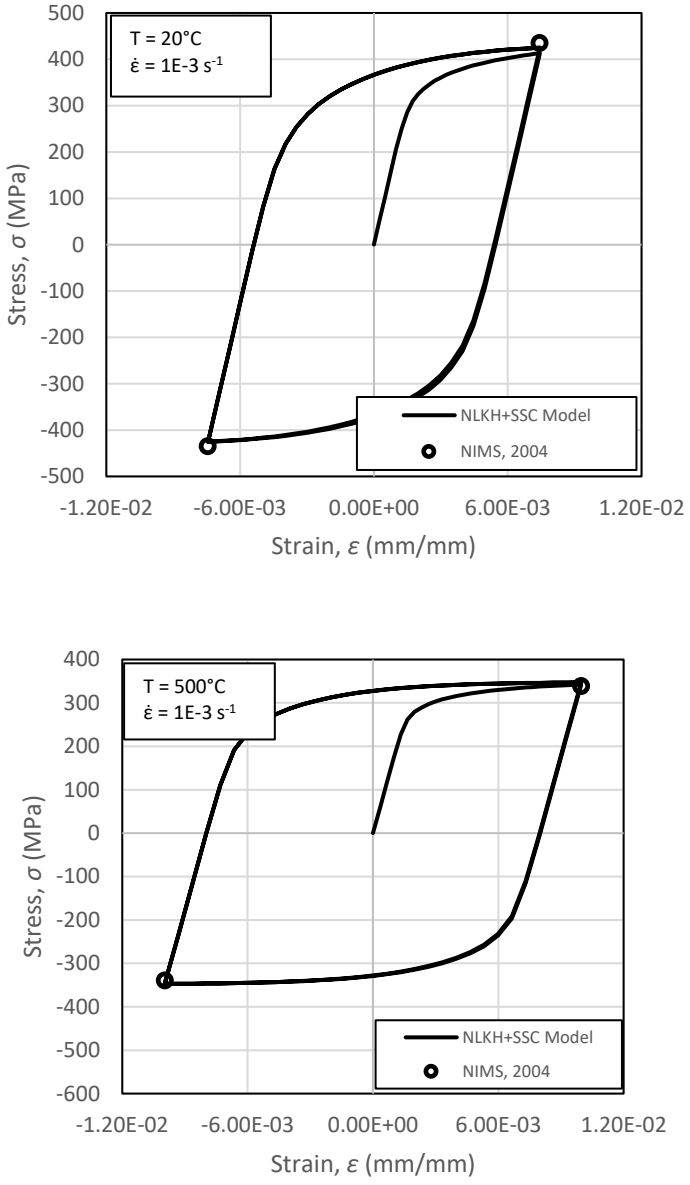

Figure 5-4. Simulated NLKH+SSC hysteresis loops compared with experimental results for isothermal conditions at 20°C and 500°C.

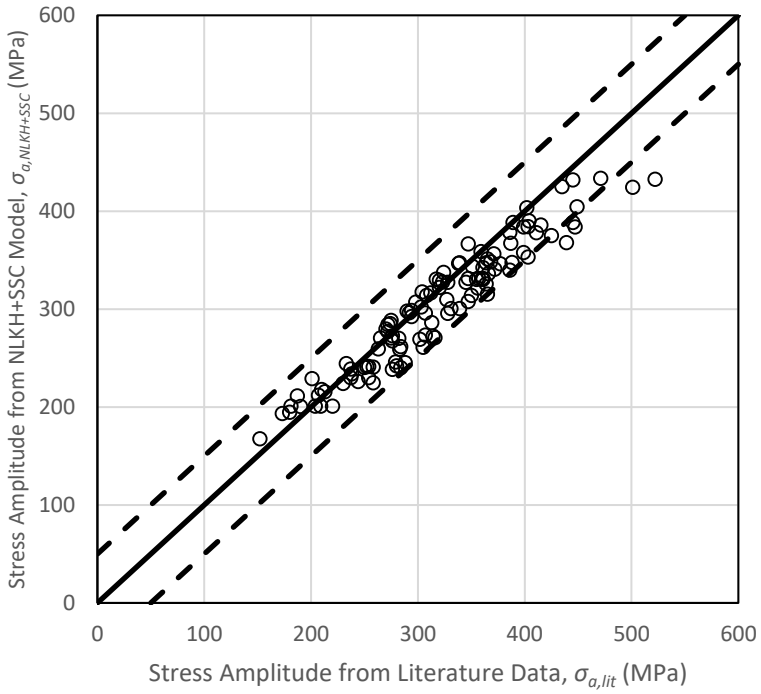

Figure 5-5. Comparison of stress amplitude from literature data (Science 2004) (Metals 1989) and simulated data using the NLKH+SSC model. Upper and lower reference lines of ±50 MPa are also plotted.

5.2.2 Creep-Fatigue

The model was also simulated with creep-fatigue conditions to compare with the literature data containing tensile dwells. Literature data include stress amplitude, strain amplitude, maximum stress, and relaxed stress which are presented with the finite element simulated data in Figure 5-6. The NI model accurately approximates the maximum stress and relaxed stress for the first cycle when it is compared with the literature data.

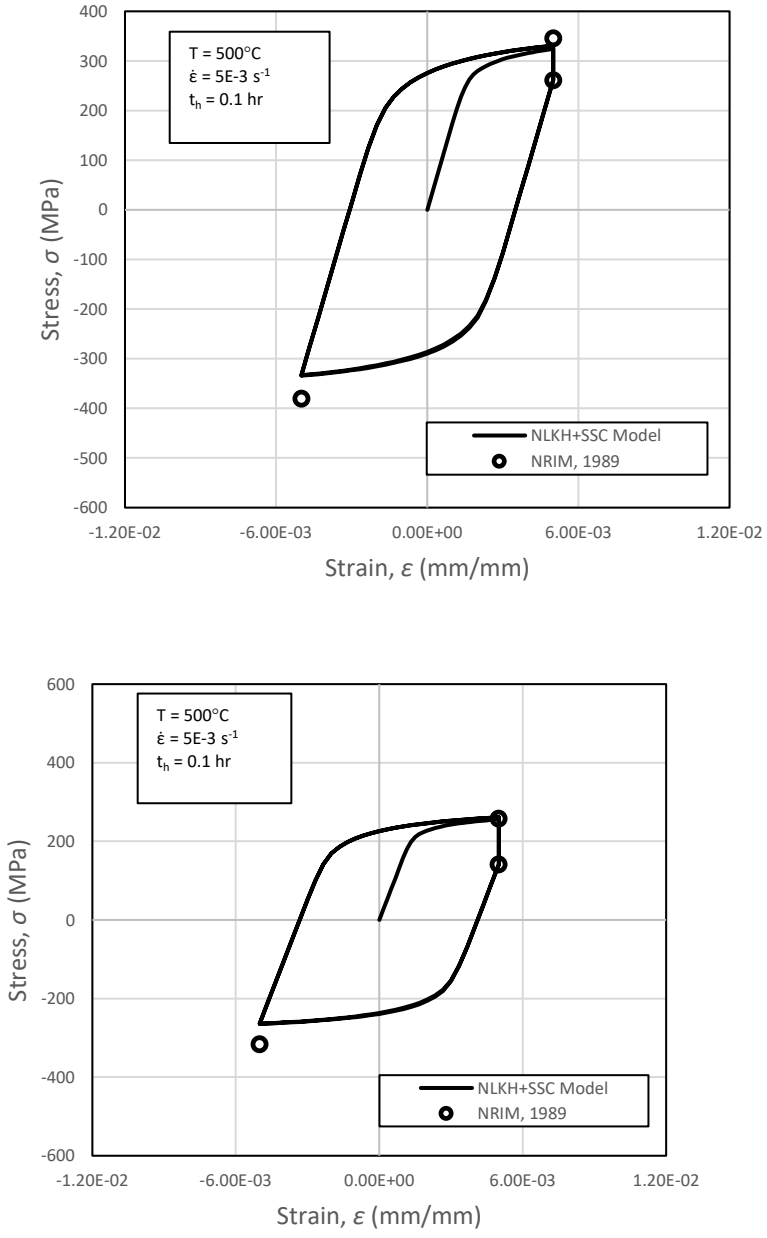

Figure 5-6. NLKH+SSC model predictions with NRIM experimental maximum, minimum, and relaxed stress values for creep-fatigue with 0.1 hr dwells for Δε=1% at (a) 500°C and (b) 500°C

5.2.3 Thermomechanical Fatigue

As previously described, 2.25Cr-1Mo is commonly used for hot components. Those structures generally experience thermal cycling with mechanical loading; therefore, the non-interaction model needs to accurately estimate the non-isothermal material response. Hysteresis loops were simulated with the material subjected to non-isothermal conditions. The constitutive model is compared with the experimental data from Iwasaki in Figure 5-7. Results indicate that the model correctly simulates the non-isothermal deformation for this material. The model calculates the important values for the fatigue life models, such as the mean stress, strain range, and stress range, with high accuracy.

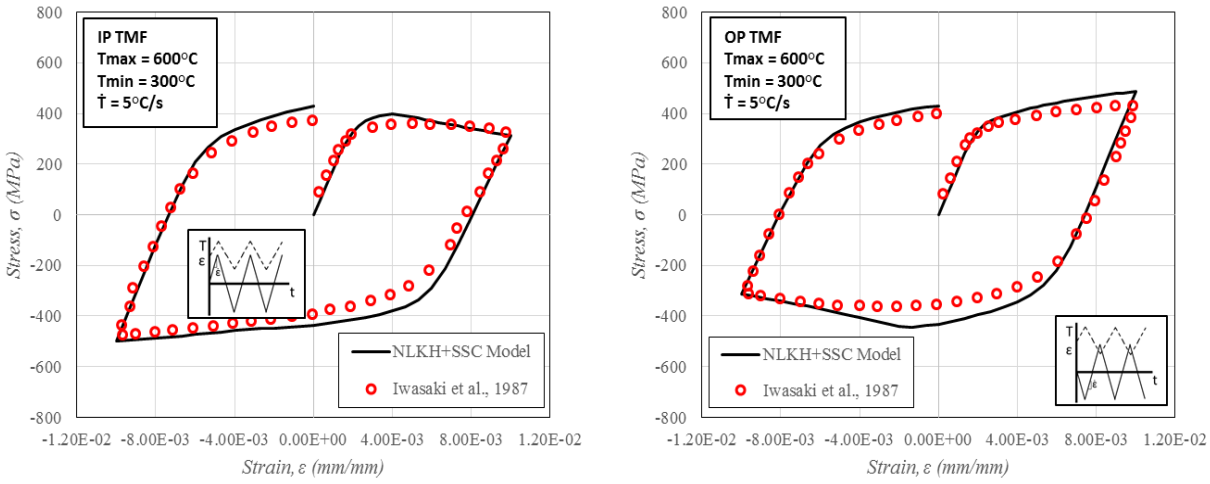

Figure 5-7. Non-isothermal response and modeling of 2.25Cr-1Mo under (left) in-phase and (right) out-of-phase conditions.

5.3 Model Predictions

Parameters that inform fatigue life models, such as the mean stress, inelastic strain range, and stress range, are predicted by the deformation model; thusly, it is important to predict the deformation of the material accurately for developing a good fatigue life approach. The accuracy of the model is shown in Section 5.2 of this chapter. The constitutive modeling approach was exercised under a variety of conditions to analyze the effect of different variables in this section.

5.3.1 Effect of Temperature, Strain Rate and Strain Ratio

Temperature is one of the most effective variables for deformation of a material. 2.25 Cr-1Mo, a low alloy steel, material frequently experiences high temperatures, such as 550°C and 600°C. Thusly, most of the experimental data presented earlier is at these high temperatures. This material is also used at lower temperatures during start-up of turbomachinery components. The model is performed under variety of temperatures, shown in Figure 5-8. Strain range of these simulations are 0.7%, also strain rate is 1e-3 per second. There are three deformation responses plotted with temperatures 20°C, 450°C and 650°C with no dwell period. As expected, stress range is the highest for the condition at 20°C. Difference between stress ranges for cases at 20°C and 450°C is approximately 90 MPa. This number increases when deformation responses for cases at 450°C and 650°C are compared. This behavior is visualized in the figure. The reason for this drop-in stress range is plasticity. Plasticity becomes more prominent after 450°C for this material

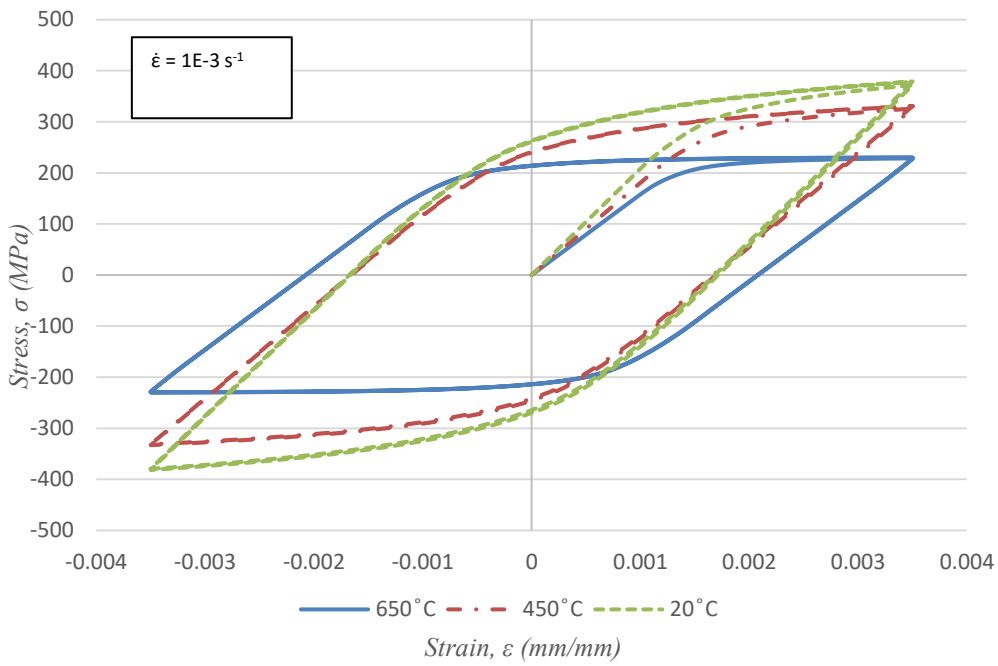

Figure 5-8. Effect of different temperatures on deformation response.

After simulating conditions with different temperatures, it was decided to analyze the effect of strain rate on the deformation of 2.25 Cr-1Mo material. The constitutive model was compared with the data from Tian with strain rate 2e-3 per second in section 5.2. The components for turbomachinery are used under various conditions; consequentially, the model is used to produce deformations responses with three different strain rates. Figure 5-9 shows three hysteresis curves with strain range 0.6%, at 650°C with no well period. Each curve represents a different strain rate; 1e-3 s^-1, 1e-4 s^-1 and 1e-5 s^-1. When the condition is slower, which means lower strain rate, the stress range is lower as well; therefore, it is expected to have a shorter life for conditions with slower strain rates. Unlike for different temperatures, difference in stress ranges does not seem to be changing for cases with different strain rates.

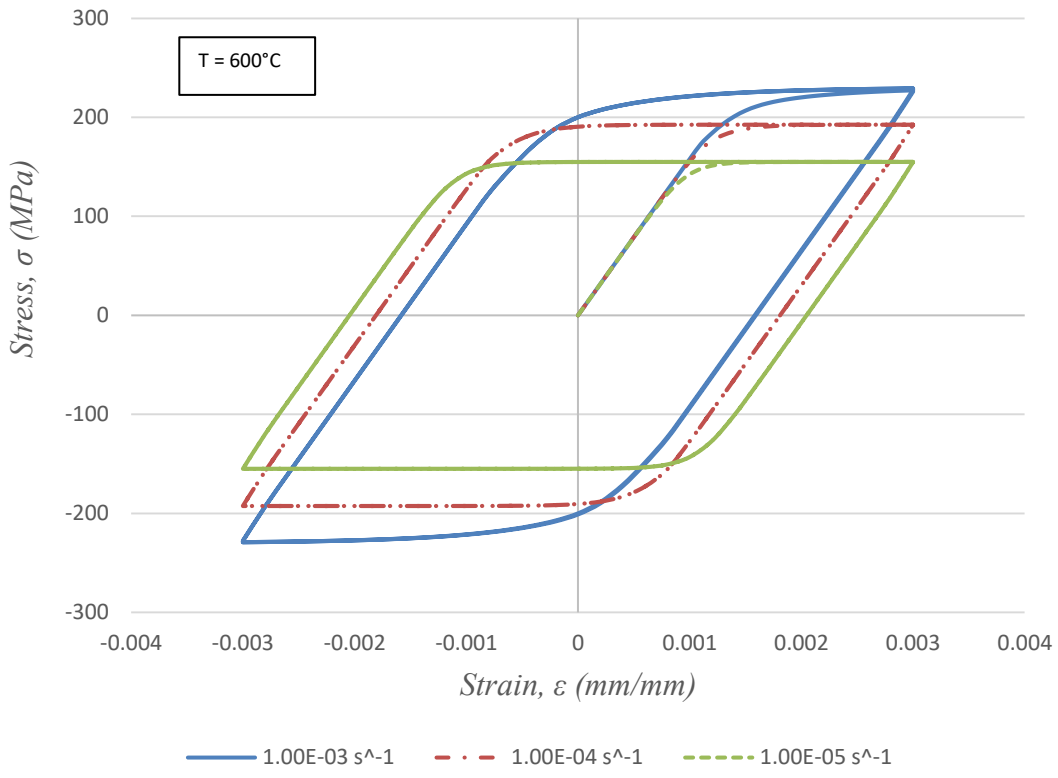

Figure 5-9. Effect of different strain rates on deformation response.

Lastly, the model is utilized to simulate conditions with different strain ratios, *R*. All the deformation and lifing data available for 2.25 Cr-1Mo material is in fully-reversed conditions. The fatigue test matrix, presented in Section 3.3, included a condition with strain ratio negative infinity to understand the effect of strain ratios; therefore, it is important to demonstrate the capability of simulating conditions other than fully reversed. Figure 5-10 presents hysteresis loops with strain range 0.5% and strain rate 1e-3 per second at 600°C for visualizing different strain ratios. As expected, stress ranges are same for each case because strain ratio does not affect the stress history.

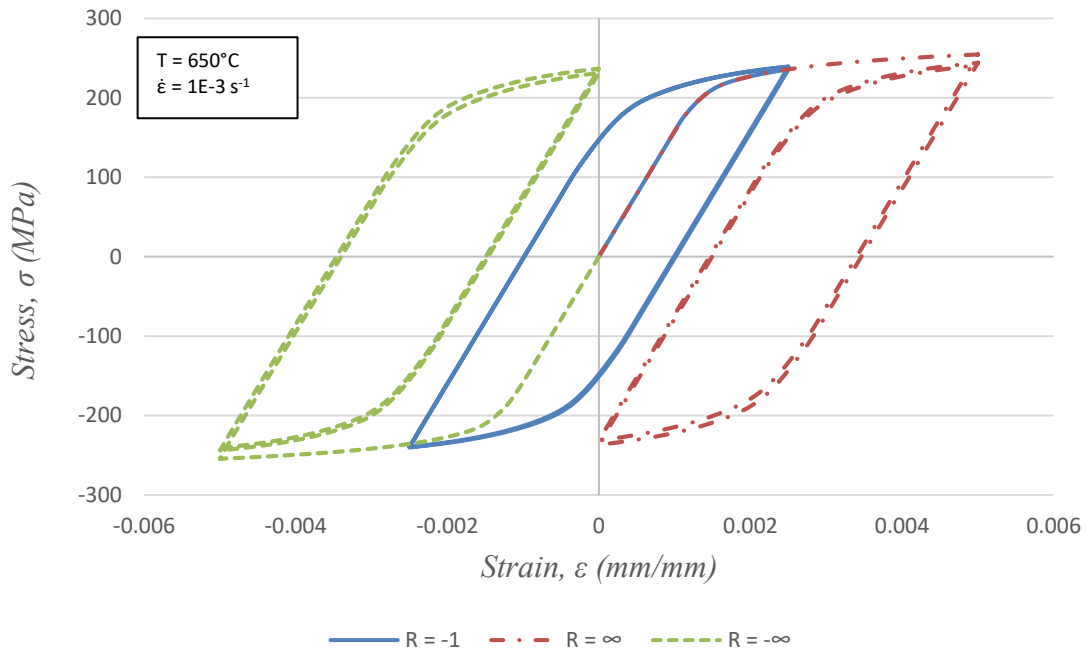

Figure 5-10. Effect of different strain ratios on deformation response.

5.3.2 Effect of Dwell Period and Dwell Type

Turbomachinery components experience very long dwell periods with their usage conditions. Main purpose of this study is to develop a life prediction approach that can simulate service like conditions for 2.25 Cr-1Mo material; thusly, the constitutive model needs to be able to simulate dwell periods with different hold times and hold types. Figure 5-11 shows deformation response of this material under variety of dwell periods. These hysteresis curves are with strain range 0.4% and strain rate 1e-3 per second at 650°C. Similar conditions are needed for capturing the effect of creep damage with the life prediction model. An LCF case is compared with 600s and 6000s tensile dwell periods in the figure.

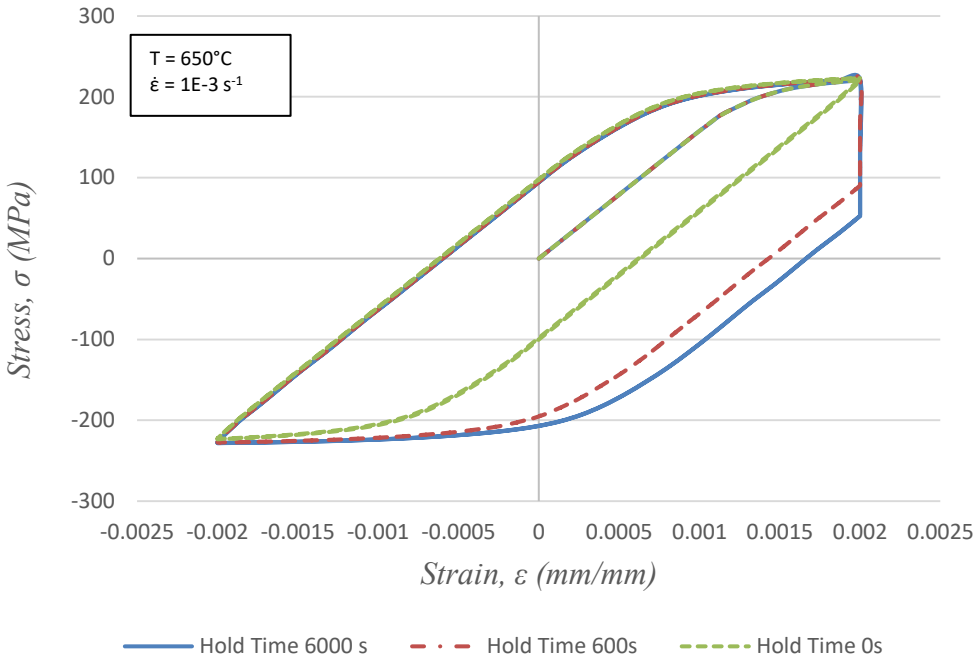

Figure 5-11. Effect of different dwell times on deformation response.

Hold time is very effective on deforming the material, but dwell type can make a difference in life-span of structures as well. As explained in Chapter 2, most of the data available with dwell periods are in tension. Thusly, multiple experiments were conducted with compressive hold times to overcome this knowledge gap for 2.25 Cr-1Mo material. Simulating fatigue life for these cases with dwell in compression, the constitutive model needs to be able to provide deformation response not just with tensile dwells. Hysteresis loops are simulated with both dwell types in Figure 5-12. Conditions are as follows; strain range 0.4%, strain rate 1e-4 per second, and temperature is 650°C. As expected, the loops are symmetric, so stress ranges are identical for both dwell types.

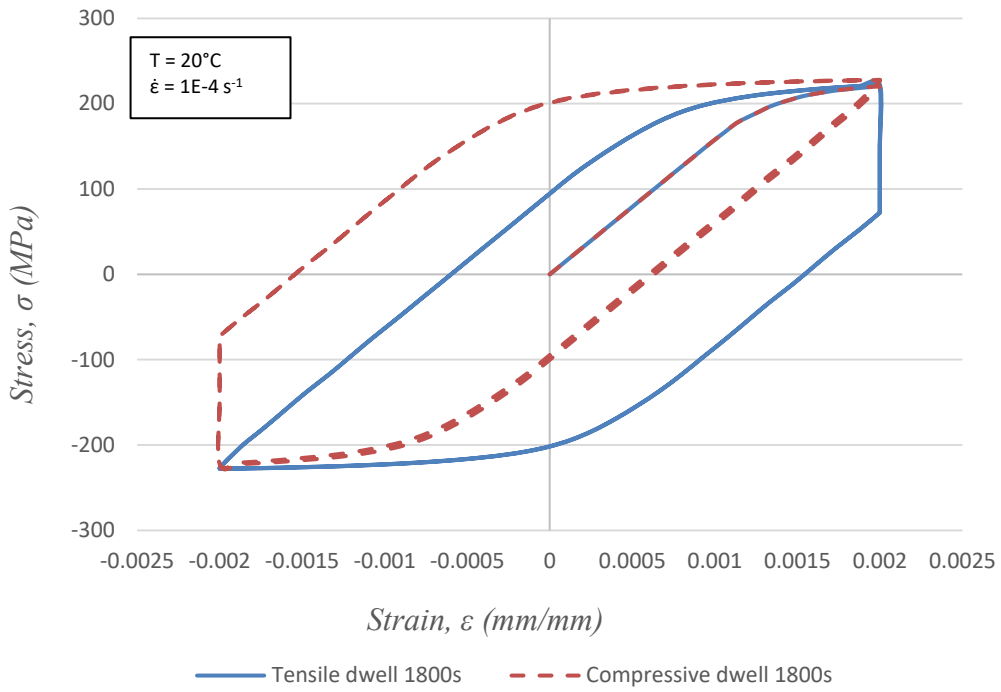

Figure 5-12. Effect of different dwell types on deformation response.

5.3.3 Effect of Maximum Temperature and Phasing for TMF cases

After performing various simulations with different dwell periods and types, the constitutive model is utilized to obtain deformation response for TMF cases with dissimilar maximum temperatures and phasing. Even though there were not any experiments with TMF cases in this study, the deformation response is needed to compare predicted life with literature data for these conditions. Figure 5-13 displays two hysteresis loops with different phasing. Blue curve represents out-phase cycling, while orange curve is for in-phase cycling. Temperature cycles between 450°C and 650°C for both cases with strain range 0.4% and strain rate 1e-3 per second.

The curves are opposite of each other. Out-phase case has the peak stress in tensile direction, while the peak stress is in compression for in-phase cycling.

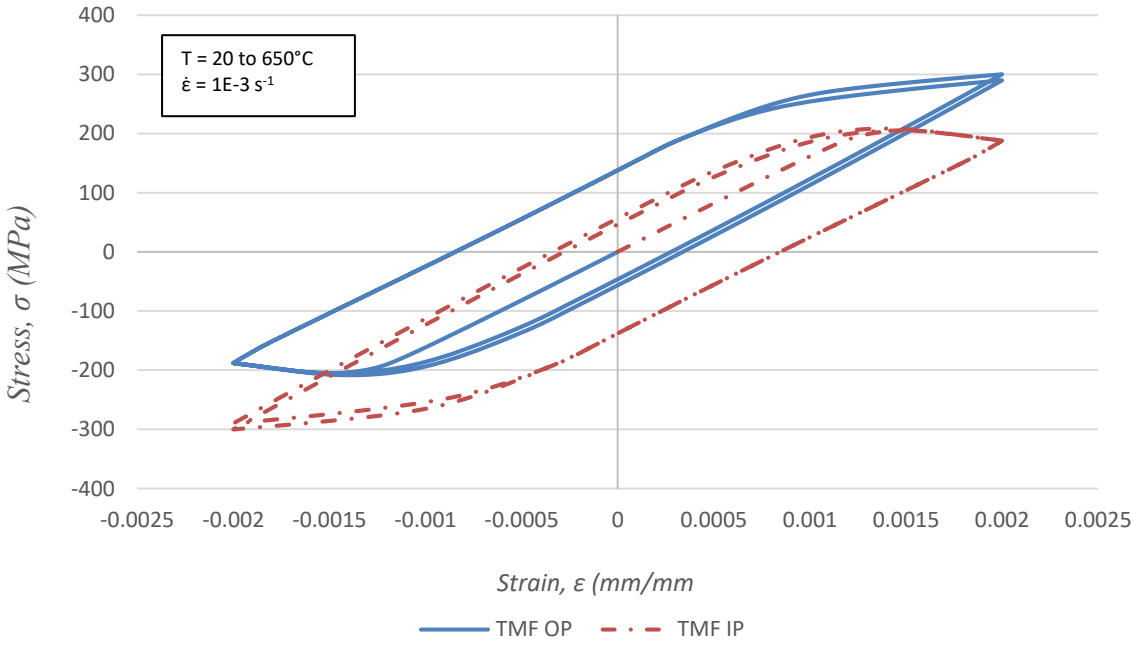

Figure 5-13. Effect of phasing on deformation response.

Additionally, the constitutive model is used to run TMF cases with cycling up to various temperatures. Deformation responses with different maximum temperatures are presented in Figure 5-14. Curve with solid line is for the case with thermal cycling from 20°C to 650°C, while the other curve has 20°C to 450°C thermal loading. Strain range and strain rate are 0.5% and 1e-4 per second for both cases, respectively. Also, mechanical loading is full reversed while both cases have out-phase thermal cycling. Maximum stress in tension for both curves are almost same; however, difference between maximum compressive stresses is approximately 123 MPa. Reason

for this behavior is maximum temperatures occur in compressive region for these cases. Thusly, higher maximum temperature, solid line curve, has a smaller peak stress in compression.

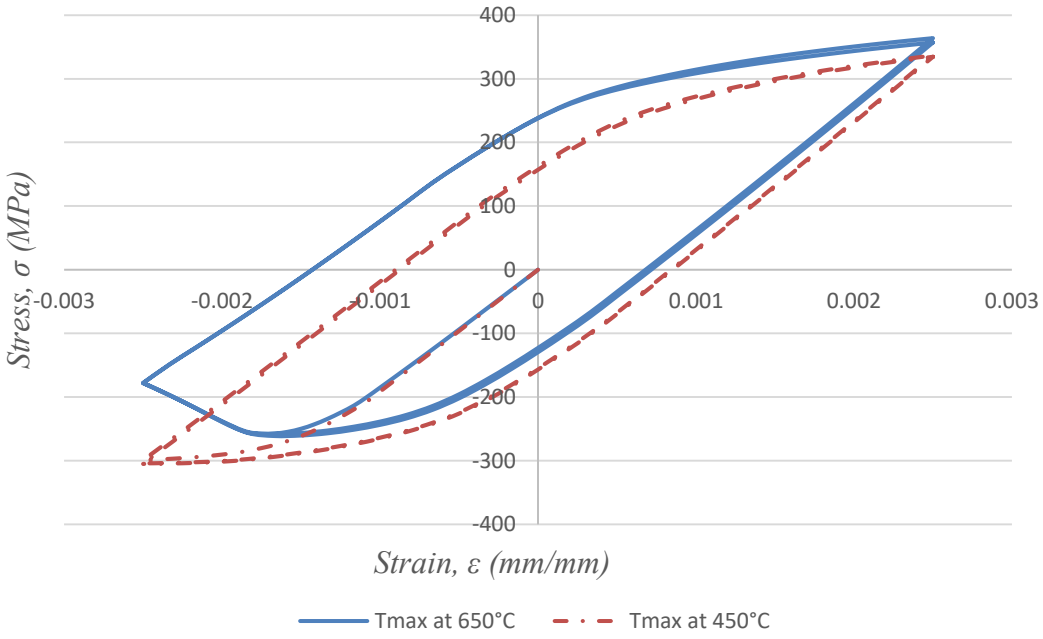

Figure 5-14. Effect of maximum temperatures on deformation response.

CHAPTER 6 LIFE PREDICTION MODELLING

The focus of this chapter is to develop a life prediction model for 2.25Cr-1Mo material. There are multiple life prediction approaches have been constructed for materials experiencing complex environments. The Palmgren-Miner rule, better known as Miner's rule, is used in this study as the fundamental method to combine damage mechanisms. Flexibility and the accuracy of this model make it more favorable over other approaches, such as dominant damage method where the most dominant damage mechanisms number of cycles to failure value is taken as the total number of cycles to failure. This cumulative damage approach is well-suited for structures experiencing variety of mechanical loadings with thermal cycling. Total damage, D_{total}, acquired by multiple damage modules is shown as

$$D_{total} = \frac{1}{N_i^{(fat)}} + \frac{1}{N_i^{(cr)}} + \frac{1}{N_i^{(env)}} \tag{6-1}$$

In this expression, the total damage is comprised of prominent modules: (*fat*), creep (*cr*), and coupled environmental fatigue (*env* or *ox*). Here, N_i is defined as the number of cycles to a fatigue crack initiation by means of a respective module; therefore, number of cycles associated with crack initiation under combined loading is obtained by taking the reciprocal of total damage, D_{total} .

6.1 Fatigue Module

The primary mechanism of crack initiation and early propagation of a material subjected to cyclic loading is termed as "fatigue." Fatigue (fat) damage progresses in metals by way of dislocation generation on preferentially-oriented grains leading to persistent slip bands facilitating intrusion and extrusion development and ultimately a Stage I crack. While both stress- and energy-life methods have been developed extensively to predict the onset of fatigue cracks, the former approach is most appropriate for high cycle fatigue (HCF) conditions and energy methods have yet to be progressed for multiaxial states of the strain/strain. The total strain approach, which merges contributions from Coffin, Manson, Basquin, and Haford, excels at life prediction for both low cycle fatigue (LCF) and high cycle fatigue (HCF) conditions, i.e.,

$$\frac{\Delta\varepsilon_{mech}}{2} = \frac{\left(\sigma'_f - \sigma_m\right)}{E}\left(2N_i^{(fat)}\right)^b + \varepsilon'_f\left(\frac{\sigma'_f - \sigma_m}{\sigma'_f}\right)^{\frac{c}{b}}\left(2N_i^{(fat)}\right)^c \tag{6-2}$$

The mechanical strain range, $\Delta\varepsilon_{mech}$, is correlated with the fatigue life, N_i, via a collection of constants and the mean stress, σ_m. Here σ'_f and b are the fatigue strength coefficient and exponent, respectively, ε'_f and c are the fatigue ductility coefficient and exponent, respectively, and E is Young's Modulus. A typical strain-life curve is shown in Figure 6-1. Both data from the present study and those harvested elsewhere agree with the model. There is plenty of LCF data available for 2.25 Cr-1Mo material.

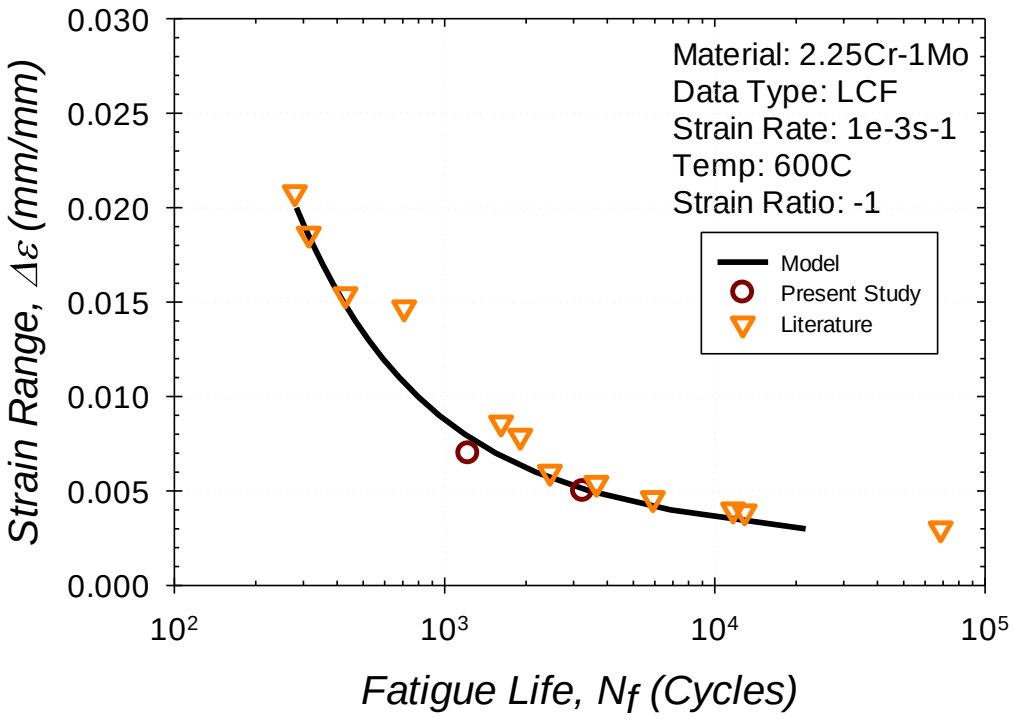

Figure 6-1. Performance of the fatigue module on the LCF response of 2.25Cr-1Mo.

Fatigue is the most dominant damage mode for isothermal cases without dwell periods; therefore, number of cycles to failure values can be accurately obtained using the fatigue module alone for these cases. Comparison of predicted fatigue life and experimental data are presented in Figure 6-2. Experimental data from other sources is shown in blue dots, and the data from this study is in green dots. Dotted lines represent the values between factor of 2, and light grey dotted lines are for the values between factor of 10. For fatigue experiments, it is expected to have difference in factor of 2 even for repeated cases. This behavior was shown in Chapter 5 of this study. Thusly, the values between black dotted lines represent accurate predictions. There are few data points out of this region because those values are for cases with very low strain ranges where

the creep damage starts to become more dominant.

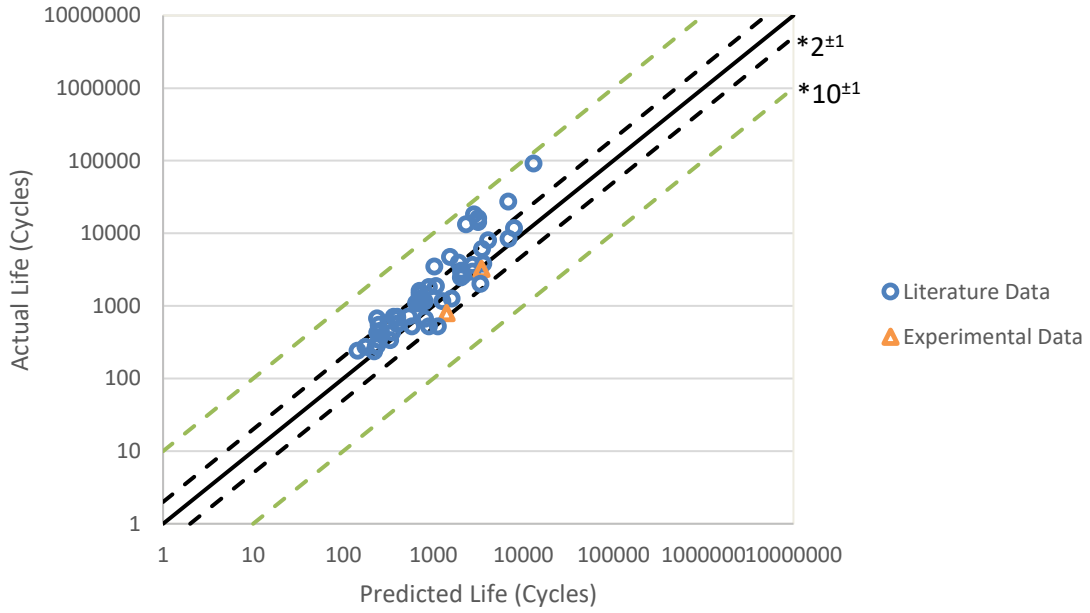

Figure 6-2. Actual versus predicted fatigue life plot for LCF cases

6.2 Creep Module

The Robinson Rule [30] for creep life fractioning is a variant of the Miner rule. It decomposes a representative cycle into a series of time increments (m) over which stress and temperature can be approximated as constant, i.e.,

$$\frac{1}{N_i^{(cr)}} = \sum_{i=1}^{m} \frac{t_c^{(\sigma_i, T_i)}}{t_r^{(\sigma_i, T_i)}} \tag{6-3}$$

Here the numerator in the creep damage fraction, t_c, is the time duration spent at a given combination of stress and temperature. The term that appears in the denominator corresponds to the rupture time of the material if it were only subjected to the given stress, σ_i, and temperature, T_i, for its full life. A general expression can be developed based on the Larson-Miller parameter to explicitly express rupture time in terms of stress and temperature, i.e.,

$$\log_{10} t_r = C_{GB} + \left(a_i + \frac{T}{T_m} \right)^{-q} \sum_{j=0}^{3} b_j \log_{10} \left(\frac{\langle \sigma \rangle + 1}{\sigma_{MUTS,RT}} \right)^j \tag{6-4}$$

where C_{GB}, q, a_i, and b_j are regression constants that allow rupture time to achieve the best fit where constant stress and constant temperature data exist at various levels, as shown in Figure 6-3.

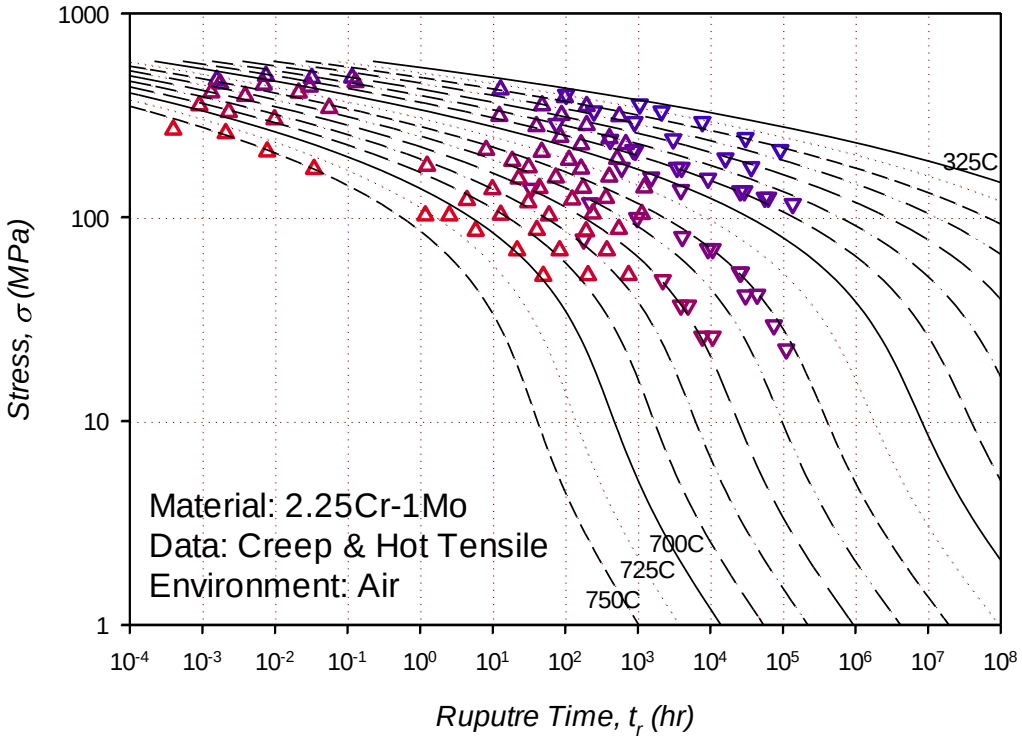

Figure 6-3. Rupture correlation for 2.25Cr-1Mo under tensile creep across a range of temperatures.

A key assumption in this creep-damage formulation is that the creep is uncoupled. Parameters for Eqs. (6-3) and (6-4) are determine independently. Damage due to creep-fatigue interaction is, thusly, accepted as negligible. This is a plausible assumption since the microstructural mechanisms associated with fatigue damage (surface-initiated) and creep damage (sub-surface grain boundaries) are nominally distinct.

Experimental data from this study and other sources having dwell periods are compared with the predicted cumulative life of fatigue and creep modules, shown in Figure 6-4. This plot is very similar to Figure 6-2, presented earlier in this chapter. The data is comprised of dwell periods ranging from 60 seconds to an hour. Also, these experiments are conducted at 550°C or 600°C,

where creep becomes more prominent. There were less data points available in the literature with dwell periods in contrast with LCF cases; in consequential, this study presents more experimental values for creep-fatigue conditions, especially for dwell in compression. The model predicts life of 2.25 Cr-1Mo material very accurately when the fatigue and creep modules are combined for these cases. All the data points are in the ideal region except one.

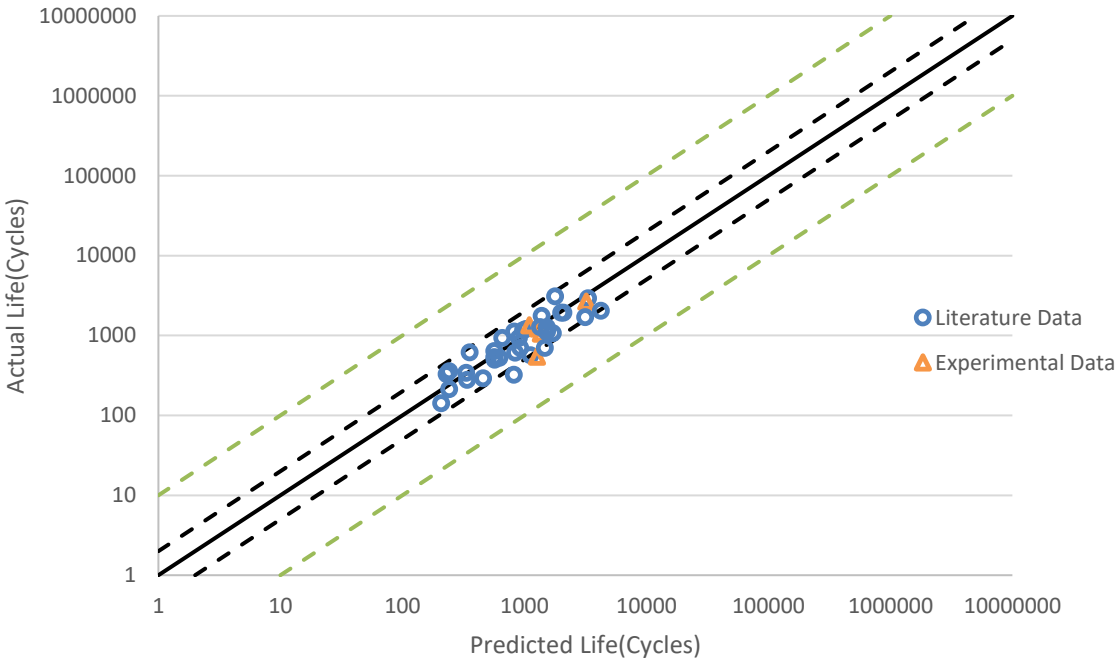

Figure 6-4. Actual life versus cumulative life for creep-fatigue conditions.

6.3 Environmental-Fatigue Module

The coupled environmental-fatigue term (env or ox) captures a distinct microstructural mechanism. Crack initiation and early propagation in this module is based on microcrack nucleation and growth through an oxide layer at free surfaces of the material. On the microstructural level, oxides formed at the surface at elevated temperatures will crack under specific conditions. Exposure of virgin material at the tip of the newly-formed crack will oxidize, and the process repeats. This process corresponds to cyclic brittle crack growth, and is depicted. Environmental-fatigue (env) damage has been shown to dominate under nominally two situations: (a) non-isothermal, out-of-phase loading and (b) creep-fatigue with compressive dwells at high temperature. A signature of oxidation damage is that the process is strongly dependent on time. There must be enough service time to allow for oxidation to occur. For instance, if the mechanical strain range is dominated by cyclic plasticity, then "fatigue" damage will dominate; consequently, environmental-fatigue damage operates in the HCF regime. The expression for cycles to crack initiation is given by

$$N_i^{(env)} = B\left(\frac{K_{env}}{\bar{K}_{env}}\right)^{m_1} \left(\Delta\varepsilon_{mech}\right)^{m_2} f\left(\Phi_{env}, \Phi_{dwell}\right)^{m_3} \tag{6-5}$$

Here B, m_1, m_2, m_3, are constants that initialized analytically and optimized through regression. The first term of the expression bears strong resemblance to common fatigue crack growth expressions. The factors K_{env} is purely a parabolic oxidation constant determined from stress-free

diffusion experiments and is its normalization constant. The diffusion expression follows classical Arrhenius diffusivity theory and integration is required to approximate its value under non-isothermal conditions.

The cycle factors, Φ_{dwell} and Φ_{env}, help the expression to adjust for attributes of the thermal and mechanical cycling profile exhibited in service. The dwell factor uses times t_{closed} (the duration of time that the material spends in compression measured in units of hours) and t_{cc}, i.e.,

$$\Phi_{dwell} \equiv \exp\left[-\frac{1}{2}\left(\frac{\dfrac{t_{closed}}{t_{closed}+t_{cc}}-1}{\xi_{dwell}}\right)^2\right] \tag{6-6}$$

The dimensionless time ratio appearing in the numerator is valued between 0 and 1. For long dwell periods in compression the ratio converges to 1; however, under continuous cycling at completely reversed conditions, the ratio is approximately 0.3. For long dwell periods in tension, creep is expected to be the dominant damage mode, and the time ratio converges to 0. In this manner, the cycle factor adjusts for various loading profiles. The influence of the time ratio is shown in Figure 6-6a. Here ξ_{dwell} is a regression constant that helps to control the sharpness of the difference in life oxidation damage under long compressive dwell and continuous cycling conditions.

Similarly, Φ_{env} accounts for phase differences between the thermal and the mechanical cycle. The formulation uses mechanical and thermal strain rates, i.e.,

$$\Phi_{env} \equiv \frac{1}{t_{cc}} \int_0^{t_{cc}} \exp\left[-\frac{1}{2} \left(\frac{\frac{\dot{\varepsilon}_{th}^{cc}}{\dot{\varepsilon}_{m}^{cc}} + 1}{\xi_{env}} \right)^2 \right] dt \tag{6-7}$$

Under isothermal conditions, the thermal strain rate is zero. When the mechanical cycle operates in-phase with the thermal cycle (i.e., the peak temperature and stress are nominally coincident), the environmental factor is reduced to approximately zero. This allows creep-damage to take precedence. Under out-of-phase TMF (e.g., OP-TMF) cycling, the ratio between the thermal and mechanical strain rates can be close to -1. These special cases are highlighted in Figure 6-6b. The phase factor approaches unity for the most severe conditions and zero elsewhere. In contrast with the dwell factor, this expression utilizes an integral. Here ξ_{env} is a regression constant that helps to control the sharpness of the difference in oxidation damage under various phase types.

The cycle factors, Φ_{dwell} and Φ_{env}, are used in function *f*, as expressed in equation 6-5. This function accounts for the effects of both long compressive dwells and phase differences. After refining creep and fatigue modules with experimental data from tensile creep-fatigue and in-phase thermomechanical tests, environmental-fatigue life, $N_i^{(env)}$, is isolated from total life, N^{total}. Compressive creep-fatigue experimental data, from this study, and out-phase thermomechanical experimental data from other sources are utilized to obtain environmental-fatigue life, $N_i^{(env)}$;

$$N_i^{(env)} = \left(\frac{1}{N^{total}} - \frac{1}{N_i^{(fat)}} - \frac{1}{N_i^{(cr)}} \right)^{-1} \tag{6-8}$$

After computing environmental fatigue life for various cases, function *f* is obtained by a numerical fit. Some materials are more sensitive to compressive dwell while others are affected more by out-phase thermal cycling. Function *f* makes this framework to adjust for other materials as needed.

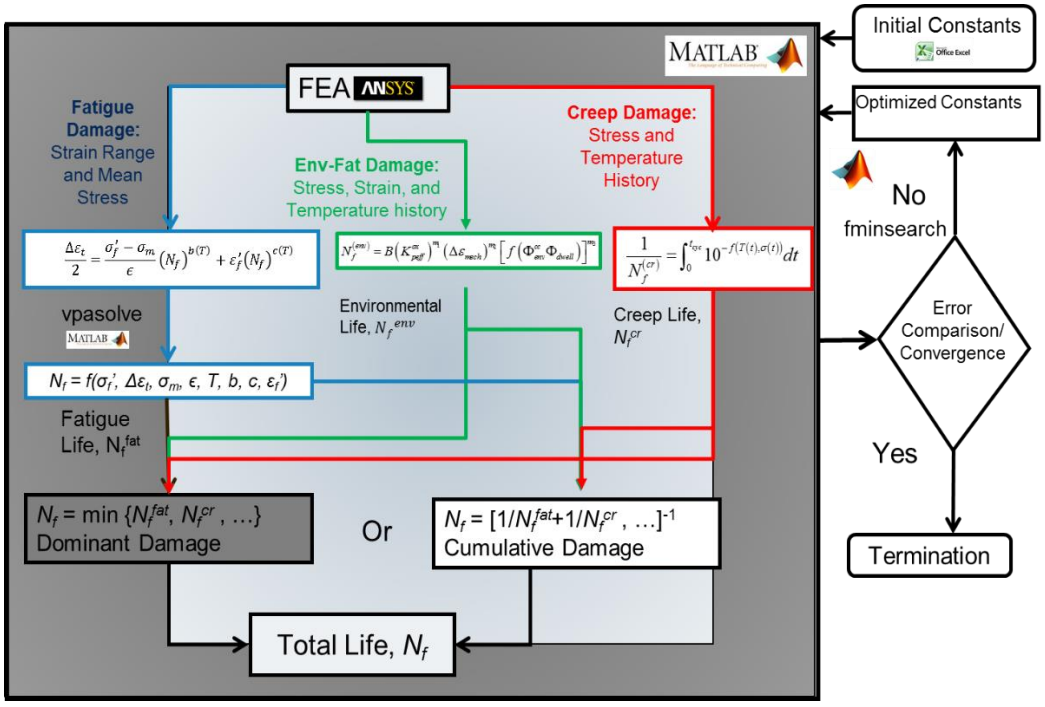

Figure 6-5. Constant determination and life prediction modeling framework.

a)

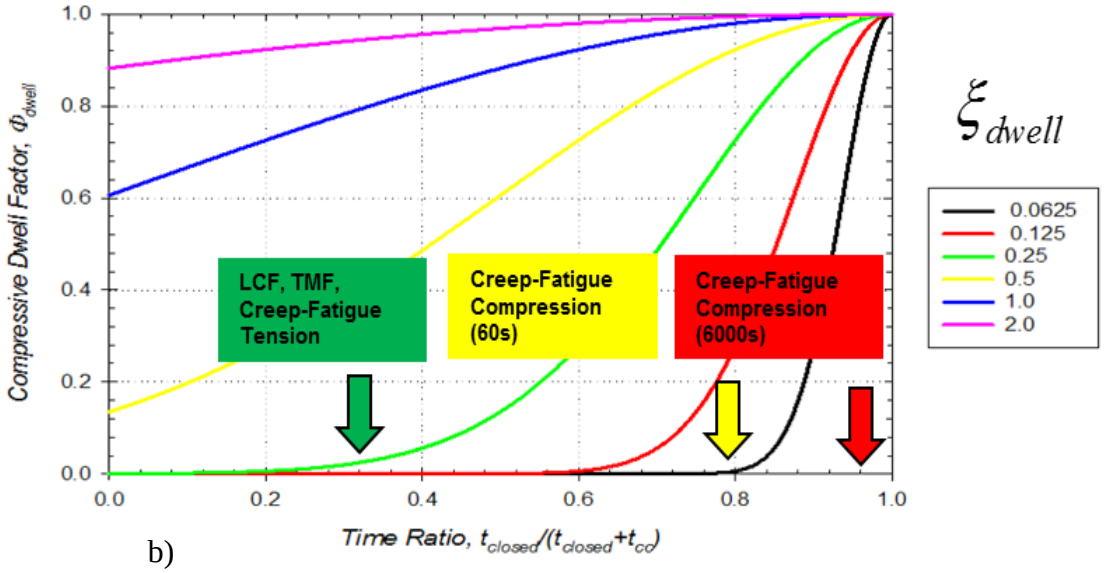

b)

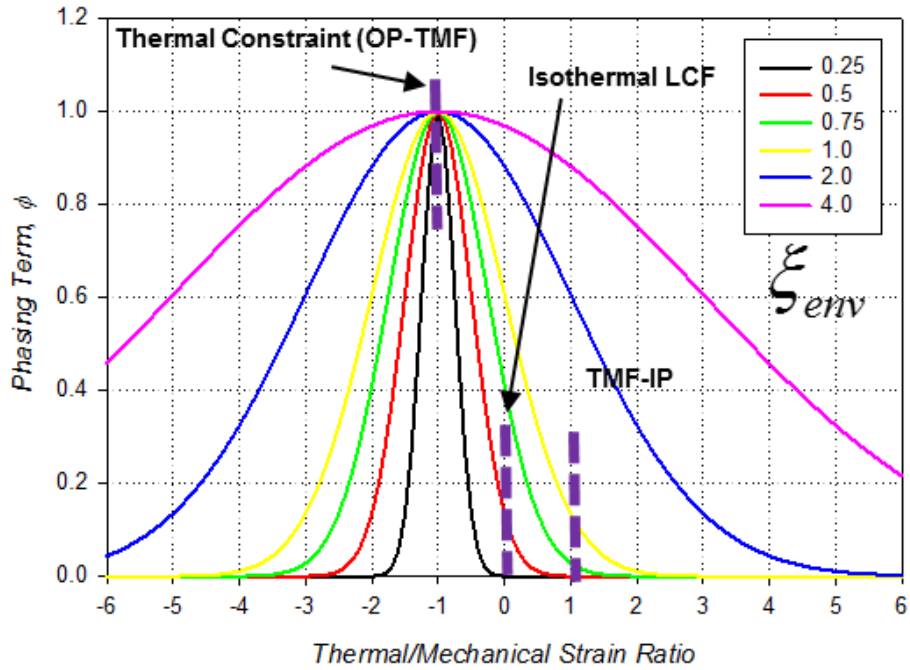

Figure 6-6. Coupled environmental-fatigue factors: (a) dwell and (b) phasing

a)

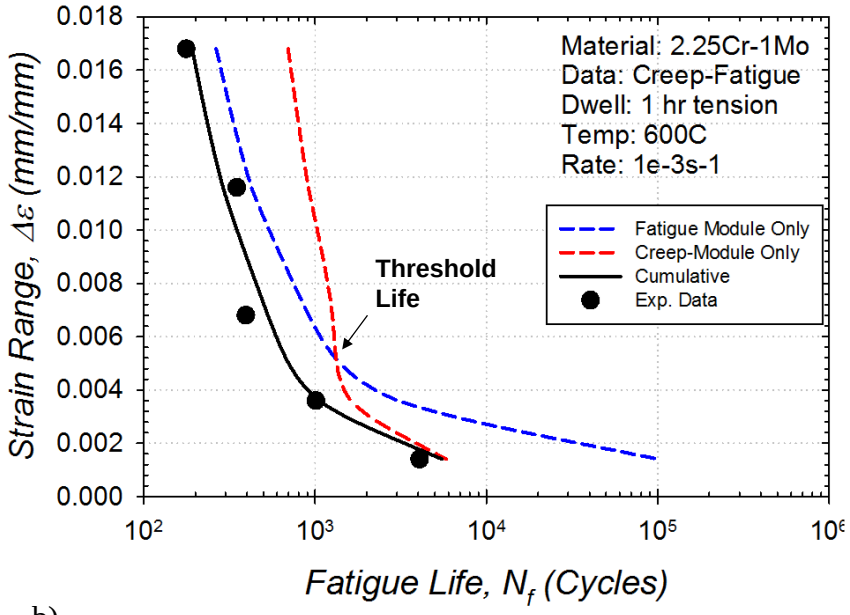

b)

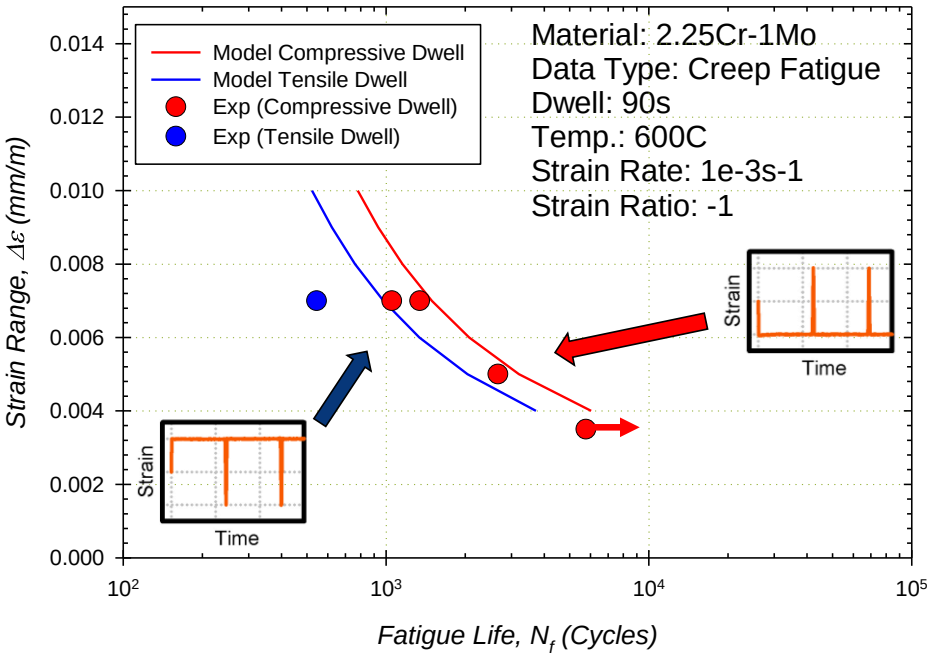

Figure 6-7. Module performance under dominantly creep-fatigue conditions: (a) 1 hour tensile dwell [data from NRIM No. 62] and (b) 90 second tensile or compressive dwell [data from present study].

6.4 Overall Model performance

The physically-based, cumulative damage lifing approach is used to predict the fatigue life under a variety of conditions, namely CF, TMF, and creep-TMF. A flowchart demonstrating how data information is processed in the course of making life estimates is provided in Figure 6-5. As displayed in the flow chart, constants obtained from various sources are applied to the deformation model, described in Chapter 5. Then, deformation data of the material is extracted to Matlab using *xlsread* command to calculate the fatigue life. In Matlab, N_i for each damage module is calculated separately and combined later using the cumulative damage approach. For the fatigue module, *vpasolve* command is utilized to solve for N_i^{fat} in Equation 6.2. Stress and temperature history extracted from the deformation response are used in Equation 6.3 for the creep module. This equation is integrated by trapezoidal rule with *trapz* command in Matlab. For environmental-fatigue module, simple for and if commands are utilized to calculate all the variable and N_i^{env}. After all the calculations, each N_i and total life are extracted to an Excel file. In this Excel file, total life values are compared with experimental data to validate the accuracy of the model. If the results are not satisfactory, then constants in the model are optimized until the criteria is met. Table 6-1 presents optimized model constants for each damage mechanism, which were used to simulate accurate simulations.

Table 6-1. Optimized life prediction model constants for each damage module.

Fatigue Module Constants	Creep-Fatigue Module Constants	Environmental Fatigue Module Constants
$\sigma_f^{'} = 970$	$T_m = 1540°C$	$\xi_{env} = 0.75$
$b = -0.078$	$\sigma_{MUTS,RT} = 580 MPa$	$\xi_{dwell} = 0.5$
$\varepsilon_f^{'} = 1.60$	$C = 0.5$	$Q_{ox} = 212kJ$
$c = -0.80$		$B = 2$
$E = 201125\ MPa$		$m1 = -0.25$
		$m2 = -0.35$

The lifing estimates generated by the model are compared with data from literature in Figure 6-7. At high strain ranges, plasticity is the dominant mode of deformation. The fatigue module compares well with data. At low strain ranges, however, the creep module is the dominant term and fatigue is less relevant. Data from the present are also used to demonstrate the accuracy of the model. Figure 6-7(b) shows the tensile-compressive asymmetry in terms of dwell-fatigue strain-life. Compressive dwells are not as detrimental to fatigue life as tensile dwells, and the life prediction model predicts the difference.

6.4.1 Effect of Temperature

Temperature is an essential quantity that effects life of a material. The 2.25 Cr-1Mo material is widely used for turbomachinery components where it experiences various temperatures; thusly, a life prediction model must be able to simulate different temperatures. Additionally, these structures are utilized with thermal cycling. Thusly, isothermal assumption is not valid, and thermomechanical fatigue conditions are to be considered for service-like cases.

High temperatures, such as 600°C and 650°C, are the main concern for this material. Most of the experimental data is regarding these temperatures. Conditions with various temperatures are simulated against the test data in Figure 6-8. The figure shows that the model matches the actual life for different temperatures, especially for high temperatures. Life of the material decreases with the increase of temperature as expected. Also, this figure displays that fatigue life of the material is very close to each other with high strain ranges at different temperatures. Especially, the curves for 20°C, 200°C and 300°C are overlapping until very low strain ranges because creep damage does not play a role until 400°C.

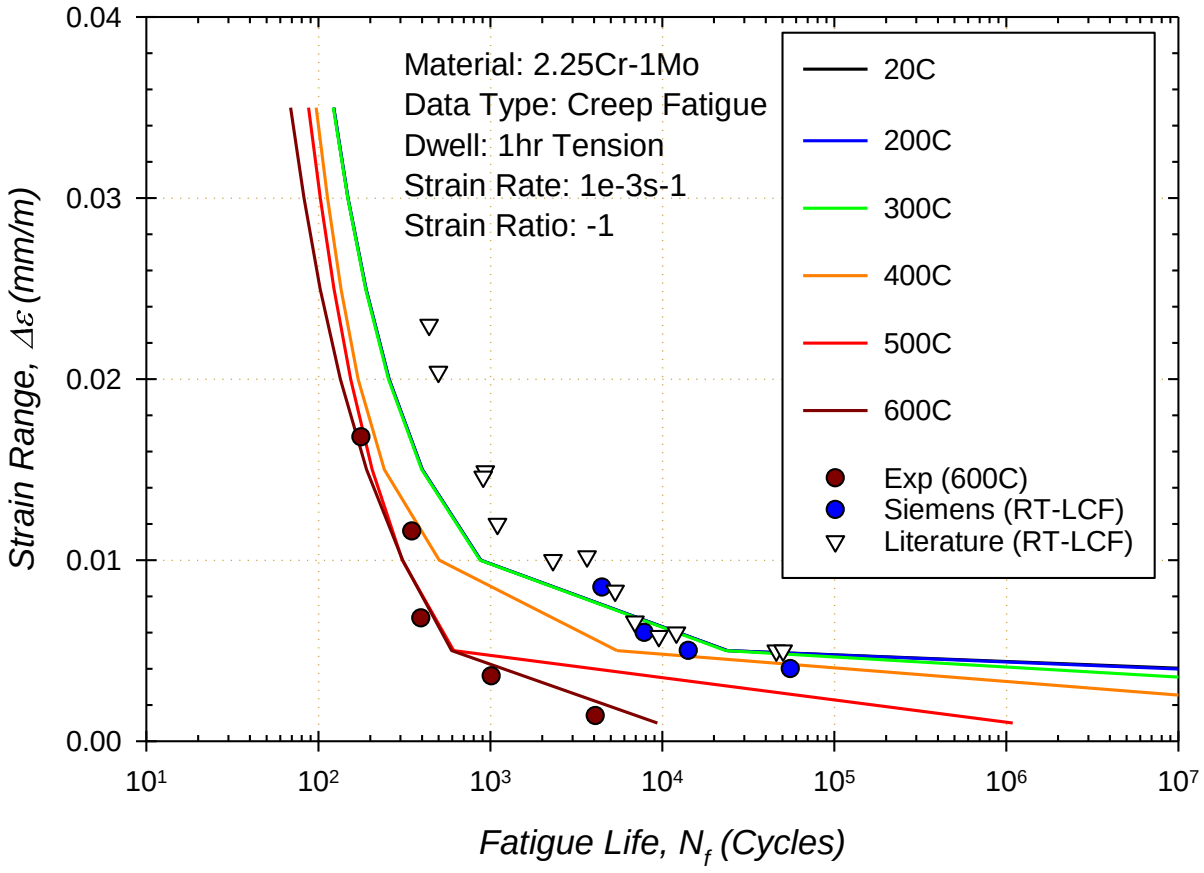

Figure 6-8. Model performance on various temperatures

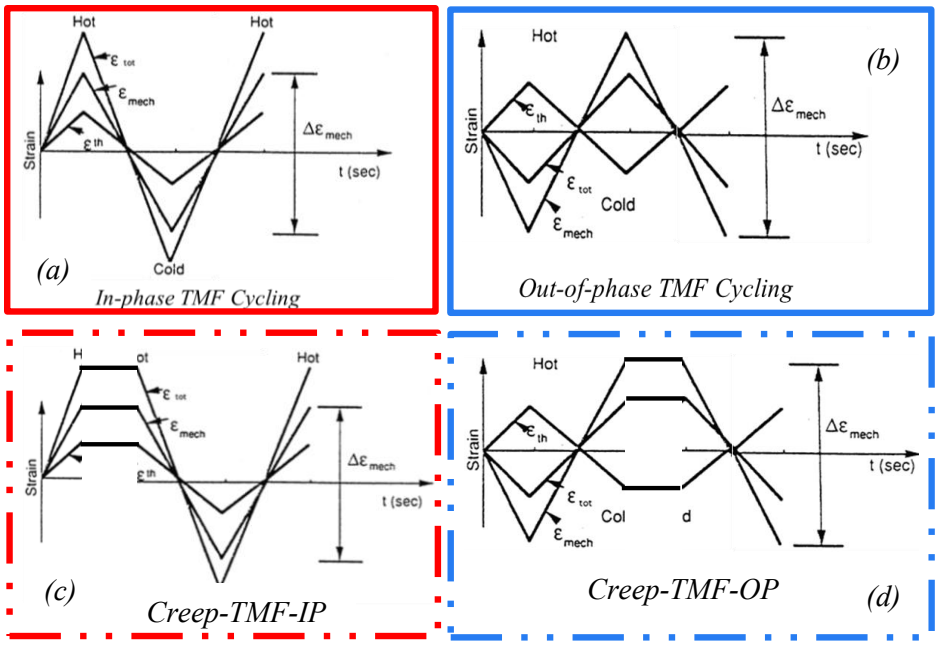

Figure 6-9. Thermomechanical fatigue (TMF) waveforms: (a) in-phase (IP) TMF, (b) out-of-phase (OP) TMF, (c) IP-TMF with creep, and (d) OP-TMF with creep.

The model is exercised under idealized service conditions, as well, namely thermomechanical fatigue (TMF). Prior studies subjected 2.25Cr-1Mo to TMF and creep-TMF conditions [15] as shown in

Figure 6-9. Specifically, two types of mechanical strain controlled TMF waveforms were used: in-phase and out-of-phase. The temperature range reported in the data was 300 to 538°C at a pace of 2°C/s. For capturing the effect of phasing accurately for TMF cases, ξ_{env} is analyzed carefully in this study. As described previously in this chapter, this term helps to regulate the difference between out-phase and in-phase cases. Separate lifing curves are constructed to visualize the effect of ξ_{env} constant in Figure 6-10. Figure 6-10a displays the model prediction with ξ_{env} equals 4 against the literature data. The model simulates the TMF out-phase case accurately

compared to experimental data with his ξ_{env} value; however, the effect of phasing is not captured for the TMF in phase case. The literature data clearly shows that the fatigue life is much higher at lower strain ranges with out of phase cycling; consequentially, another value is needed for ξ_{en} constant. Same conditions, with ξ_{en} constant is 2.5, are simulated against the literature data, shown in Figure 6-10b. Similarly, TMF OP case is predicted accurately with this ξ_{en} value. Even though TMF IP curve is closer to the literature data in this figure, ξ_{en} constant is needed to be lower for better results.

Lastly, ξ_{en} is lowered until 1.25 to capture the true effect of phasing for this material, displayed in Figure 6-11. The model predicts that TMF with out-phase temperature cycling leads to the shortest life correctly. TMF IP and TMF OP simulated curves match the literature closely with this value for. ξ_{en} Figure 6-12illustrates the performance of the model with another actual versus predicted plot. All predictions are within a factor of 2 compared to actual data. Some scatter exists within the data.

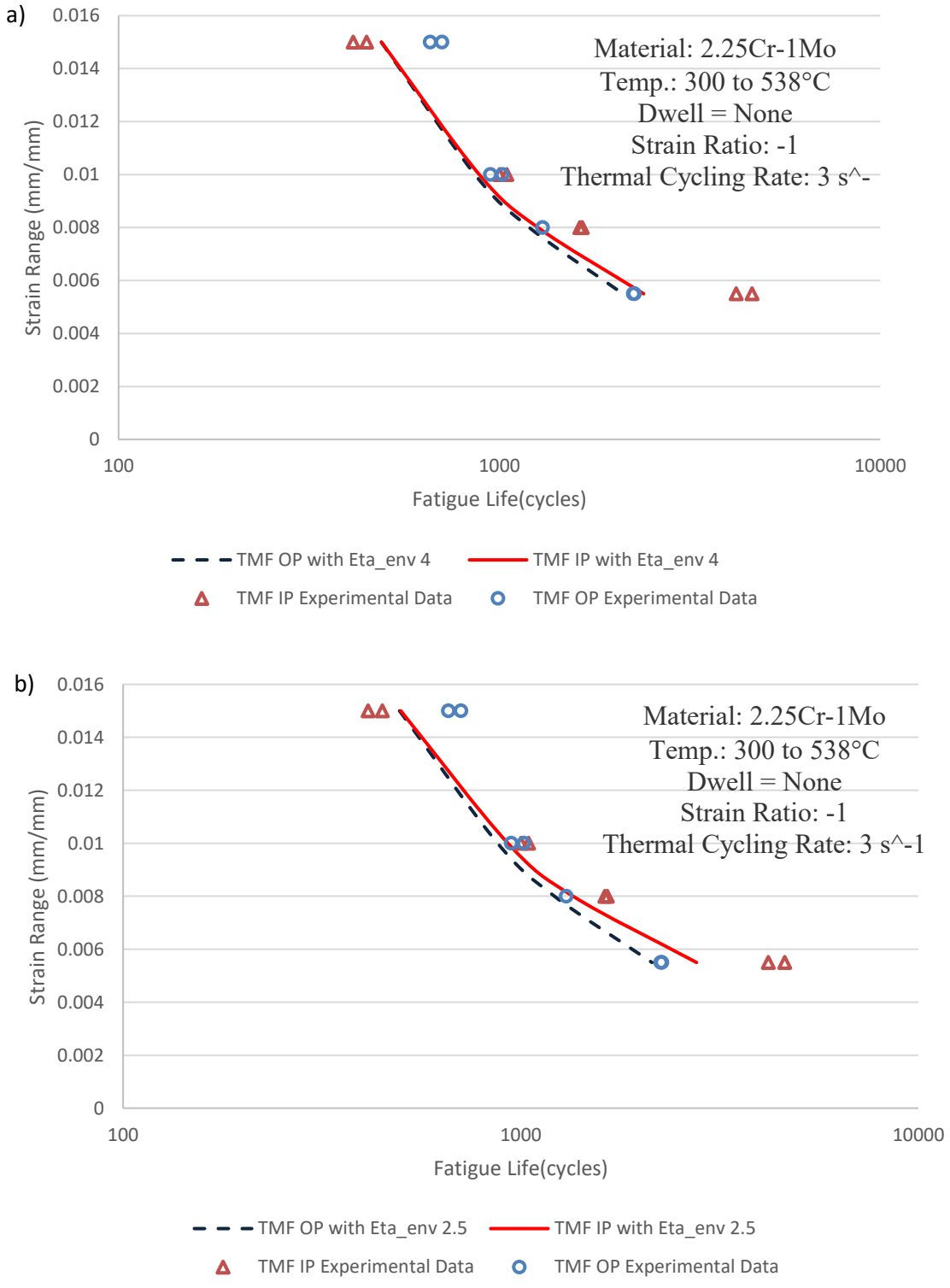

Figure 6-10. Model prediction for TMF cases against the literature data with ξ_{en} is 4 (a) and ξ_{en} is 2.5(b).

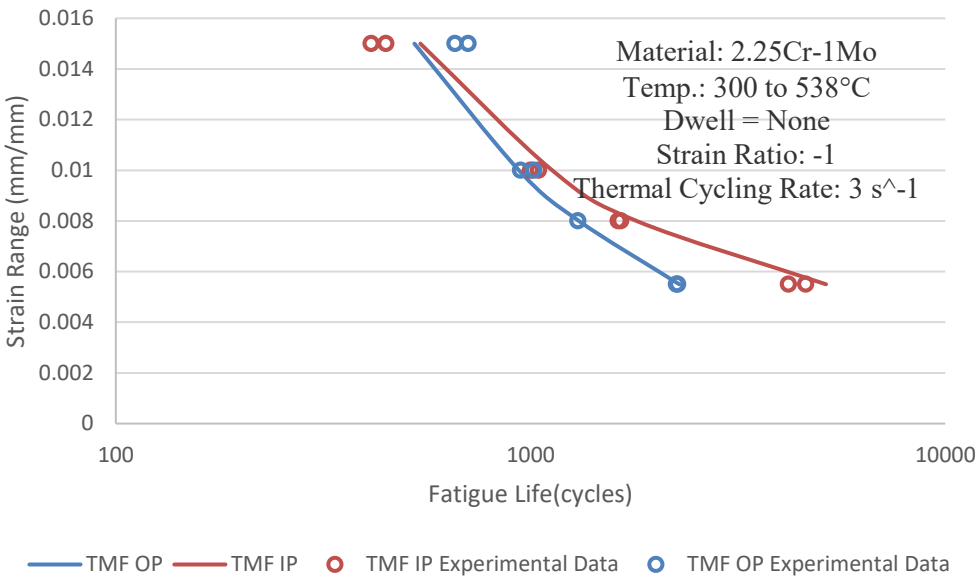

Figure 6-11. Cumulative life prediction against literature data for TMF cases

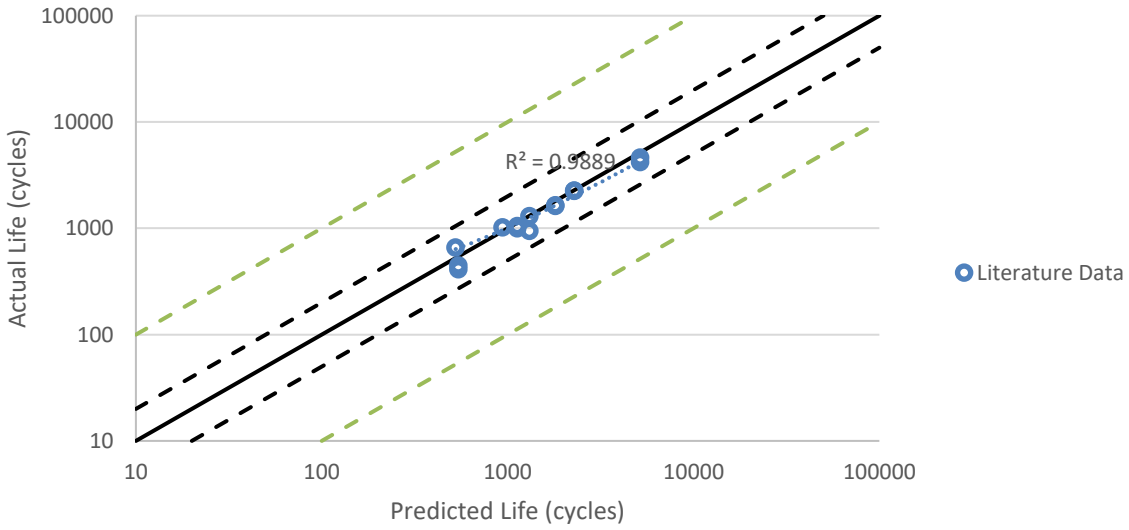

Figure 6-12. Comparison of actual and predicted fatigue behavior of 2.25Cr-1Mo steel under non-isothermal fatigue loading.

6.4.2 Effect of Dwell Periods

Another important influence on fatigue life of 2.25 Cr-1Mo material is dwell periods or hold times. Conditions with dwell periods at high temperatures are dominated by creep damage. Structures in the energy industry undergo very long dwell periods; however, there is not any test data over 1-hour dwell for this material. Experiments with long dwells can be very expensive and time consuming; therefore, longest dwell period that was tested in this study is 90 seconds. The model predicts the fatigue life of conditions with hold times very accurately, as shown in the section 2 of this chapter. Thusly, the model is used to analyze the effects of dwell periods longer than 1 hour on this material.

Various dwell periods, ranging from 20 seconds to 48 hours, at 600^{o}C are simulated using the model with cumulative damage, presented in Figure 6-13. Additionally, experimental data from NRIMS are included in the figure to compare with the predicted life with no dwell and 1- hour dwell periods. The line with highest life represents a LCF condition with no dwell, which matches the experimental data very well. Also, similar results for the curve with 1-hour dwell when it is compared to the data from NRIMS. As expected, LCF condition has the longest life while the condition with 48-hour dwell has the shortest. It is important to point out in this figure that all the lifing curves are almost overlapping at high strain ranges because creep has no effect in these regions. Additionally, effect of dwell times is decreasing after certain point as can be seen in the figure. After the condition with 5-hour dwells, creep damage hits its maximum point, the curves starting to overlap after this value in the plot.

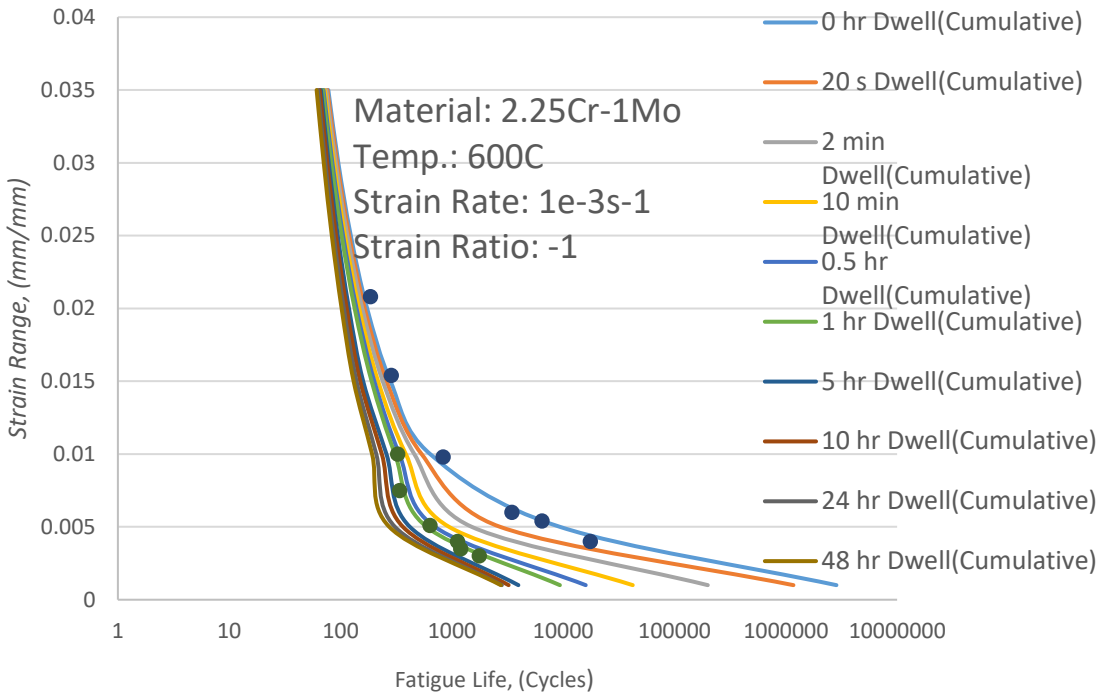

Figure 6-13**.** Overall model performance for various dwell times against data from NRIMS.

6.4.3 Effect of Strain Rate

Strain rate is defined as the variation in deformation of a material with respect to time. It is another variable that effects the life-span of a structure. Most of the experimental data available for 2.25 Cr-1Mo has a strain rate of 1e-3 per second in the literature. Strain rate is also 1e-3 per second for the fatigue experiments in this study, because using slower strain rates result in very long tests; therefore, it is very time and budget consuming; however, the life prediction model, presented in this study, is able to simulate conditions with various strain rates. The model was utilized to compare a condition with four different strain rates, displayed in Figure 6-14. The

simulations were run at 600°C with 1-hour dwell times. The plot shows that fatigue life decreases with slower strain rates until very low strain ranges. Life is shorter because the material experiences more time in high stress levels for slower strain rates. This behavior is supported by experimental data from NRIMS [8]. They experimented 2.25 Cr-1Mo material at 500°C with a strain range of 1% for three different strain rates. Number of cycles to failure values for strain rates at 1e-3, 1e-4, and 1e-5 are 1450 cycles, 1080 cycles, and 751 cycles, respectively. Also, the figure shows that all the curves starts to overlap at very low strain ranges. This happens because creep damage is really dominant in this region where strain rate becomes ineffective on fatigue life.

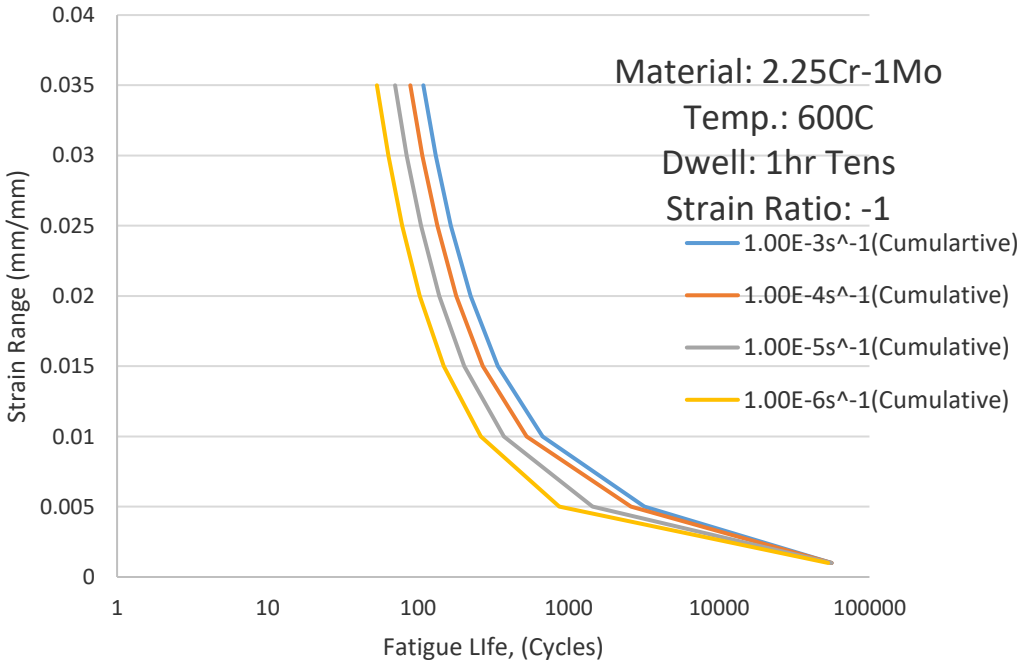

Figure 6-14. Overall model performance for strain rates

6.4.4 Effect of Function *f*

As described earlier in section 3 of current chapter, function *f* is utilized to capture the effect of compressive dwells and thermal cycling. This function could be different for other materials, where thermal phasing is more prominent or compressive dwells behave like dwells in tension. Thusly, it is important to analyze the effect of different values for function *f* on total life, N^{total}. This section includes comparison of total life values calculated with different function *f* numbers.

Accuracy of the life prediction approach, presented in this study, for conditions with thermal cycling is shown in section 4.1 of this chapter. Figure 6-15 presents a lifing curve with a different function *f* where the material is more sensitive to out-phase cycling. Simulated conditions are with various strain ranges at strain rate 1e-3 per second and without any dwell periods. Literature data and simulated life curve from Figure 6-11 are included here to compare with the new lifing curve with a different function *f*. Instead of changing the regression constant ξ_{en}, function *f* is modified to make it more sensitive to phasing here. For higher strain ranges, difference between both curves is not very noteworthy; however, total life is much lower for the lifing curve with the new function *f* at low strain ranges. Additionally, function *f* can be used to eliminate the difference between compressive and tensile dwells for materials that are less sensitive to compressive dwells. Figure 6-16 shows two lifing curves with different type of dwells compared against experimental data from this study. It was observed that total life is longer for conditions with compressive dwells for 2.25 Cr-1Mo material from literature and experimental data; however,

function *f* is utilized to lower total life with dwell in compression. As shown in the figure, predicted life is much lower than actual for the condition with compressive dwells. Thusly, total life is not sensitive to different types of dwell with the use of function *f*, if it is needed.

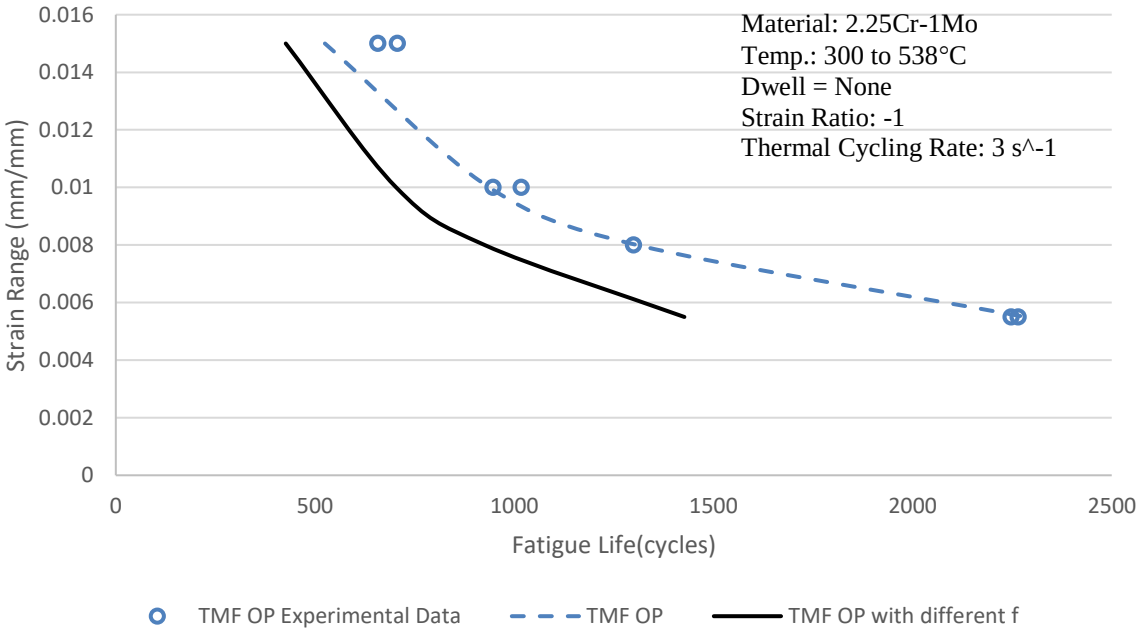

Figure 6-15. Effect of more phasing sensitive function *f*.

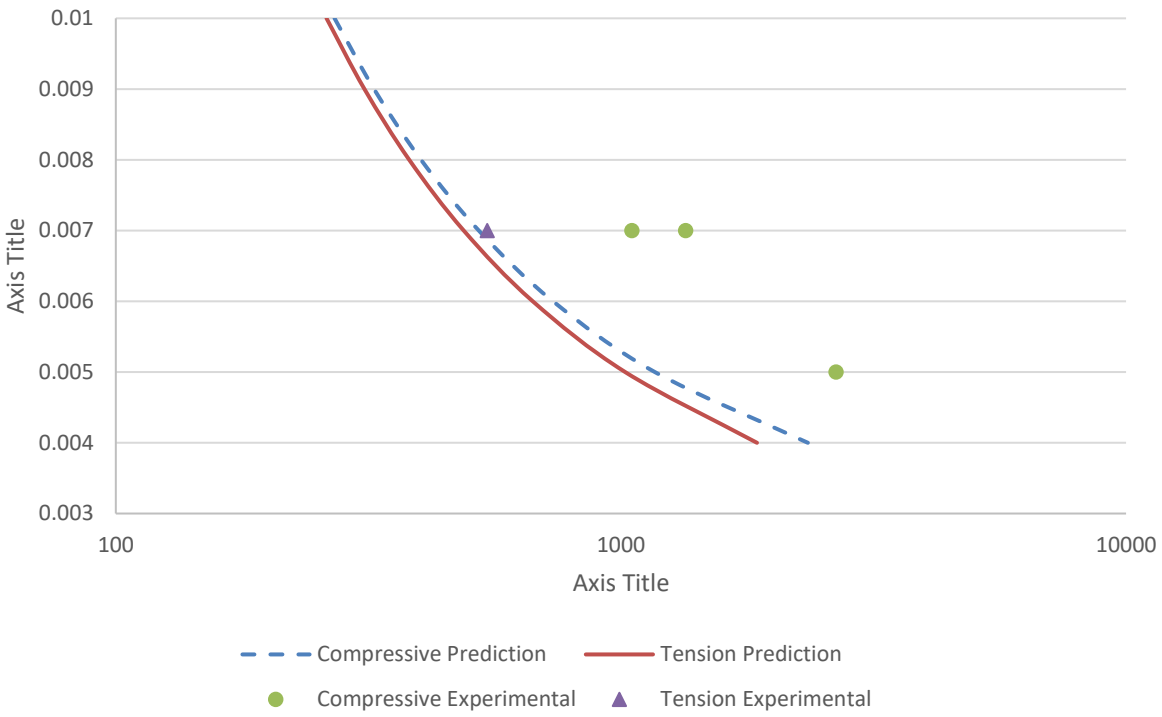

Figure 6-16. Different function *f* to eliminate the effect of different dwell types.

CHAPTER 7 CONCLUSION

A highly accurate, flexible approach for life prediction of a low alloy steel was presented in this thesis. The method is developed to be used for materials under complex loading conditions although it was tuned to basic experiments. Despite the significant progress in the development of modern alloys, low alloy steels remain to be the materials of choice for turbomachinery components. The candidate material is 2.25 Cr-1Mo alloy in this work. This approach assumes cumulative damage with modules that are related to classical fatigue crack initiation, creep rupture, and coupled environmental-fatigue cracking instead of using dominant damage method. A material database was developed to analyze the experimental data on 2.25 Cr-1Mo. For simulating deformation response of the material under variety of conditions, a non-interaction (NI) constitutive model is used in the present work. This model was established on the basis of uncoupled creep and plasticity. Instead of correlating the creep damage module with creep-fatigue data, creep rupture data and the Larson-Miller parameter was employed. Similarly, creep-fatigue data were not essential for tuning the constitutive model; the creep portion of the constitutive model was fit with creep deformation data alone. The environmental-fatigue damage component of the model makes use of oxidation kinetics data which are typically available from stress-free oxidation ingression studies. A flexibility function was built in the environmental-fatigue module to make this approach flexible to be used for different materials. Accuracy of the life prediction approach was shown by comparing simulated lifing data with experimental data for variety of conditions.

APPENDIX A: EXPERIMENTAL DATA

Tensile Experiments

BR 23

Test Conditions and Results

Speciemen No.	Temperature(s), T (°C)	Strain Rate, $d\varepsilon/dt$ (mm/mm/s)	Elastic Modulus, ϵ (MPa)	Ultimate Tensile Strength (MPa)	0.2% Yield Strength (MPa)
BR23	20	0.001	1.04E+06	687	686

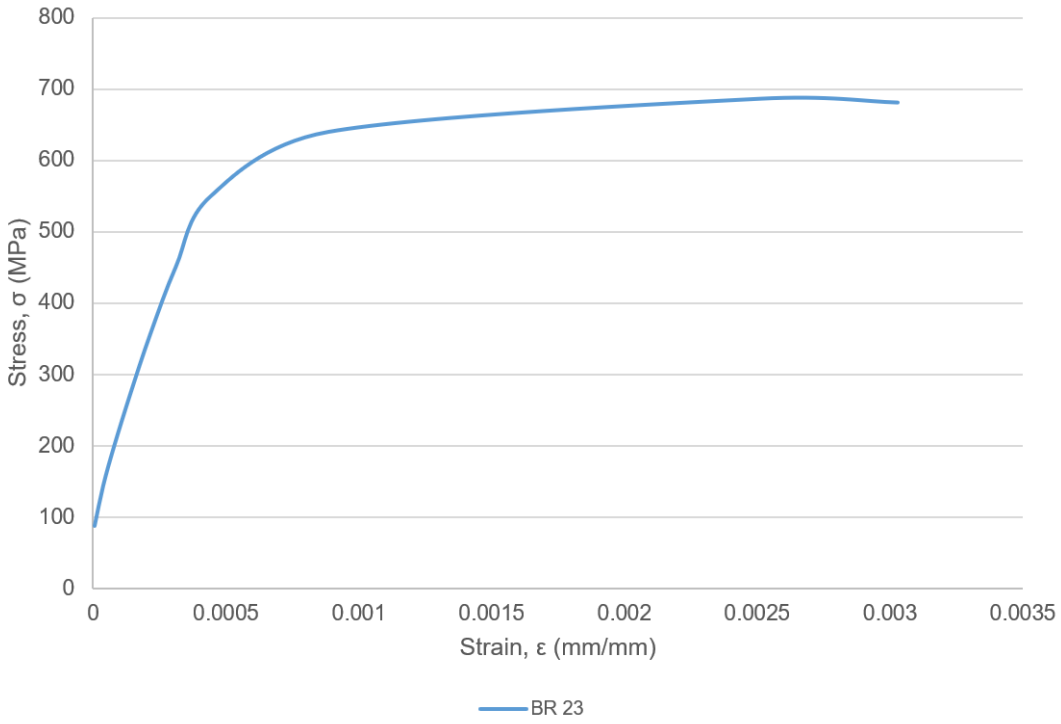

Figure A- 1. Deformation response of specimen BR23.

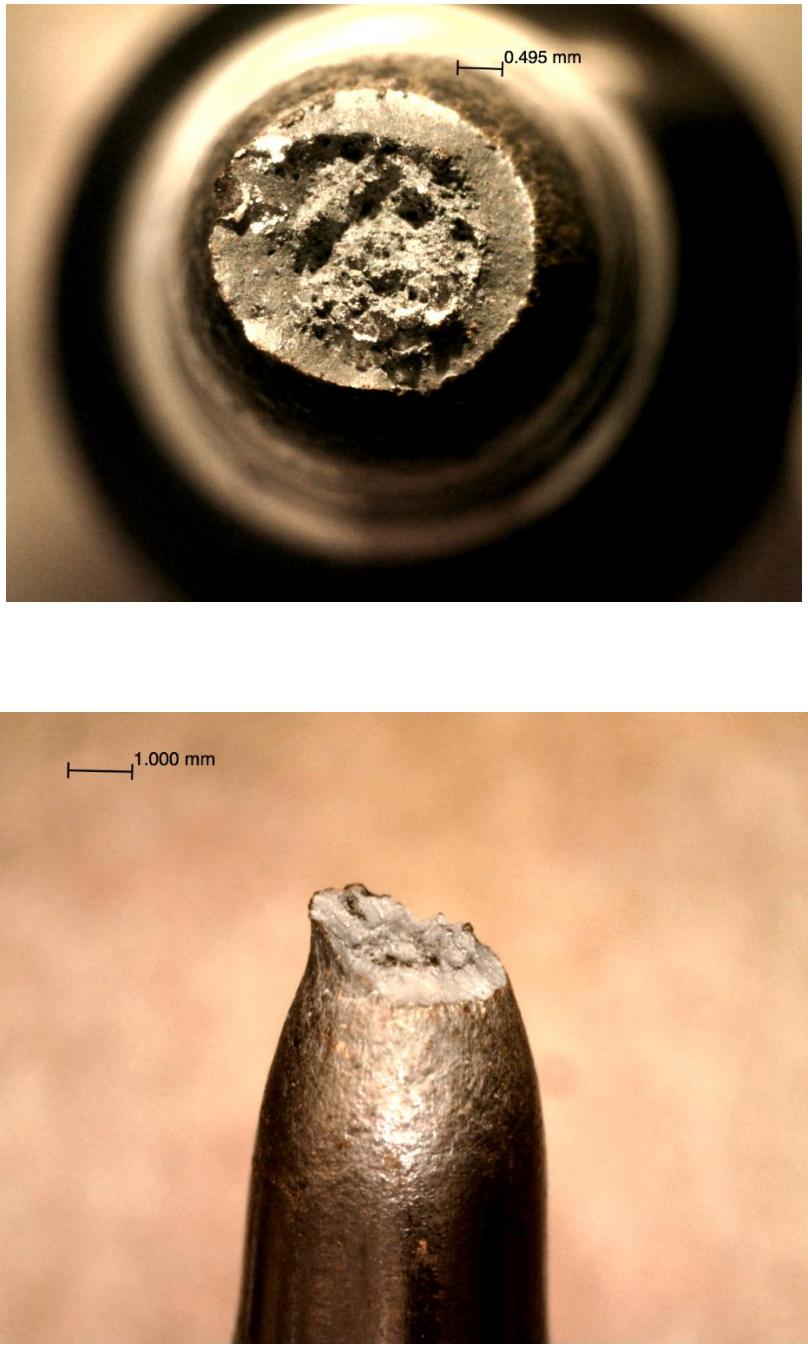

Figure A- 2. Pictures of deformed specimen BR23.

BR 25

Speciemen No.	Temperature(s), T (°C)	Strain Rate, $d\varepsilon/dt$ (mm/mm/s)	Elastic Modulus, ϵ (MPa)	Ultimate Tensile Strength (MPa)	0.2% Yield Strength (MPa)
BR25	650	0.001	1.32E+05	393	372

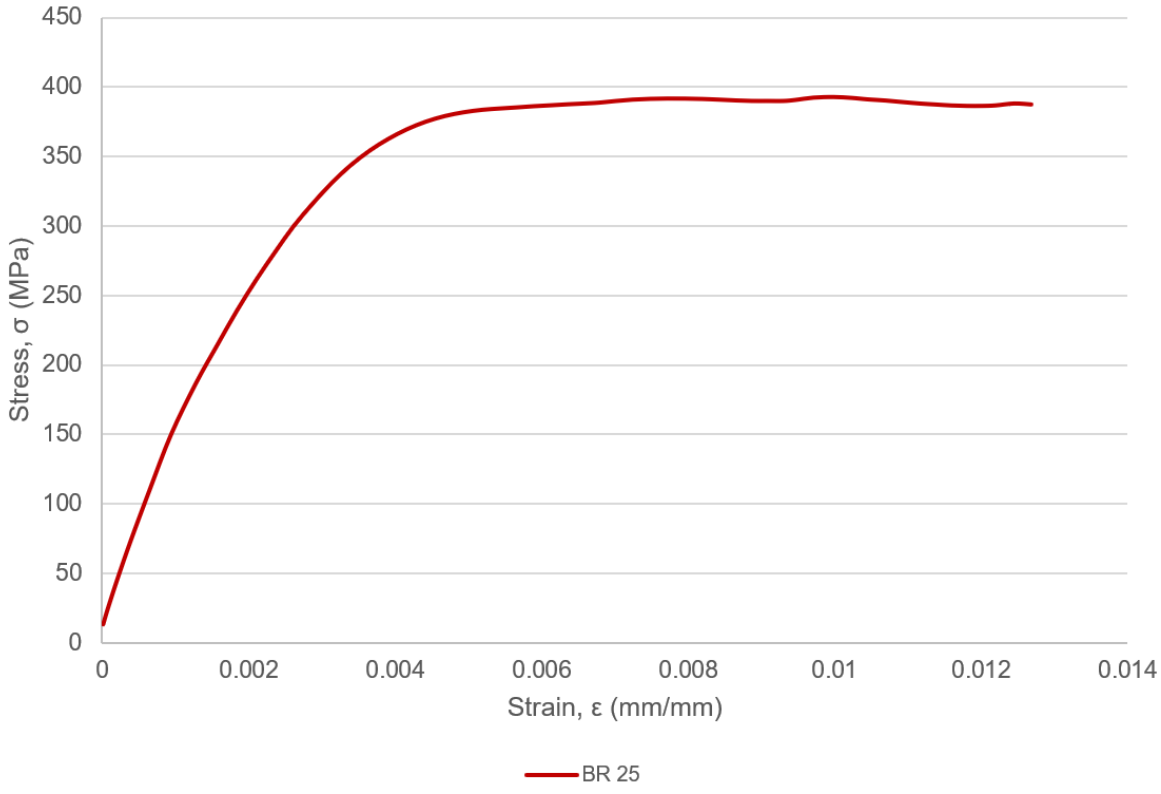

Figure A- 3. Deformation response of specimen BR25.

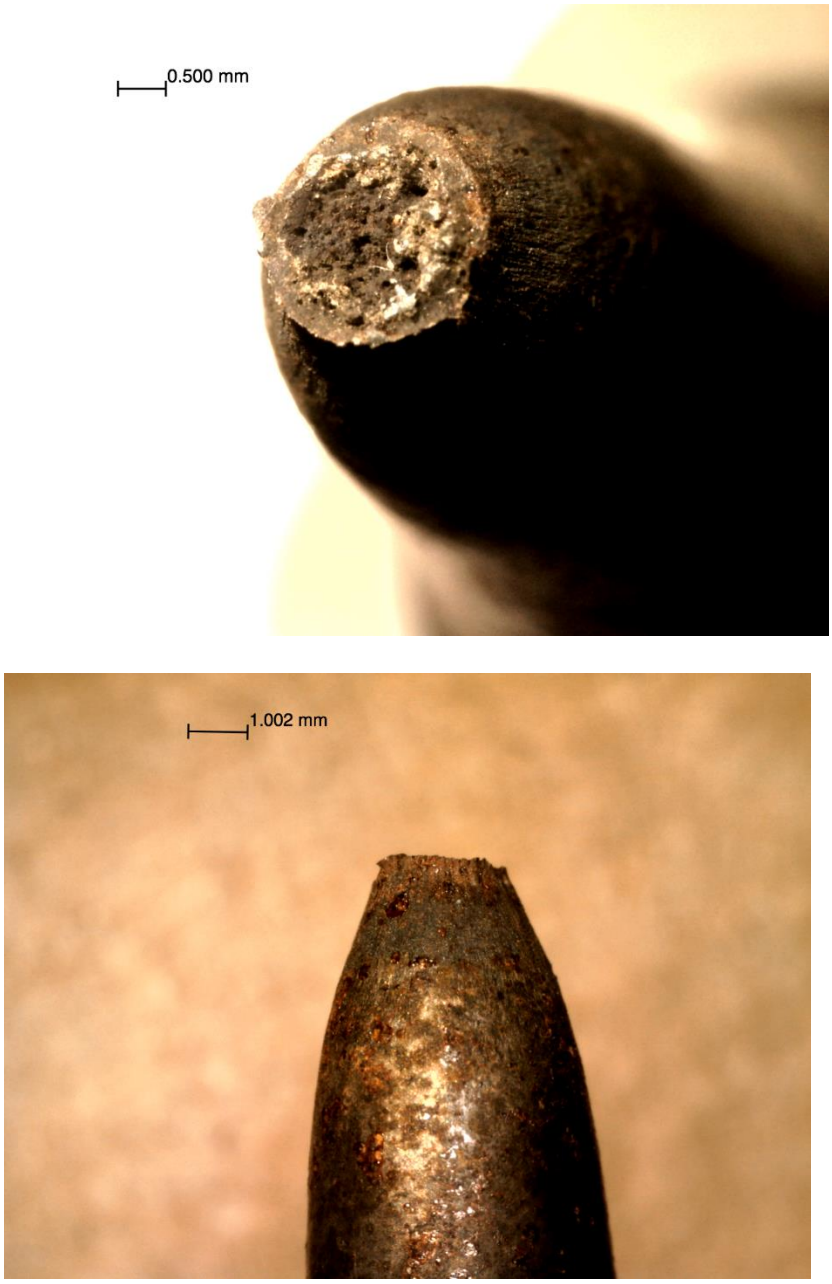

Figure A- 4. Pictures of deformed specimen BR25.

BR 26

Speciemen No.	Temperature(s), T (°C)	Strain Rate, $d\varepsilon/dt$ (mm/mm/s)	Elastic Modulus, ϵ (MPa)	Ultimate Tensile Strength (MPa)	0.2% Yield Strength (MPa)
BR26	600	0.00001	1.64E+05	367	355

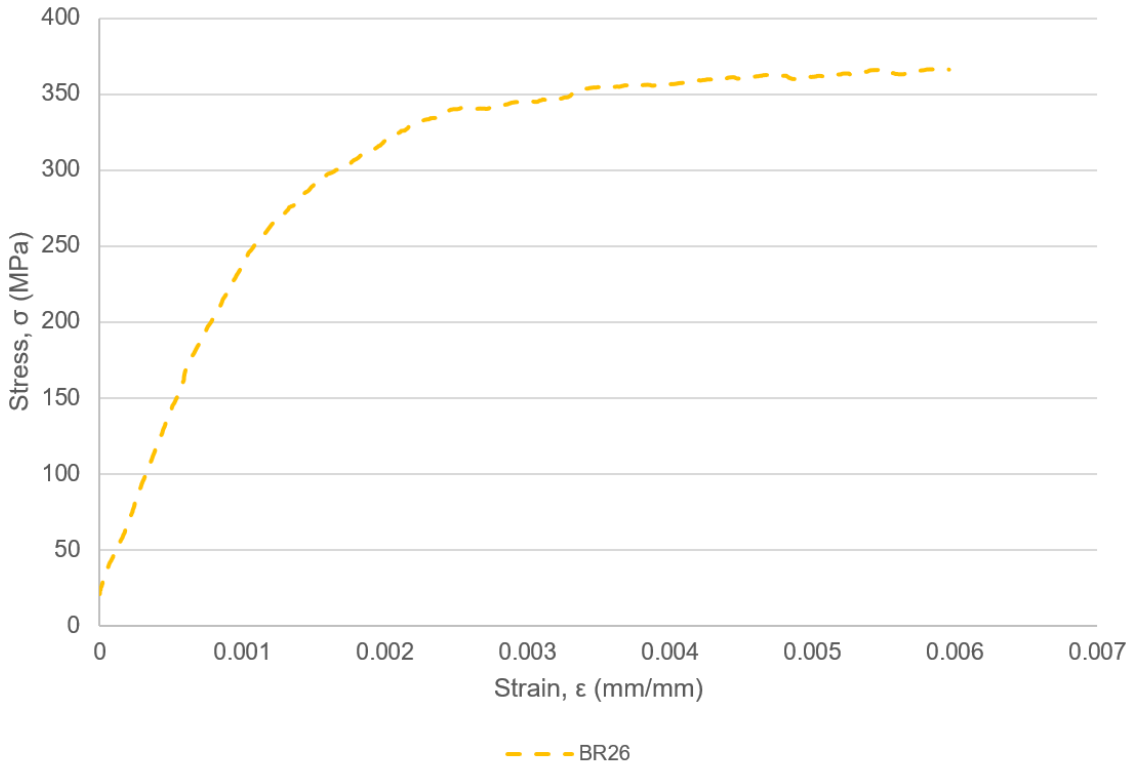

Figure A- 5. Deformation response of specimen BR26.

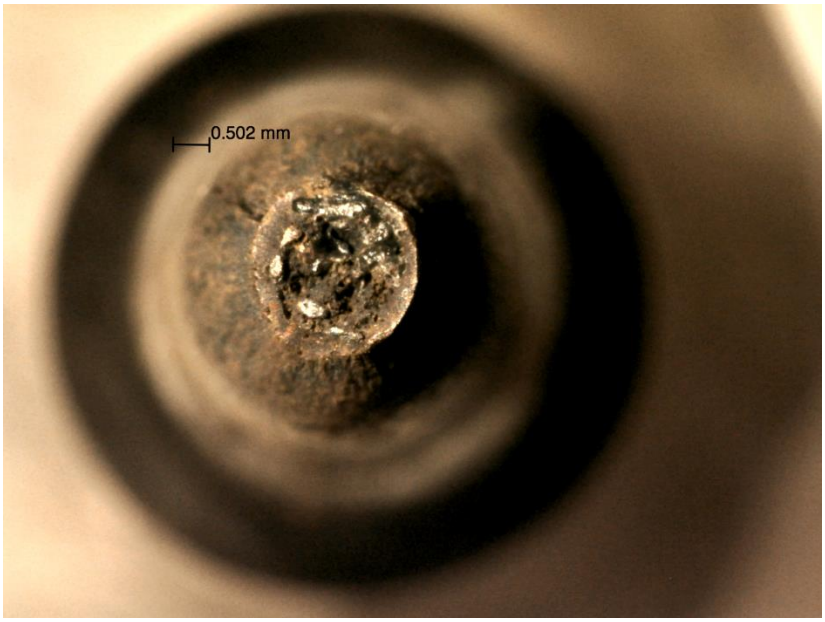

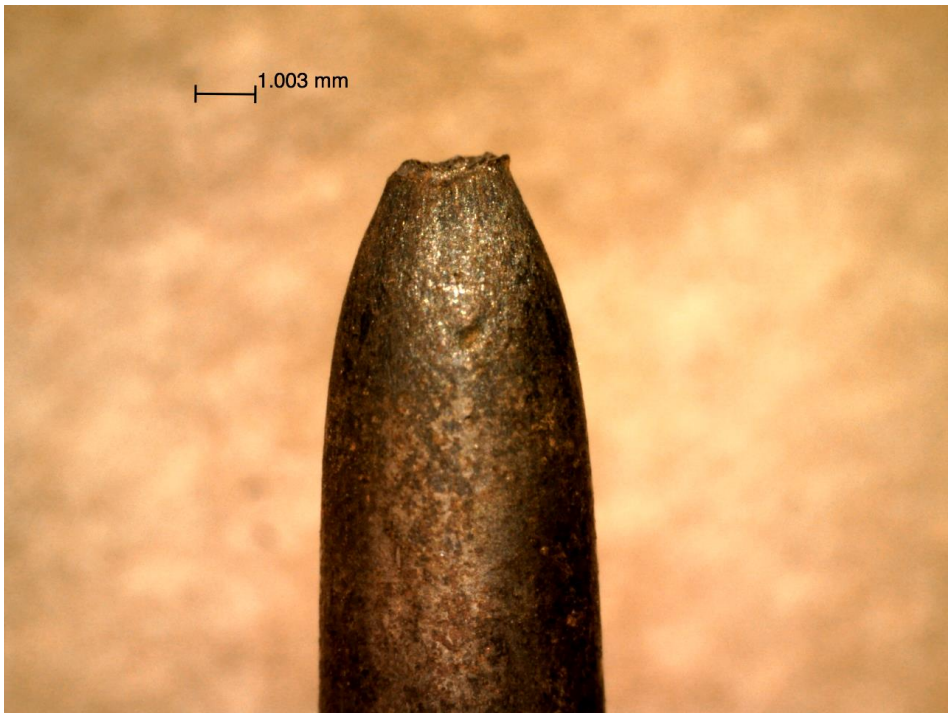

Figure A- 6. Pictures of deformed specimen BR26.

BR 27

Speciemen No.	Temperature(s), T (°C)	Strain Rate, $d\varepsilon/dt$ (mm/mm/s)	Elastic Modulus, ϵ (MPa)	Ultimate Tensile Strength (MPa)	0.2% Yield Strength (MPa)
BR27	650	0.00001	1.41E+05	258	238

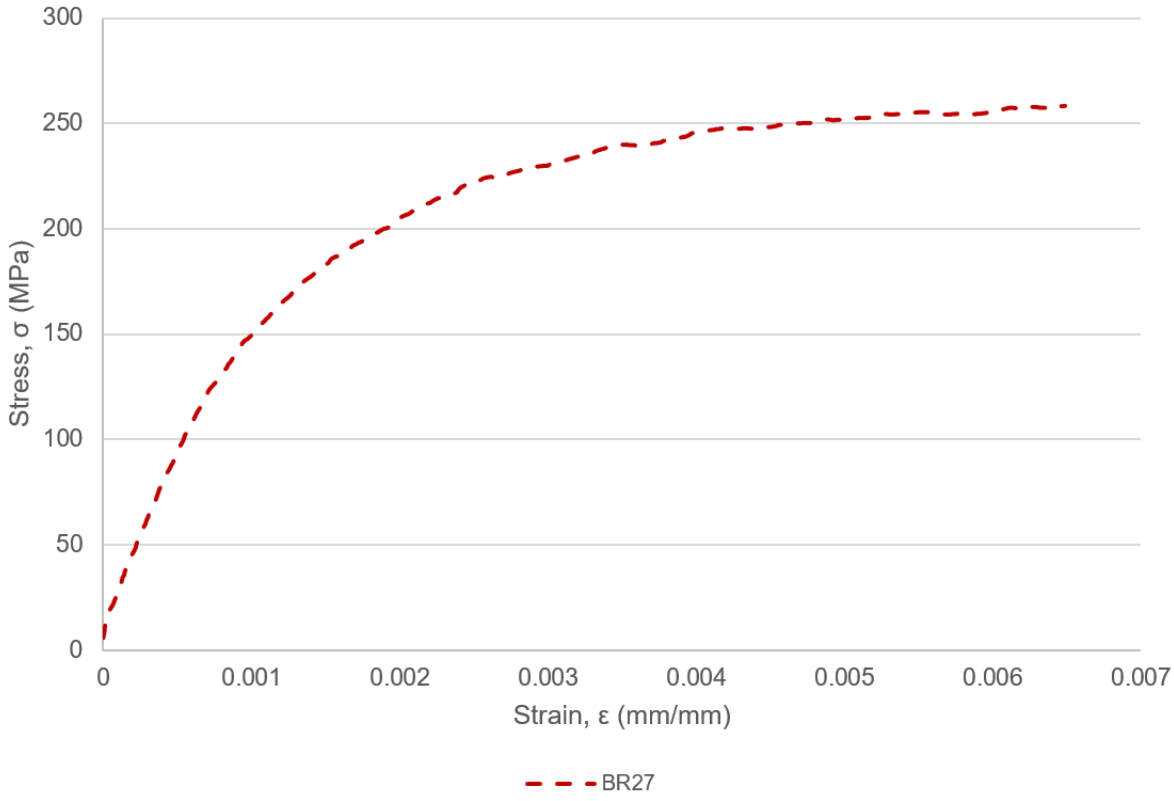

Figure A- 7. Deformation response of specimen BR27.

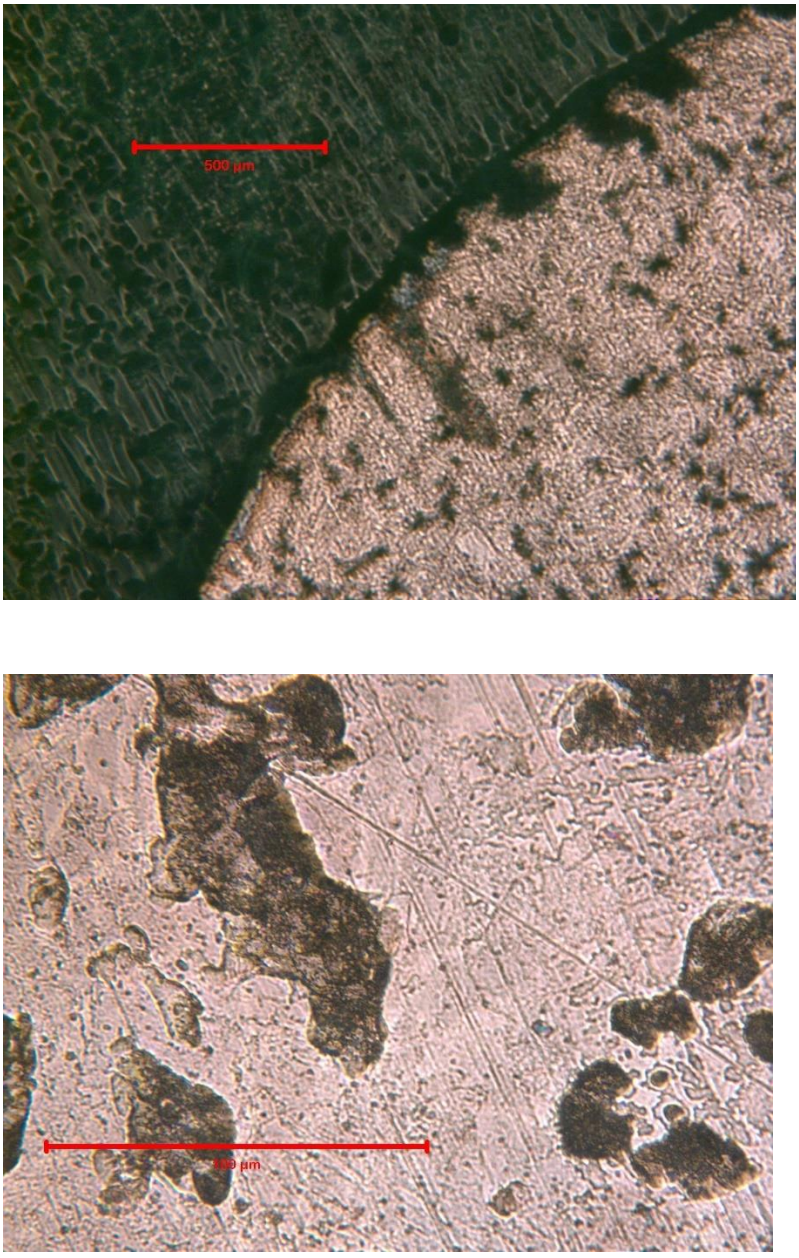

Figure A- 8. Microscopic pictures of BR27 using LOM.

BR 28

Speciemen No.	Temperature(s), T (°C)	Strain Rate, $d\varepsilon/dt$ (mm/mm/s)	Elastic Modulus, ϵ (MPa)	Ultimate Tensile Strength (MPa)	0.2% Yield Strength (MPa)
Spare	600	0.001	1.94E+05	468	452

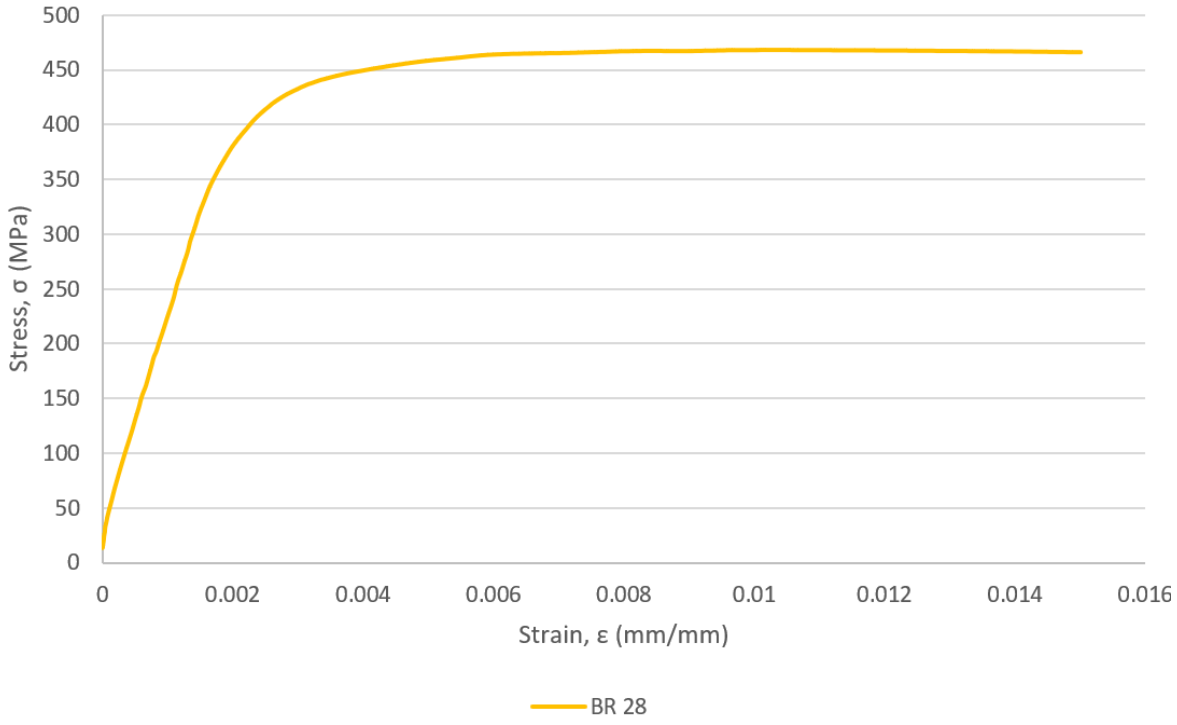

Figure A- 9. Deformation response of specimen BR28.

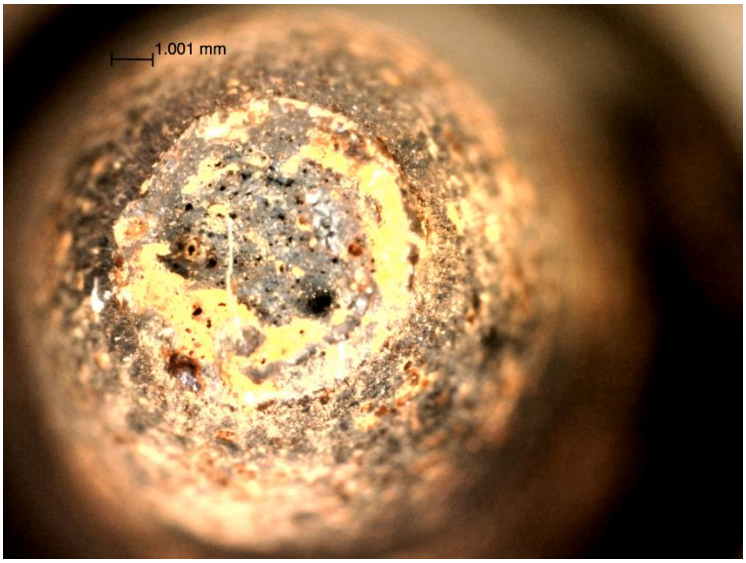

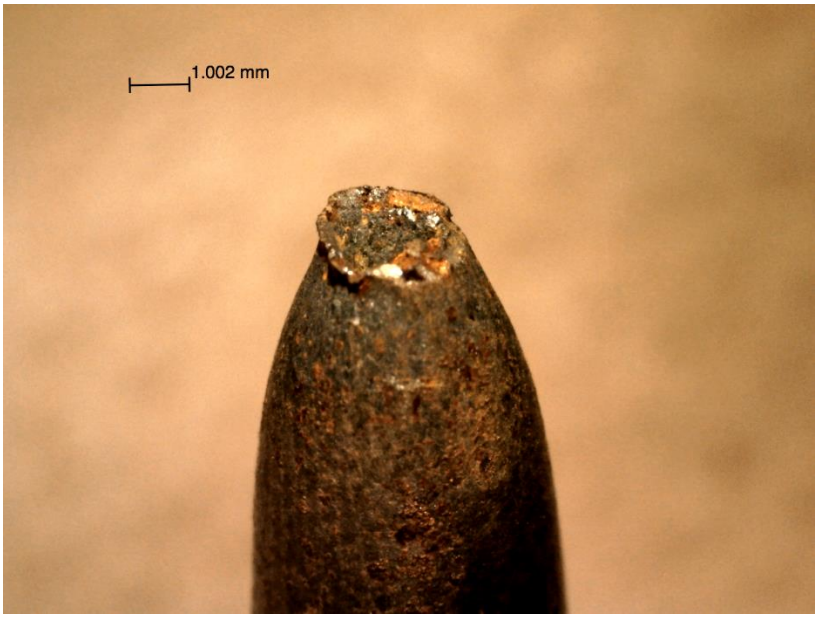

Figure A- 10. Pictures of deformed specimen BR28.

Fatigue Experiments

BR 15

Specimen No.	Total Strain Range, $\Delta\varepsilon$ (mm/mm)	Temperature(s), T (°C)	Strain Rate, $d\varepsilon/dt$ (mm/mm/s)	Strain Ratio, R_e	Dwell Time, t_h (sec) and Type	Cycles to Failure	Stress Range (MPa)	Mean Stress (MPa)
BR 15	0.007	600	0.001	-1	90s in Tens.	544	640.42	4.48

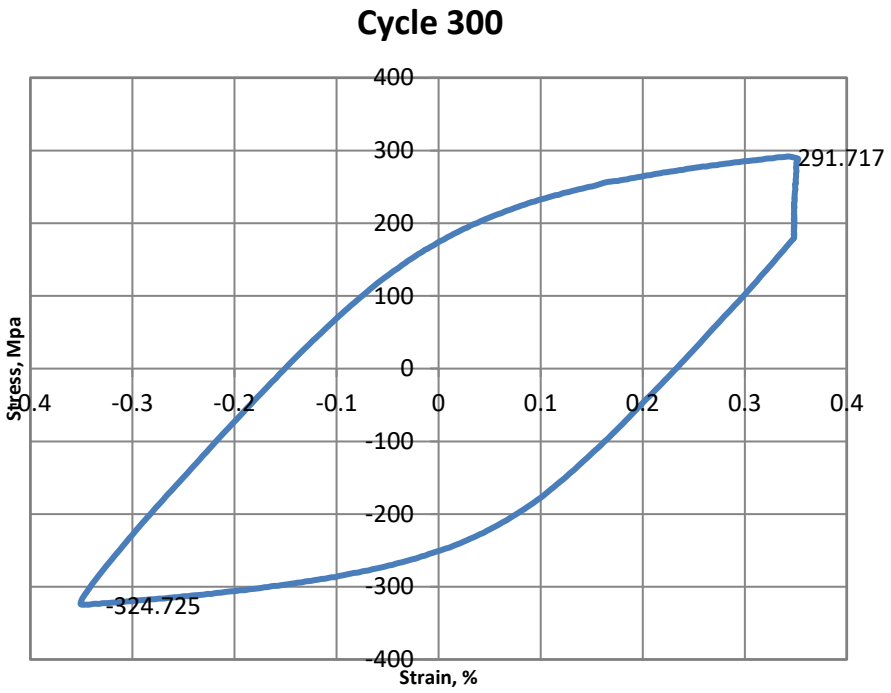

Figure A- 11. Deformation response of specimen BR15.

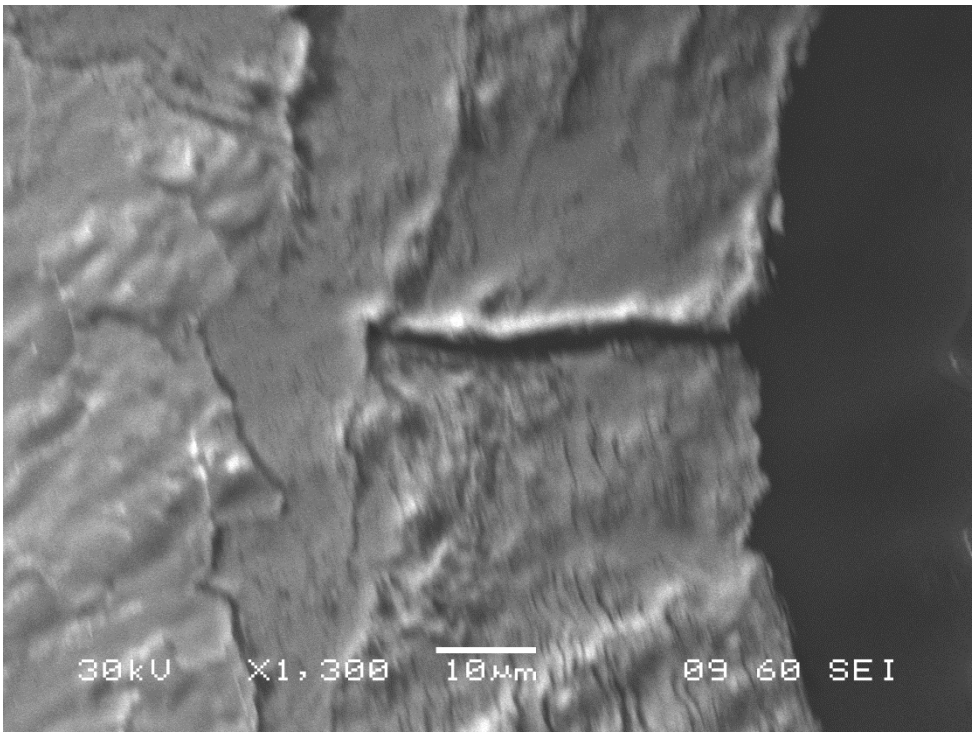

Figure A- 12. Microscopic picture of specimen BR15 using SEM.

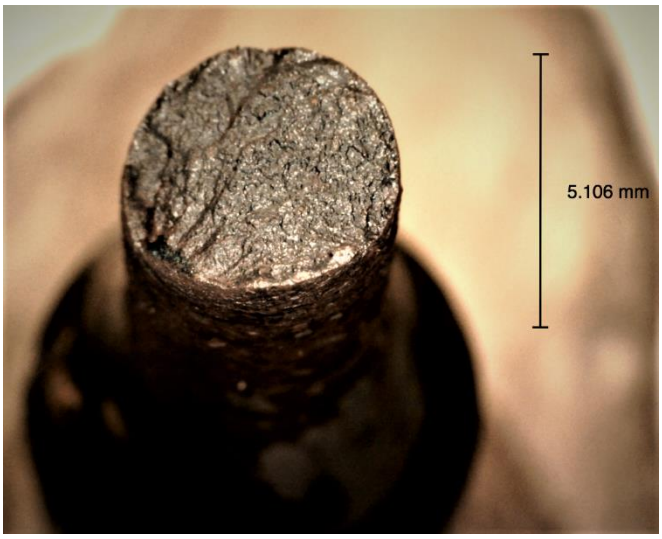

Figure A- 13. Pictures of deformed specimen BR15.

BR 17

Specimen No.	Total Strain Range, $\Delta\varepsilon$ (mm/mm)	Temperature(s), T (°C)	Strain Rate, $d\varepsilon/dt$ (mm/mm/s)	Strain Ratio, R_e	Dwell Time, t_h (sec) and Type	Cycles to Failure	Stress Range (MPa)	Mean Stress (MPa)
BR 17	0.007	600	0.001	-1	90s in Comp.	1051	611.81	-4.20

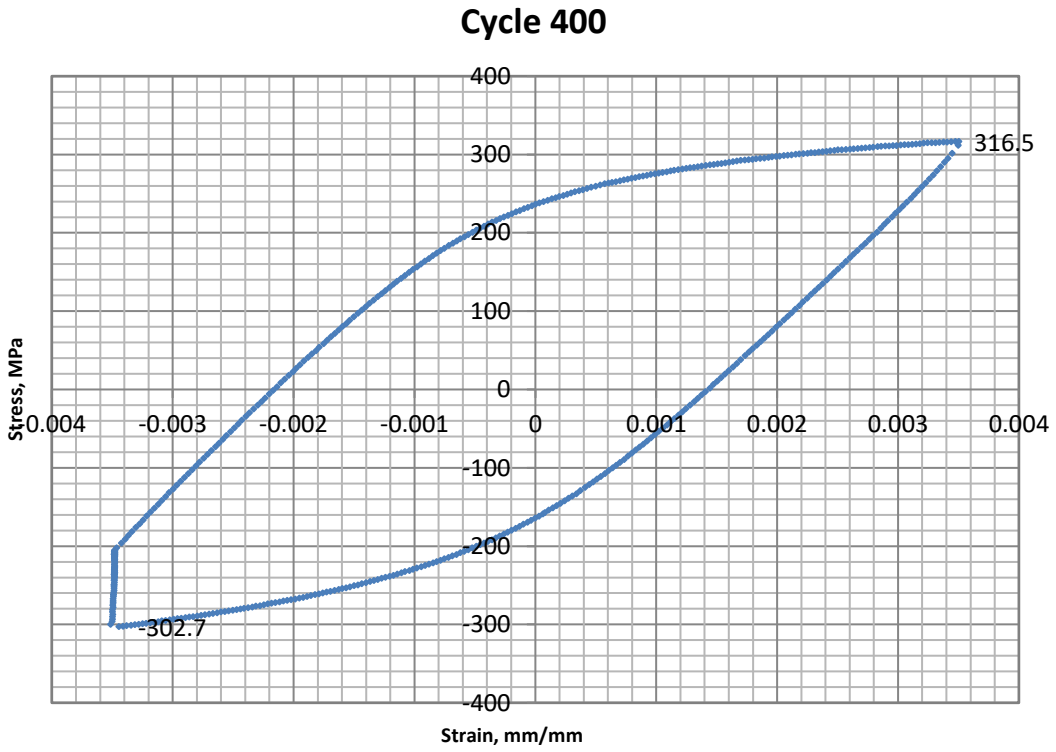

Figure A- 14. Deformation response of specimen BR17.

Figure A- 15. Pictures of deformed specimen BR17.

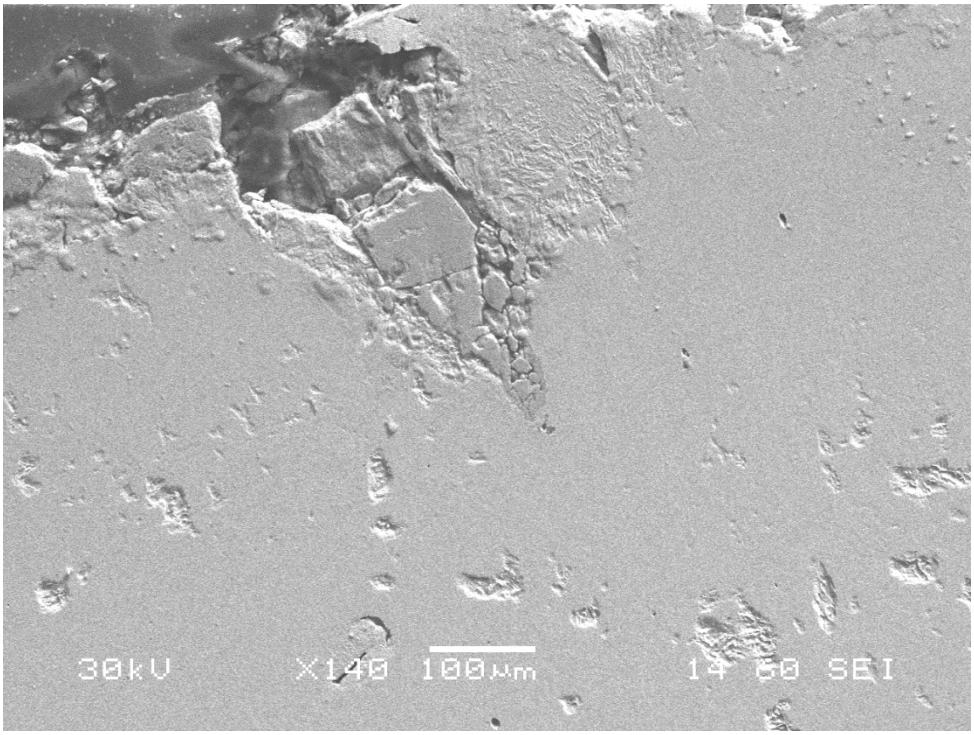

Figure A- 16. Microscopic picture of specimen BR17 using SEM.

BR 35

Specimen No.	Total Strain Range, $\Delta\varepsilon$ (mm/mm)	Temperature(s), T (°C)	Strain Rate, $d\varepsilon/dt$ (mm/mm/s)	Strain Ratio, R_e	Dwell Time, t_h (sec) and Type	Cycles to Failure	Stress Range (MPa)	Mean Stress (MPa)
BR 35	0.005	600	0.001	-1	90s in Comp.	2664	595.00	9.60

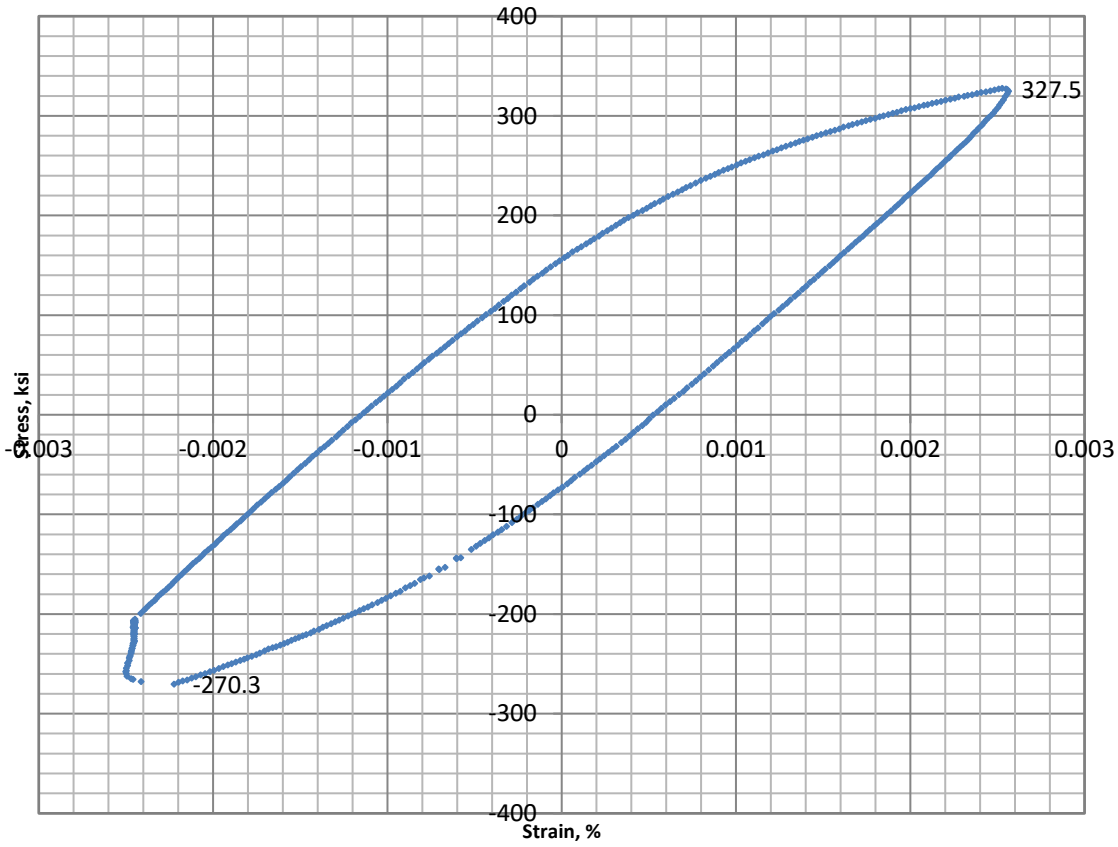

Figure A- 17. Deformation response of specimen BR35.

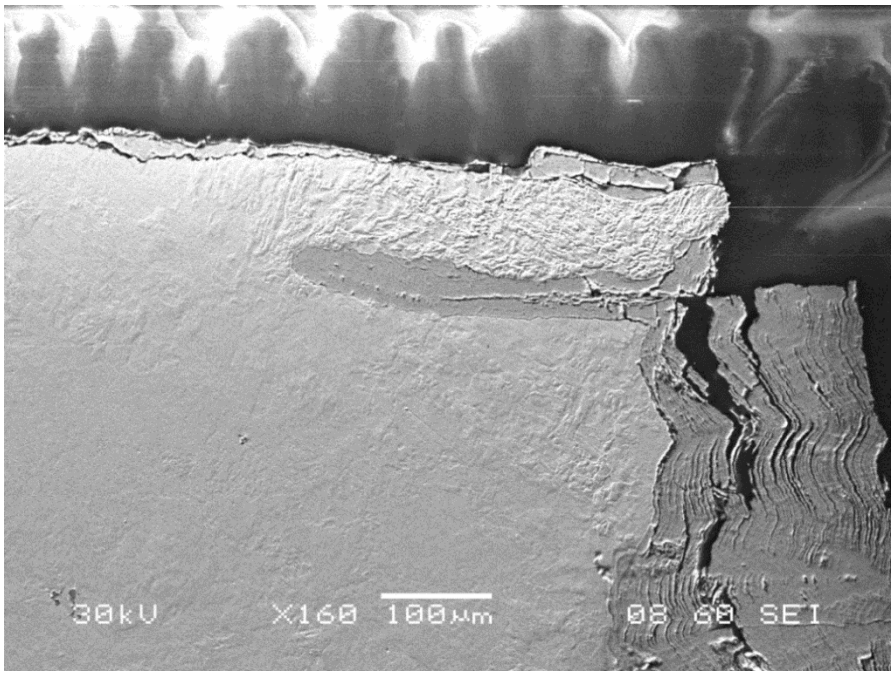

Figure A- 18. Microscopic pictures of specimen BR35 using SEM.

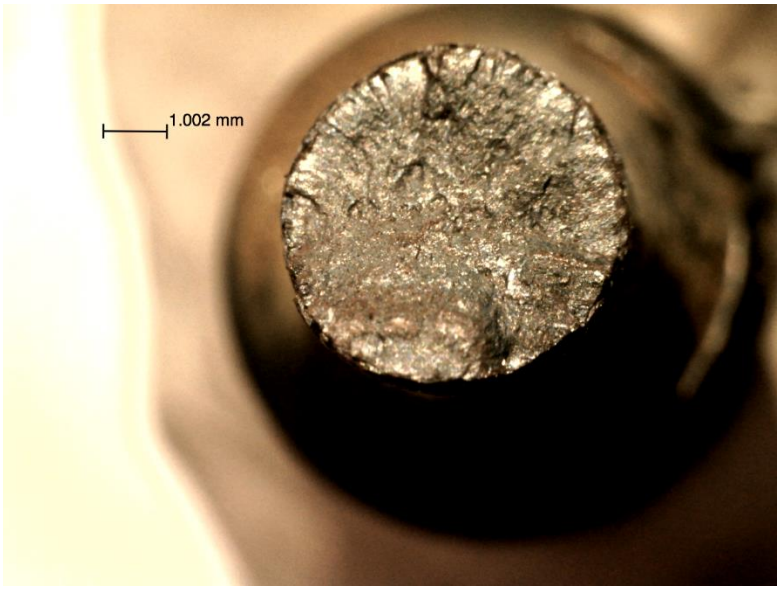

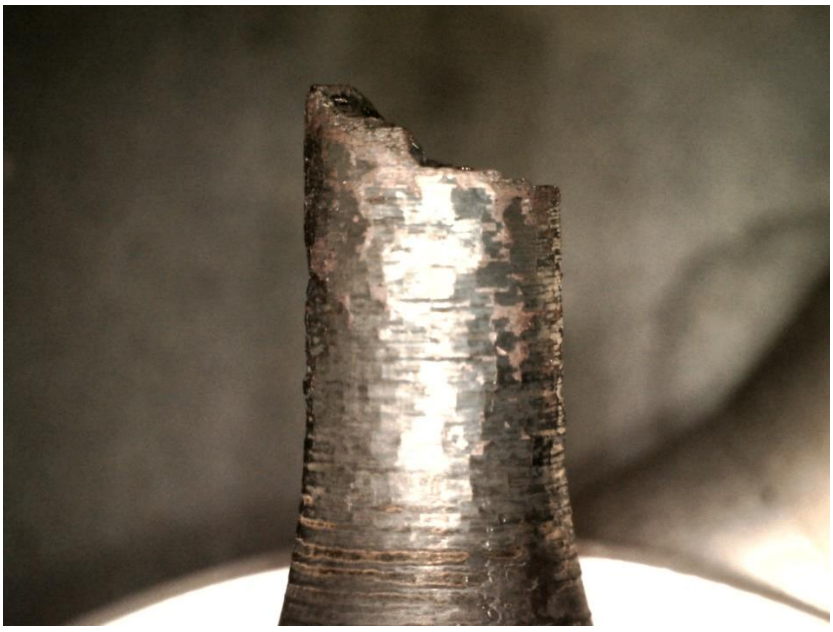

Figure A- 19. Pictures of deformed specimen BR35.

BR 29

Specimen No.	Total Strain Range, $\Delta\varepsilon$ (mm/mm)	Temperature(s), T (°C)	Strain Rate, $d\varepsilon/dt$ (mm/mm/s)	Strain Ratio, R_e	Dwell Time, t_h (sec) and Type	Cycles to Failure	Stress Range (MPa)	Mean Stress (MPa)
BR 29	0.007	600	0.001	-1	90s in Comp.	1342	622.91	-13.03

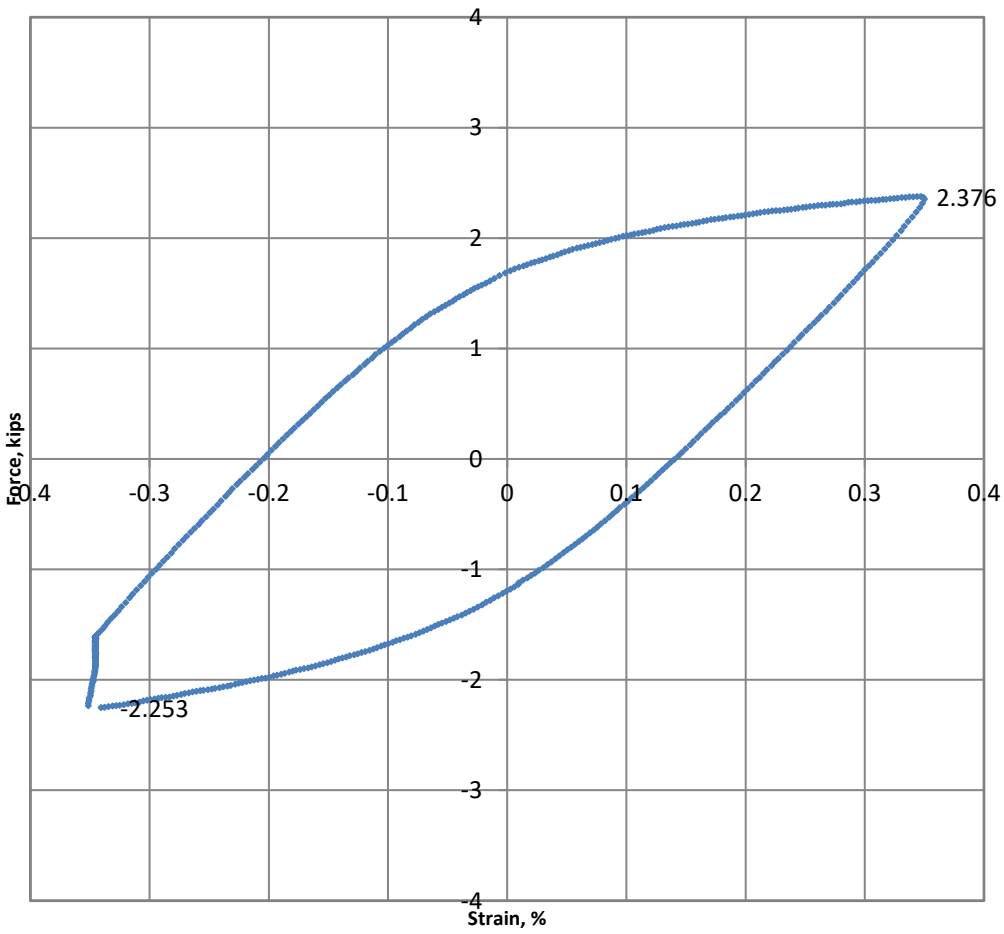

Figure A- 20. Deformation response of specimen BR29.

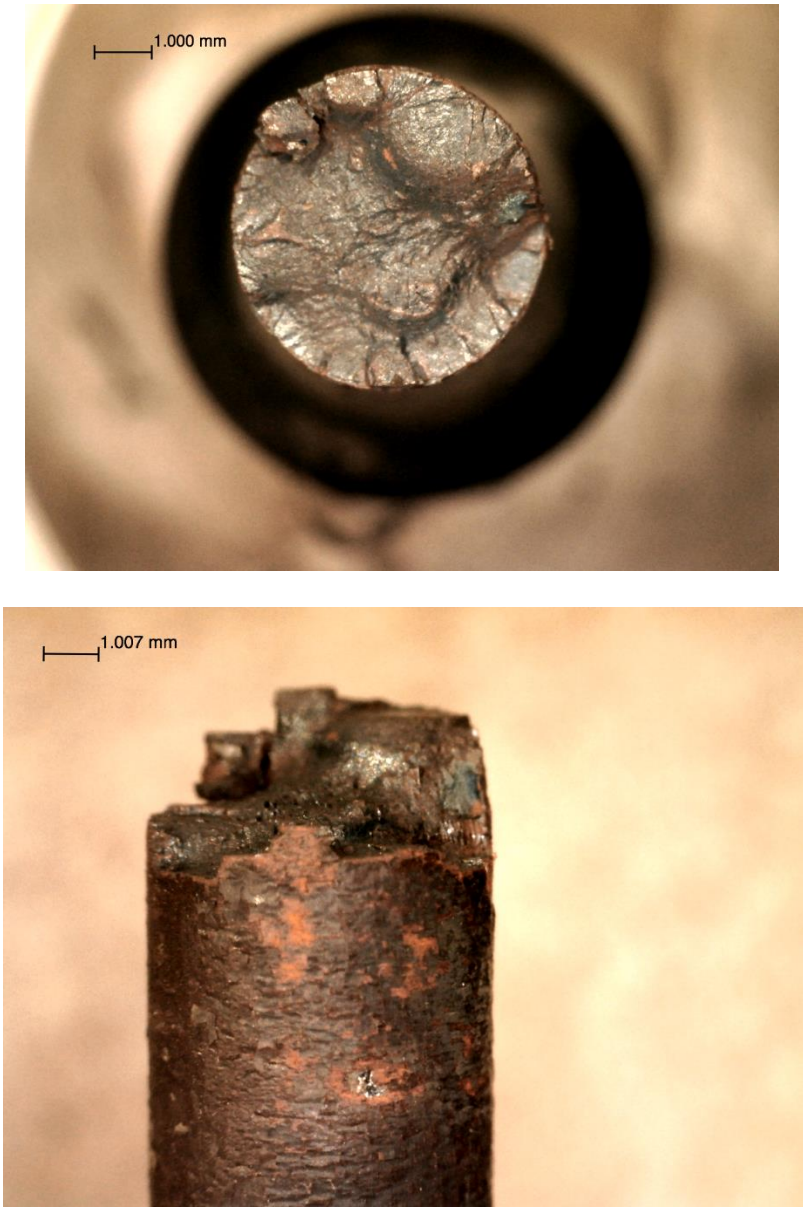

Figure A- 21. Pictures of deformed specimen BR29.

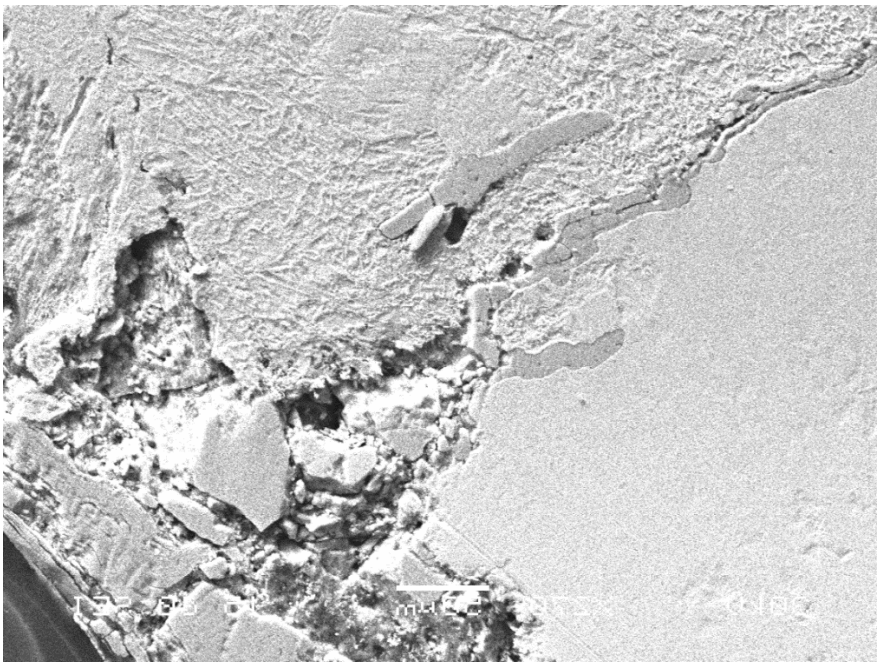

Figure A- 22. Microscopic picture of specimen BR29 using SEM.

BR 32

Specimen No.	Total Strain Range, $\Delta\varepsilon$ (mm/mm)	Temperature(s), T (°C)	Strain Rate, $d\varepsilon/dt$ (mm/mm/s)	Strain Ratio, R_e	Dwell Time, t_h (sec) and Type	Cycles to Failure	Stress Range (MPa)	Mean Stress (MPa)
BR 32	0.005	600	0.001	-1	0s	3242	642.74	0.46

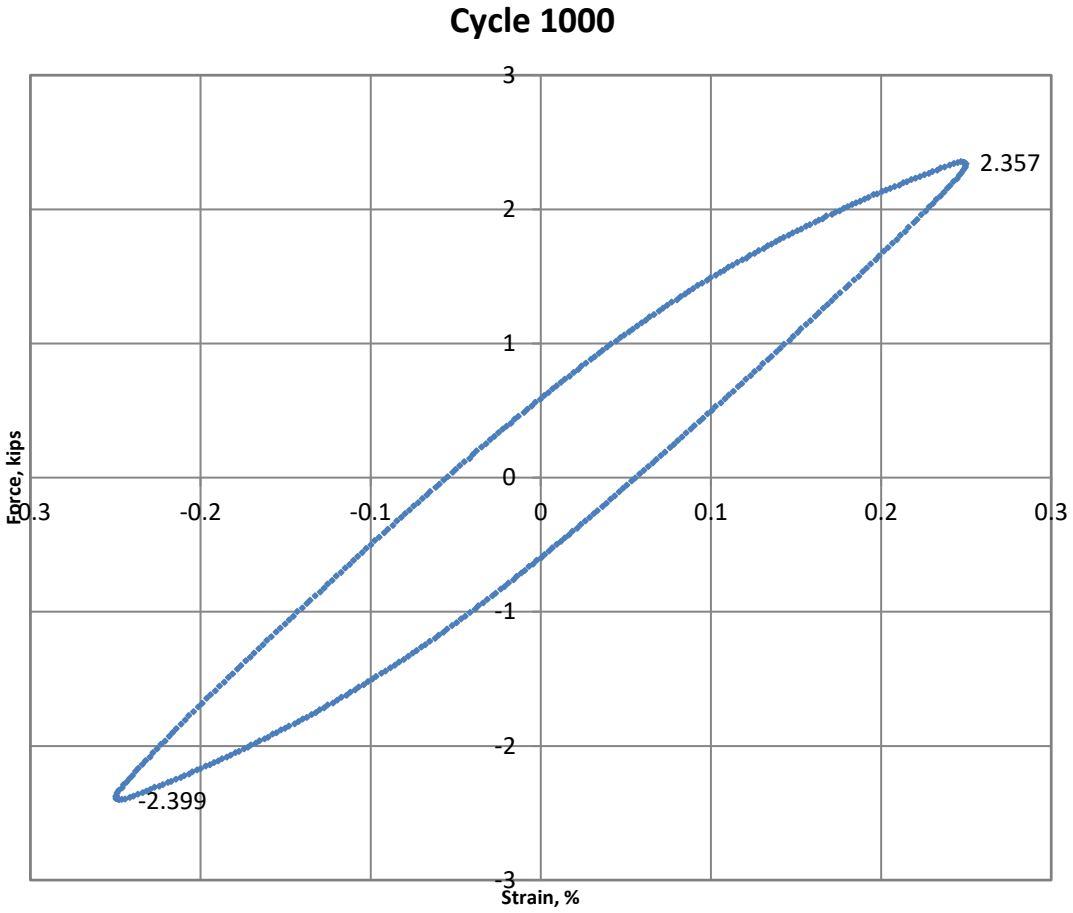

Figure A- 23. Deformation response of specimen BR32.

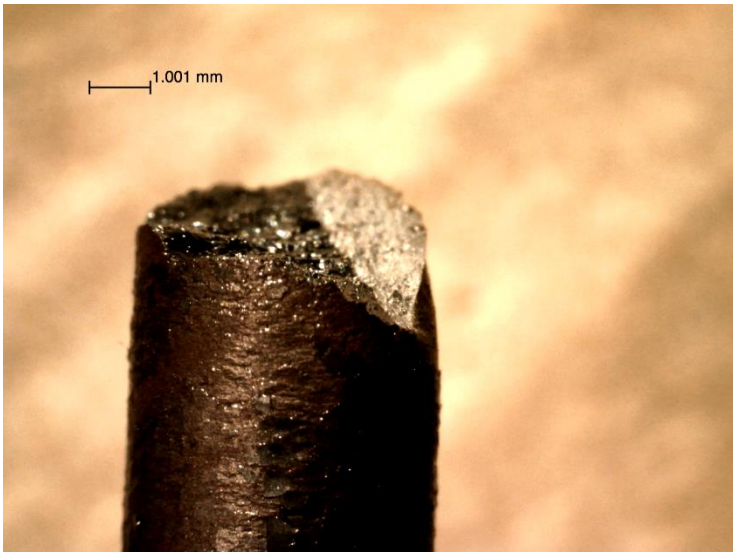

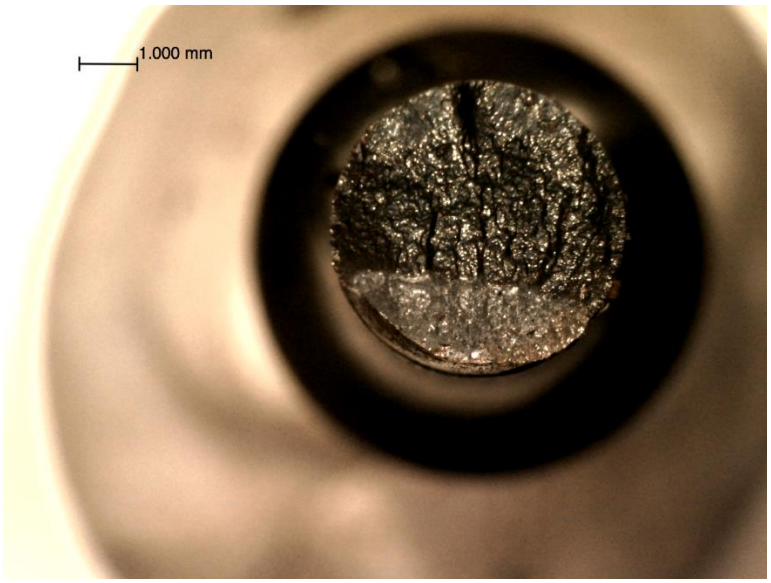

Figure A- 24. Pictures of deformed specimen BR32.

BR 33

Specimen No.	Total Strain Range, $\Delta\varepsilon$ (mm/mm)	Temperature(s), T (°C)	Strain Rate, $d\varepsilon/dt$ (mm/mm/s)	Strain Ratio, R_e	Dwell Time, t_h (sec) and Type	Cycles to Failure	Stress Range (MPa)	Mean Stress (MPa)
BR 33	0.007	650	0.001	-1	90s in Comp.	797	N/A	N/A

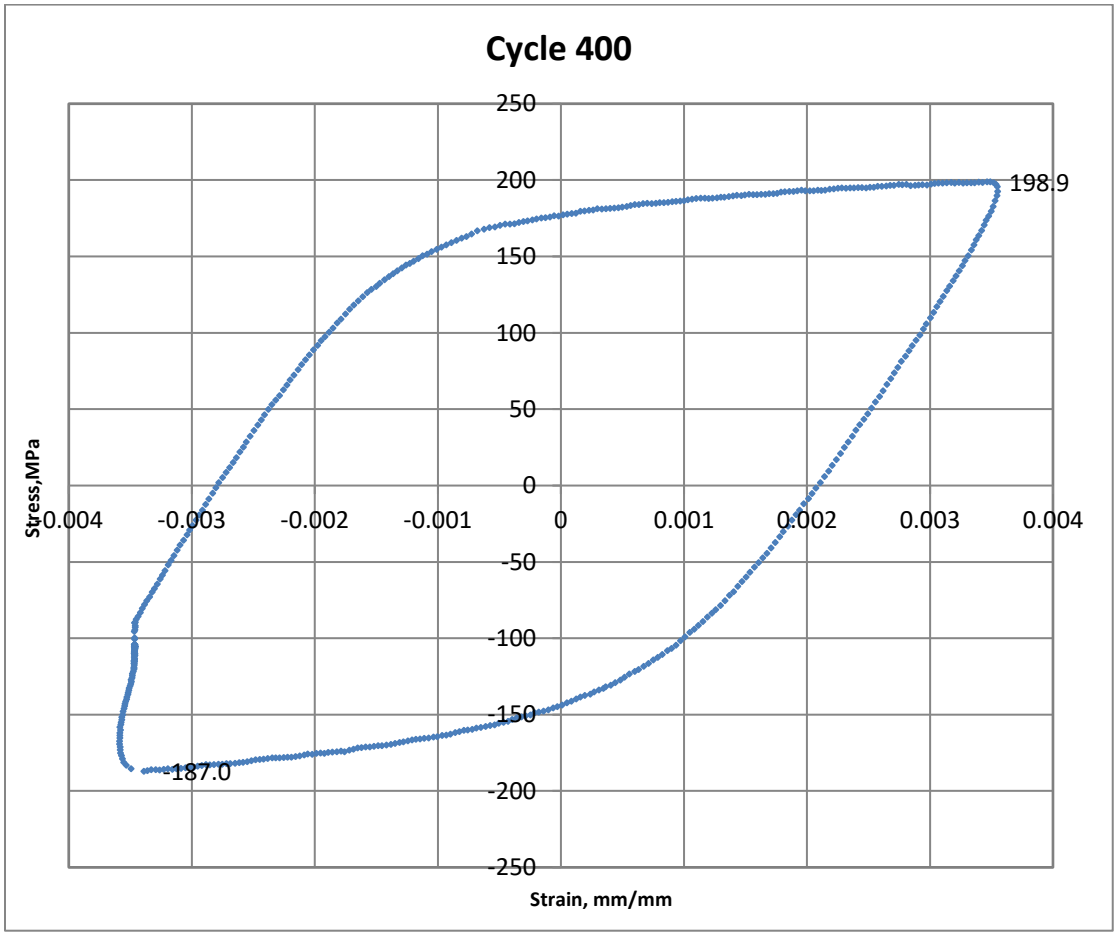

Figure A- 25. Deformation response of specimen BR33.

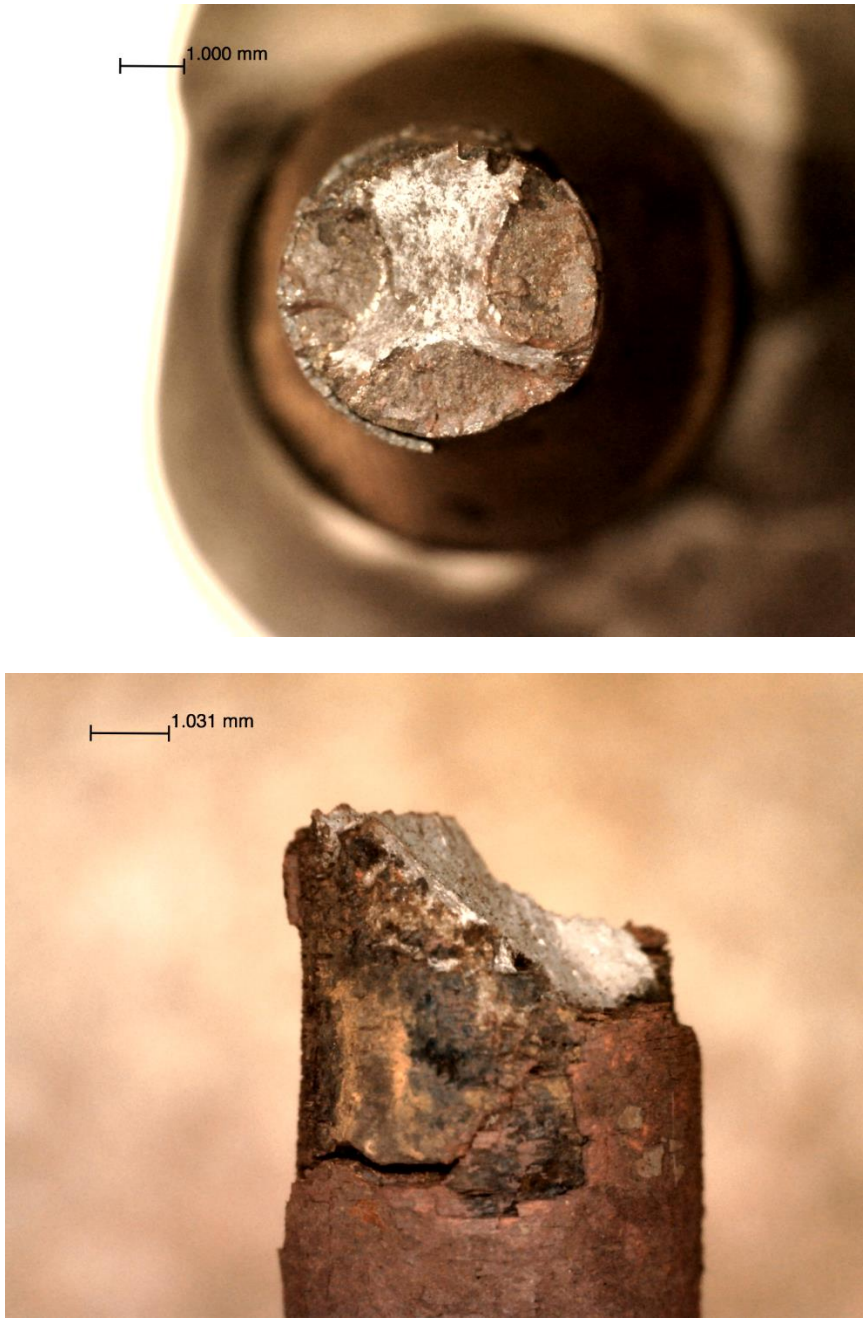

Figure A- 26. Pictures of deformed specimen BR33.

BR 34

Specimen No.	Total Strain Range, $\Delta\varepsilon$ (mm/mm)	Temperature(s), T (°C)	Strain Rate, $d\varepsilon/dt$ (mm/mm/s)	Strain Ratio, R_e	Dwell Time, t_h (sec) and Type	Cycles to Failure	Stress Range (MPa)	Mean Stress (MPa)
BR 34	0.007	600	0.001	-1	0	1220	636.64	-3.72

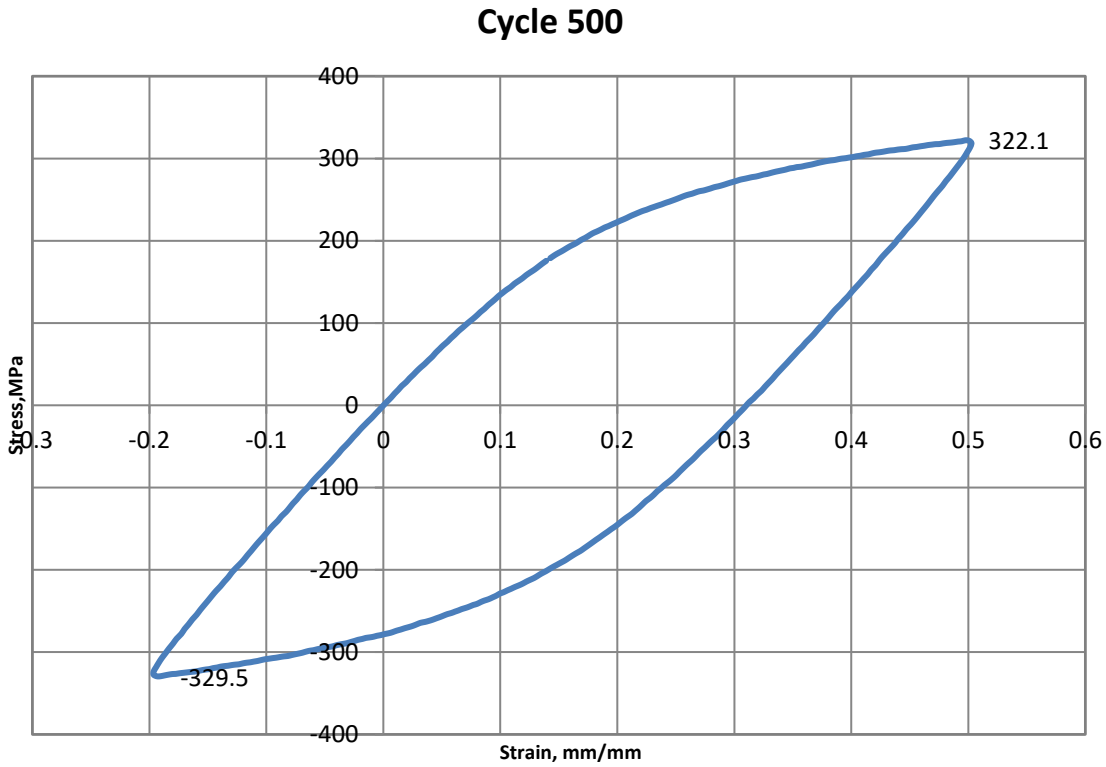

Figure A- 27. Deformation response of specimen BR34.

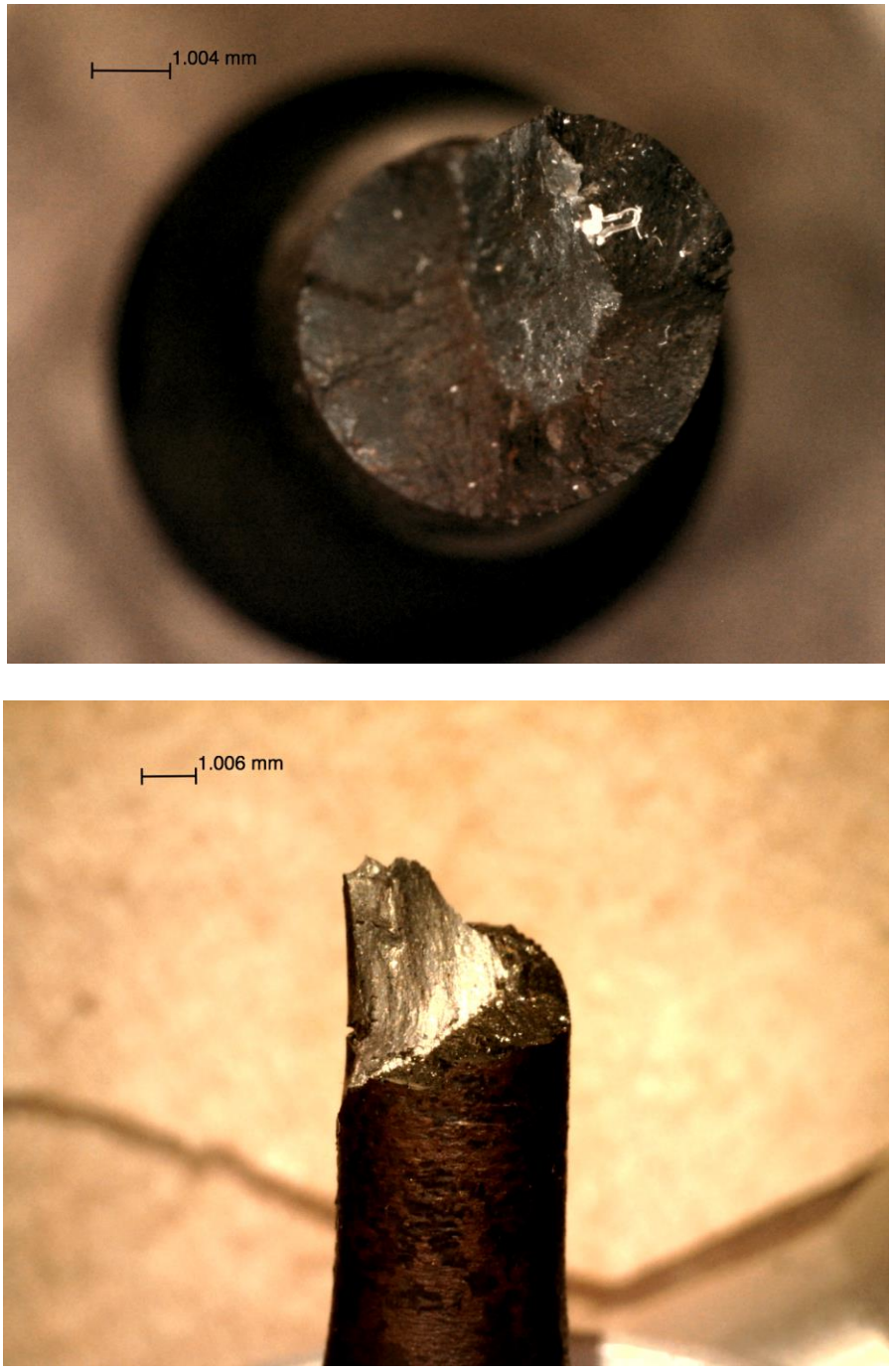

Figure A- 28. Pictures of deformed specimen BR34.

BR 31

Specimen No.	Total Strain Range, $\Delta\varepsilon$ (mm/mm)	Temperature(s), T (°C)	Strain Rate, $d\varepsilon/dt$ (mm/mm/s)	Strain Ratio, R_e	Dwell Time, t_h (sec) and Type	Cycles to Failure	Stress Range (MPa)	Mean Stress (MPa)
BR 31	0.0035	600	0.001	-1	90s in Tens.	5778(Runout)	476.00	-33.00

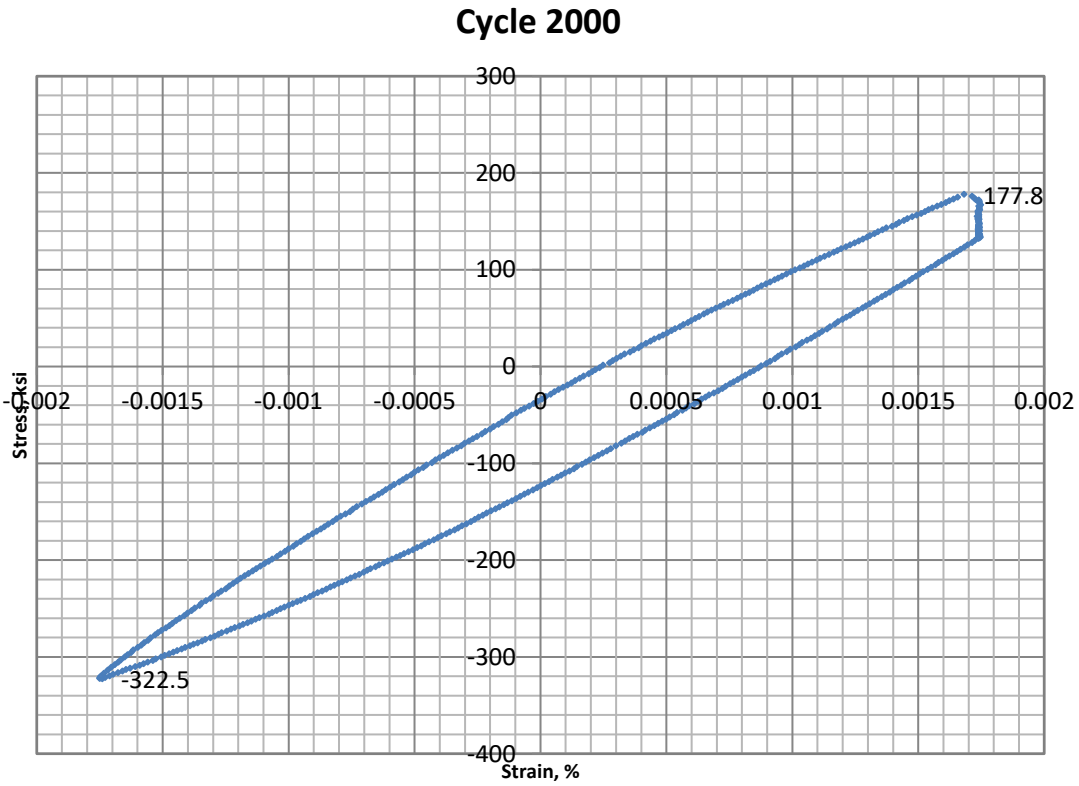

Figure A- 29. Deformation response of specimen BR31.

BR 36

Specimen No.	Total Strain Range, $\Delta\varepsilon$ (mm/mm)	Temperature(s), T (°C)	Strain Rate, $d\varepsilon/dt$ (mm/mm/s)	Strain Ratio, R_e	Dwell Time, t_h (sec) and Type	Cycles to Failure	Stress Range (MPa)	Mean Stress (MPa)
BR 36	0.007	600	0.001	-∞	90s in Comp.	938	606.18	-3.98

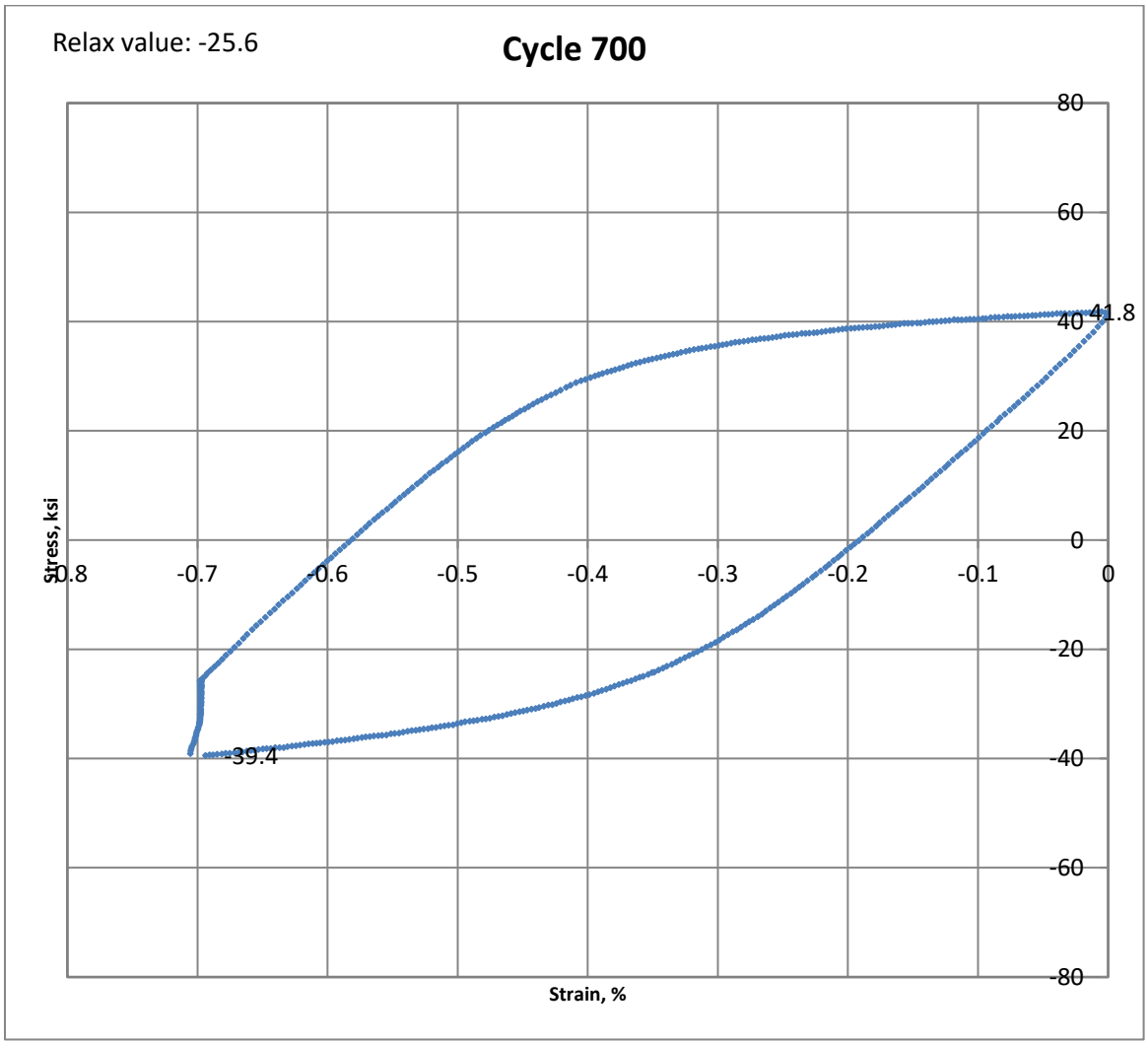

Figure A- 30. Deformation response of specimen BR36.

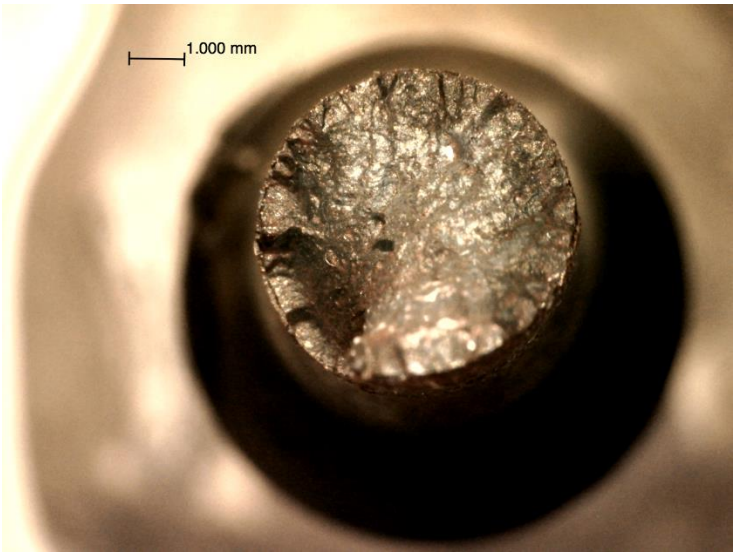

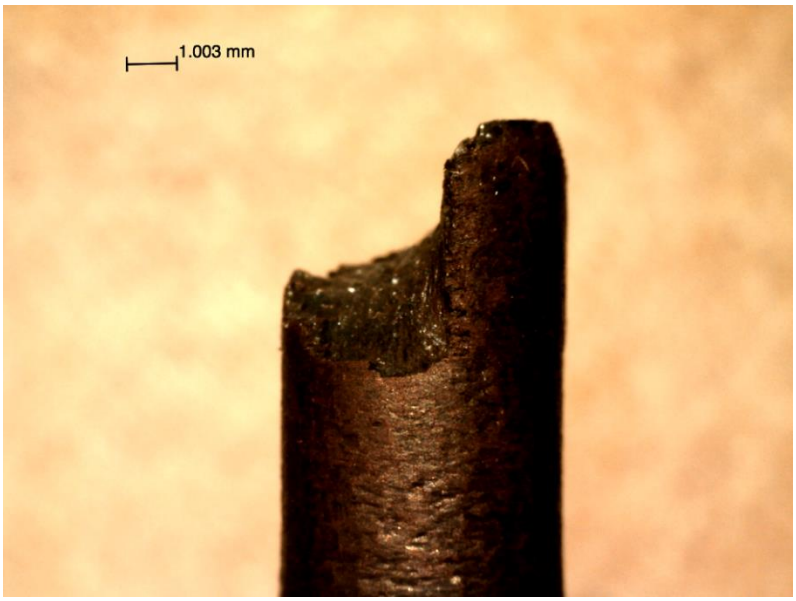

Figure A- 31. Pictures of deformed specimen BR36.

APPENDIX B: CODE

```
!!!!!!!!!!!!!!!!!!!!!!!!!!!!!!!!!!!!!!!!!!!!!!!!!!!!!!!!!!!!!!!!!!!!!!!!!!!
! ANSYS Finite Element Modeling (FEM) Simulation of Fatigue
!!!!!!!!!!!!!!!!!!!!!!!!!!!!!!!!!!!!!!!!!!!!!!!!!!!!!!!!!!!!!!!!!!!!!!!!!!!
! Author: Various ( Bouchenot, Keller, Mutter, Irmak)
! ver. 22
! Date: 4/28/17
!!!!!!!!!!!!!!!!!!!!!!!!!!!!!!!!!!!!!!!!!!!!!!!!!!!!!!!!!!!!!!!!!!!!!!!!!!!
Finish
/Clear
/Prep7
Cl='Cl1'    ! Class: 1-Single Element Parametric Simulation
St='St1'    ! Study: 1-Isothermal Fatigue in L-orientation
Ph='Ph1a'   ! Phase: 1a
!        Strain Rate:   0.01s^-1 or 0.01/300S^-1
!        Temperatures:  20 to 1050C
!        Strain Ranges: 0% to 3% (by 0.1%)
!        M Ratio:  -1,0,or 1 (Note: M = A^-1)
!
!!!!!!!!!!!!!!!!!!!!!!!!!!!!!!!!!!!!!!!!!!!!!!!!!!!!!!!!!!!!!!!!!!!!!!!!!!!
!
! Description: A Solid185 Element is subjected to strain-controlled
! fatigue in units of (m, N, MPa). Results are collected in a text file
! for later post-processing.
!
!!!!!!!!!!!!!!!!!!!!!!!!!!!!!!!!!!!!!!!!!!!!!!!!!!!!!!!!!!!!!!!!!!!!!!!!!!!

/inquire, numtes,lines,testconditions,csv

!!!!!!!!!!!!!!!!!!!!!!!!!!!!!!!!!!!!!!!!!!!!!!!!!!!!!!!!!!!!!!!!!!!!!!!!!!!
! Parametric File Setup
!
! Thermal Cycling
isotherm=1.0           ! 0=Yes, 1=No
SINGLEHOLD=1           ! 0=two holds (normal), 1= single hold at the max
temperature
firstholdon=0          ! Different first hold than rest of cycles
holdnumber_ini=1 ! For use when singlehold=1
holdnumber_inc=2 ! 1=0hr, 2=2/60hr, 3=20hr
holdnumber_fin=1
!tmt_ini=100.0   !100  ! Initial Min temperature [degrees C]
!tmt_inc=850.0         ! Increment Min temperature [degrees C]
!tmt_fin=950.0         ! Final Min temperature [degrees C]
!tmc_ini=100.0   !100  ! Initial Max temperature [degrees C]
!tmc_inc=850.0         ! Increment Max temperature [degrees C]
!tmc_fin=950.0 !1050.0       ! Final Max temperature [degrees C]
!
! Mechanical Cycling
!sr_ini=0.002    !0.001      ! Initial Strain range [mm/mm]
!sr_inc=0.002          ! Increment Strain range  [mm/mm]
!sr_fin=0.01     !0.03       ! Final Strain range [mm/mm]
```

```
!mrat_ini=0            ! -1=ZtC, 0=CR, 1=ZtT, 2= SR of 0.05
!mrat_inc=-1
!mrat_fin=0
!
! Material Orientation
ang_ini=0.0         ! 90 is L-oriented 0 is T-oriented
ang_inc=-45.0
ang_fin=0.0 !90.0

!!!!!!!!!!!!!!!!!!!!!!!!!!!!!!!!!!!!!!!!!!!!!!!!!!!!!!!!!!!!!!!!!!!!!!!!!!!
! Parametric Simulation Initiation
!
I=1
J=1
K=1
L=1
M=1
!*DO,tmc,tmc_ini,tmc_fin,tmc_inc        ! Compressive temperature [degrees
C]
!*DO,tmt,tmt_ini,tmt_fin,tmt_inc        ! Tensile temperature [degrees C]
!*DO,tempstuff,2,4,1         ! temperature stuff [degrees C]
!*DO,mrat,mrat_ini,mrat_fin,mrat_inc          ! Strain ratio [unitless]
!*DO,sr,sr_ini,sr_fin,sr_inc      ! Strain range [mm/mm]
*DO,ang,ang_ini,ang_fin,ang_inc         ! Strain range [mm/mm]
*DO,holdnumber,holdnumber_ini,holdnumber_fin,holdnumber_inc    !hold  time
for single hold
!*DO,strainstuff,1,4,1
*DO,csvlist,1,numtes,1

PARSAV,,FEA_Parameters1,txt
*IF,I,GT,1,THEN
!!!!!!!!!!!!!!!!!!!!!!!!!!!!!!!!!!!!!!!!!!!!!!!!!!!!!!!!!!!!!!!!!!!!!!!!!!!


!!!!!!!!!!!!!!!!!!!!!!!!!!!!!!!!!!!!!!!!!!!!!!!!!!!!!!!!!!!!!!!!!!!!!!!!!!!
!
! File Naming Convention
Finish
/clear
/PREP7
PARRES,,FEA_Parameters1,txt
*ENDIF
Finish
/FILNAME, C1-S1-Ph1a
/title, C1-S1-Ph1a Isothermal Fatigue Simulation
/prep7
/OUTPUT, FEA_Junk1,txt,,
!!!!!!!!!!!!!!!!!!!!!!!!!!!!!!!!!!!!!!!!!!!!!!!!!!!!!!!!!!!!!!!!!!!!!!!!!!!

! Simulations set conditions
```

```
/inquire, numtes,lines,testconditions,csv
*DIM,tespar,array,numtes,7
*VREAD,tespar(1,1),testconditions,csv,,JIK,7,numtes
(E11.5,F10.0,F10.0,F10.0,E11.5,F10.0,F10.0)


sr=tespar(csvlist,1)         ! Strain Range
tmc=tespar(csvlist,2)        ! Temperature in compression
tmt=tespar(csvlist,3)        ! Temperature in tension
mrat=tespar(csvlist,4)       ! Strain Ratio -1=ZtC, 0=CR, 1=ZtT
strain_rate=tespar(csvlist,5)     ! Strain rate mm/mm/sec
holdtime=tespar(csvlist,6)   ! Dwell in seconds
dwelltype=tespar(csvlist,7)       !1=dwell   in   tension,   0=dwell   in
compression

holdtime=holdtime/3600
*IF, holdtime, eq, 0, then
holdtime=1.02e-2/3600
*ENDIF
!!!!!!!!!!!!!!!!!!!!!!!!!!!!!!!!!!!!!!!!!!!!!!!!!!!!!!!!!!!!!!!!!!!!!!!!!!!
!
! Dwells
!
!*IF, holdnumber, EQ, 1, THEN
!holdtime=1.02e-2/3600
!*ENDIF

!*IF, holdnumber, EQ, 2, THEN
!holdtime=20/60
!*ENDIF

!*IF, holdnumber, EQ, 3, THEN
!holdtime=20
!*ENDIF
!!!!!!!!!!!!!!!!!!!!!!!!!!!!!!!!!!!!!!!!!!!!!!!!!!!!!!!!!!!!!!!!!!!!!!!!!!!


!!!!!!!!!!!!!!!!!!!!!!!!!!!!!!!!!!!!!!!!!!!!!!!!!!!!!!!!!!!!!!!!!!!!!!!!!!!
!
! Define the specimen dimensions
!
side_length=1.00   ! in units of mm
!!!!!!!!!!!!!!!!!!!!!!!!!!!!!!!!!!!!!!!!!!!!!!!!!!!!!!!!!!!!!!!!!!!!!!!!!!!


!!!!!!!!!!!!!!!!!!!!!!!!!!!!!!!!!!!!!!!!!!!!!!!!!!!!!!!!!!!!!!!!!!!!!!!!!!!
!
! Define the nodes
! Total of 8 Nodes
```

```
N, 1 ,0,0,0                                ! Node,number,xcord,ycord,zcord

N, 2 ,side_length,0,0
N, 3 ,side_length,side_length,0
N, 4 ,0,side_length,0
N, 5 ,0,0,side_length
N, 6 ,1,0,side_length
N, 7 ,side_length,side_length,side_length
N, 8 ,0,side_length,side_length
!
! Create Node Groups
!
! All Nodes - NDALL
NSEL, S , node , , 1 , 8 , 1
CM, NDALL , NODE
!
! Bottom Nodes - BOTTOM
NSEL, S , node , , 1 , 4 , 1
CM, BOTTOM , NODE
!
! Top Nodes - TOP
NSEL, S , node , , 5 , 8 , 1
CM, TOP , NODE
!
! Clear Selected Nodes
NSEL, ALL
!!!!!!!!!!!!!!!!!!!!!!!!!!!!!!!!!!!!!!!!!!!!!!!!!!!!!!!!!!!!!!!!!!!!!!!!!!!!!!!

!!!!!!!!!!!!!!!!!!!!!!!!!!!!!!!!!!!!!!!!!!!!!!!!!!!!!!!!!!!!!!!!!!!!!!!!!!!!!!!
!
! Define a local system to transform material properties into desired
orientation
local,11,0,0,0,0,0,0,ang,,        ! use this one to rotate in the transverse
plane..
!local,11,0,0,0,0,0,ang,0,,         ! ...or this one to rotate from T to L
ESYS,11                             ! the local system is selected for all
defined elements
!
! Define the elements
ET, 1 , Solid185 , 0
!
! Assign elements to nodes
E, 1 , 2 , 3 , 4 , 5 , 6 , 7 , 8
!
!!!!!!!!!!!!!!!!!!!!!!!!!!!!!!!!!!!!!!!!!!!!!!!!!!!!!!!!!!!!!!!!!!!!!!!!!!!!!!!

!!!!!!!!!!!!!!!!!!!!!!!!!!!!!!!!!!!!!!!!!!!!!!!!!!!!!!!!!!!!!!!!!!!!!!!!!!!!!!!
! Define the material: Generic materials
!!!!!!!!!!!!!!!!!!!!!!!!!!!!!!!!!!!!!!!!!!!!!!!!!!!!!!!!!!!!!!!!!!!!!!!!!!!!!!!
!
```

```
! Elastic Properties (Hooke's Law):
MPTEMP,1,20,300,400,500,600,650
MPDATA,EX,1,1,210250,194000,192000,175750,150111,135000     !   Long
MPDATA,EY,1,1,210250,194000,192000,175750,150111,135000     !   Trans
MPDATA,EZ,1,1,210250,194000,192000,175750,150111,135000     !   Trans
MPDATA,PRYZ,1,1,0.28,0.28,0.28,0.28,0.28,0.28     !   TT
MPDATA,PRXZ,1,1,0.28,0.28,0.28,0.28,0.28,0.28    !   TL
MPDATA,PRXY,1,1,0.28,0.28,0.28,0.28,0.28,0.28    !   TL
!MPDATA,GXY,1,1,82128.90625,75781.25,75000,68652.34375,58637.10938,52734.3
75    !   TL
!MPDATA,GYZ,1,1,82128.90625,75781.25,75000,68652.34375,58637.10938,52734.3
75     !   TT
!MPDATA,GXZ,1,1,82128.90625,75781.25,75000,68652.34375,58637.10938,52734.3
75     !   TL

!Chaboche Nonlinear Kinematic Hardening
TB,CHABOCHE,1,6,3
TBTEMP,20.0
TBDATA,1,222.485067943644
TBDATA,2,698795.564851908,12470.3174452236
TBDATA,4,72594.4833738968,687.870306390038
TBDATA,6,23674.4103784525,12361.8866420616
TBTEMP,300.0
TBDATA,1,222.485067943644
TBDATA,2,698795.564851908,12470.3174452236
TBDATA,4,72594.4833738968,687.870306390038
TBDATA,6,23674.4103784525,12361.8866420616
TBTEMP,400.0
TBDATA,1,183.854862043917
TBDATA,2,675699.819324699,12565.8484992949
TBDATA,4,71805.7860174683,676.72024660815
TBDATA,6,23472.1777430697,12365.2284838343
TBTEMP,500.0
TBDATA,1,153.847065876695
TBDATA,2,492328.168153631,13014.8925795605
TBDATA,4,50624.0517109629,697.52862288703
TBDATA,6,16234.8831948607,12382.4552966344
TBTEMP,600.0
TBDATA,1,113.882540456542
TBDATA,2,269943.63579227,12337.610864522
TBDATA,4,26181.3447915656,697.45813125425
TBDATA,6,8319.23980621895,12360.1942855914
TBTEMP,650.0
TBDATA,1,101.848172325387
TBDATA,2,175829.159728268,12271.9878699204
TBDATA,4,16518.2421066805,713.161220823948
TBDATA,6,5270.86586470823,12358.1998213818
```

```
TB,Creep,1,64,,8
TBTEMP,20
TBDATA,1,1.04321036178893E-26,1.36402571928738E-21,202387563394369000
TBTEMP,30
TBDATA,1,2.10267690491891E-24,3.86146825215365E-19,1398742508781110
TBTEMP,40
TBDATA,1,9.07341609139978E-23,2.12043236703163E-17,41008785541761
TBTEMP,50
TBDATA,1,1.6825734106384E-21,4.74044189814308E-16,2653980022426.58
TBTEMP,60
TBDATA,1,1.82882217843288E-20,6.00280636233843E-15,283420238915.46
TBTEMP,70
TBDATA,1,1.37487731928092E-19,5.13493348477528E-14,42762923921.0111
TBTEMP,80
TBDATA,1,7.89168537652321E-19,3.29629666037701E-13,8309406286.65602
TBTEMP,90
TBDATA,1,3.68614260234154E-18,1.69935550805492E-12,1958776168.70891
TBTEMP,100
TBDATA,1,1.46343338009681E-17,7.36920594144434E-12,537762774.285356
TBTEMP,110
TBDATA,1,5.09394430048429E-17,2.77831011628015E-11,167012132.241021
TBTEMP,120
TBDATA,1,1.59063456325782E-16,9.33160183400045E-11,57428033.6249267
TBTEMP,130
TBDATA,1,4.53399714637635E-16,2.84440032618856E-10,21509540.8809253
TBTEMP,140
TBDATA,1,1.19581193299036E-15,7.98245884202266E-10,8664838.62349911
TBTEMP,150
TBDATA,1,2.94967121007139E-15,2.08617435757263E-09,3716590.28557646
TBTEMP,160
TBDATA,1,6.86386444252921E-15,5.1242245884141E-09,1683693.67501521
TBTEMP,170
TBDATA,1,1.51746862894798E-14,1.19189381089857E-08,800268.945026347
TBTEMP,180
TBDATA,1,3.20605573222315E-14,2.64171589393171E-08,396897.074502411
TBTEMP,190
TBDATA,1,6.50510154532827E-14,5.60843361906666E-08,204451.678754043
TBTEMP,200
TBDATA,1,1.27283436457549E-13,1.14557244607703E-07,108964.196777442
TBTEMP,210
TBDATA,1,2.4102580133632E-13,2.25978227219182E-07,59884.5003672486
TBTEMP,220
TBDATA,1,4.43050394030303E-13,4.318993852469E-07,33840.837841397
TBTEMP,230
TBDATA,1,7.92662130229135E-13,8.02031504076079E-07,19614.9898761369
TBTEMP,240
TBDATA,1,1.38346873942576E-12,1.45063471203488E-06,11636.3568764383
TBTEMP,250
TBDATA,1,2.36034282612863E-12,2.56104354242808E-06,7051.87431392224
TBTEMP,260
```

```
TBDATA,1,3.94348485915592E-12,4.42173371891888E-06,4358.37130648588
TBTEMP,270
TBDATA,1,6.46207092160048E-12,7.47852618274407E-06,2743.03816107324
TBTEMP,280
TBDATA,1,1.04006820028863E-11,1.24090505463236E-05,1755.71316194288
TBTEMP,290
TBDATA,1,1.64625882673325E-11,2.02275319546282E-05,1141.5000614551
TBTEMP,300
TBDATA,1,2.5655031048489E-11,3.24304121873854E-05,753.074207780295
TBTEMP,310
TBDATA,1,3.94029399687191E-11,5.11963725680151E-05,503.643519492298
TBTEMP,320
TBDATA,1,5.96990792683787E-11,7.96581143564453E-05,341.158476729995
TBTEMP,330
TBDATA,1,8.9300477196681E-11,0.000122267911863631,233.881062786923
TBTEMP,340
TBDATA,1,1.31983200899962E-10,0.000185284645220206,162.154516769235
TBTEMP,350
TBDATA,1,1.9287014740952E-10,0.000277416927040761,113.625107287382
TBTEMP,360
TBDATA,1,2.78849585243707E-10,0.00041066526875469 8,80.4212805245645
TBTEMP,370
TBDATA,1,3.99105762731809E-10,0.000601416224336303,57.4619821936661
TBTEMP,380
TBDATA,1,5.65787066535227E-10,0.000871853368016418,41.4270269727004
TBTEMP,390
TBDATA,1,7.9484204164013E-10,0.00125176410779136,30.1216098123312
TBTEMP,400
TBDATA,1,1.1070591539583E-09,0.0017808380436626 8,22.078873338028
TBTEMP,410
TBDATA,1,1.52935257763561E-09,0.00251157222318058,16.3082318065366
TBTEMP,420
TBDATA,1,2.09634361811484E-09,0.00351292164410451,12.1340985169663
TBTEMP,430
TBDATA,1,2.85229574411571E-09,0.00487486016785121,9.09137560929322
TBTEMP,440
TBDATA,1,3.85347071093311E-09,0.00671404815047798,6.85700068875875
TBTEMP,450
TBDATA,1,5.17098403701914E-09,0.00918083913632274,5.20465234633217
TBTEMP,460
TBDATA,1,6.89425027865994E-09,0.0124678995166636,3.97448785757109
TBTEMP,470
TBDATA,1,9.13512227688092E-09,0.0168207628171951,3.05273654954142
TBTEMP,480
TBDATA,1,1.20328439805068E-08,0.0225506949952919,2.35781712882926
TBTEMP,490
TBDATA,1,1.57599537448476E-08,0.0300503096233086,1.83081326060791
TBTEMP,500
TBDATA,1,2.05292943439424E-08,0.0398124430056856,1.42888622481007
TBTEMP,510
```

```
TBDATA,1,2.66023075052403E-08,0.0524528801042812,1.12068356272479
TBTEMP,520
TBDATA,1,3.42988147816118E-08,0.0687376136931571,0.883115104611307
TBTEMP,530
TBDATA,1,4.40085132328374E-08,0.0896154225876375,0.699072984230785
TBTEMP,540
TBDATA,1,5.62044439275609E-08,0.116256671346847,0.555808182052799
TBTEMP,550
TBDATA,1,7.14587239423025E-08,0.150099364891466,0.443766929483896
TBTEMP,560
TBDATA,1,9.04608685871299E-08,0.192903638476136,0.355751427229084
TBTEMP,570
TBDATA,1,1.14039070304608E-07,0.246816027991576,0.286310792359436
TBTEMP,580
TBDATA,1,1.43184844363275E-07,0.31444504935118,0.231296481023903
TBTEMP,590
TBDATA,1,1.79081499409801E-07,0.39894982057553,0.18753593151083
TBTEMP,600
TBDATA,1,2.23136943484289E-07,0.504143688098746,0.152591681850115
TBTEMP,610
TBDATA,1,2.77021393588514E-07,0.634615071899379,0.124582638050322
TBTEMP,620
TBDATA,1,3.42710619694718E-07,0.795868024574668,0.102050781846273
TBTEMP,630
TBDATA,1,4.22535422580095E-07,0.994485309859089,0.0838612764379509
TBTEMP,640
TBDATA,1,5.19238119478202E-07,1.23831714893439,0.0691272456337286
TBTEMP,650
TBDATA,1,6.36036892683135E-07,1.536699160962,0.0571528713708136



!!!!!!!!!!!!!!!!!!!!!!!!!!!!!!!!!!!!!!!!!!!!!!!!!!!!!!!!!!!!!!!!!!!!!!!!!!!
!
! Create Boundary Conditions
!
! Left Boundary
D, 1 , UX , 0          ! Fixed X displacement on LEFT nodes
D, 4 , UX , 0          ! Fixed X displacement on LEFT nodes
D, 5 , UX , 0          ! Fixed X displacement on LEFT nodes
D, 8 , UX , 0          ! Fixed X displacement on LEFT nodes
!
! Bottom Boundary
D, BOTTOM , UZ , 0     ! Fixed Z displacement on BOTTOM nodes
!
D, 1, UY, 0
!!!!!!!!!!!!!!!!!!!!!!!!!!!!!!!!!!!!!!!!!!!!!!!!!!!!!!!!!!!!!!!!!!!!!!!!!!!
```

```
!!!!!!!!!!!!!!!!!!!!!!!!!!!!!!!!!!!!!!!!!!!!!!!!!!!!!!!!!!!!!!!!!!!!!!!!!!
!
! Define Fatigue Cycling Parameters:
!
! Mechanical Loading
strain_range = sr                       ! Difference in Max and Min strains
[mm/mm]
tol=0.0001
re=(mrat-1+tol)/(mrat+1+tol)                 ! Strain ratio (0 = Z-to-T, -
1 = CR, -900 = Z-to-C)
strain_ratio=re
*IF, mrat, EQ, 2, THEN
strain_ratio=0.05
*ENDIF
tens_hold = 18        !1.01e-2/3600                        ! Tension hold
[hr]
comp_hold = 1.02e-2/3600                !1.00e-2/3600         !18.0
           ! Compression hold [hr]
first_hold = 20       !5000.0                      !5000.00 !
      ! First hold [hr] ex:5000 hr hold
displ_range = strain_range*side_length            ! Displacement [mm]
displ_max = displ_range/(1.0-strain_ratio)                ! Displacement
[mm]
displ_min = displ_max-displ_range            ! Displacement [mm]
displ_mean = 0.5*(displ_max+displ_min)            ! Displacement [mm]
strain_rate_hr = strain_rate*3600.0               !     Strain     rate
[mm/mm/hr]
half_cycle = strain_range/strain_rate_hr/2.0      !  Half  cycle  [hr]  !
needs to be modified for z-t and z-c
full_cycle = 2.0*half_cycle                  ! Full cycle [hr]
!displ_rate = displ_range/half_cycle
!
! Cycle Stepping and Ramping Time
num_cycles = 2
tot_load_steps=num_cycles*4+2
load_init_time = 1.0E-2/3600.0                    !  Initial  Load  Time
[hr]
load_mini_time = 1.0E-4/3600.0                    ! Minimum  Deltim  step
time [hr]
load_mini_dwell_time = 1.0E-4/3600.0                   ! Minimum  Deltim
step time [hr]
load_maxi_time = 1.0E-1/3600.0                    ! Maximum  Deltim  step
time [hr]
load_maxi_dwell_time = 300       !10000.0/3600.0           !   Maximum
Deltim step time [hr]
load_ramp_time = 1.0E-10/3600.0                   !  Ramp  time  used  in
Deltim [hr]
data_freq = 1.0                              ! Frequency of data capture
!
```

```
! Temperature Cycling
tmca=tmc*isotherm+(1-isotherm)*tmt
max_temp=0.5*(tmt+tmca+abs(tmt-tmca))
min_temp=0.5*(tmt+tmca-abs(tmt-tmca))
temp_range=abs(tmt-tmca)
!temp_rate=temp_range/full_cycle
!
*IF, tmt, NE, tmca, THEN                        !temp controlled strain rate
for TMF
temp_rate = 2          !3 degress per second for TMF
temp_rate_hr = temp_rate*3600.0
half_cycle = temp_range/temp_rate_hr/2.0           !  Half  cycle  [hr]  !
needs to be modified for z-t and z-c
full_cycle = 2.0*half_cycle                     ! Full cycle [hr]
*ENDIF

load_init_time = half_cycle/100.0               ! Initial Load Time [hr]
load_mini_time = half_cycle/200.0               !  Minimum  Deltim  step  time
[hr]
load_maxi_time = half_cycle/50.0                     !  Maximum  Deltim  step
time [hr]


!
!!!!!!!!!!!!!!!!!!!!!!!!!!!!!!!!!!!!!!!!!!!!!!!!!!!!!!!!!!!!!!!!!!!!!!!!!!!


!!!!!!!!!!!!!!!!!!!!!!!!!!!!!!!!!!!!!!!!!!!!!!!!!!!!!!!!!!!!!!!!!!!!!!!!!!!!
!
! Assign the Peak-Valley-Period Values (based on strain ratio and phasing)
!
! Cycling rules:
!     Rule #2: If CR and compression hold exceeds tensile hold, then go to
compression first
!        Rule #3: If zero-to-compression, proceed to minimum displacement
first
!       Rule #4: If zero-to-tension, proceed to maximum displacement first
!       Rule #5: Initial portion of the cycle goes from zero-displacement
and mean temp
!
!
peak_displ=displ_max
valley_displ=displ_min
mean_temp=0.5*(tmt+tmca)
temp_init=mean_temp
peak_temp=tmt
valley_temp=tmca
*IF,dwelltype,EQ,1,THEN
peak_hold=holdtime
```

```
valley_hold=1.01e-2/3600
*ENDIF
*IF,dwelltype,EQ,0,THEN
peak_hold=1.01e-2/3600
valley_hold=holdtime
*ENDIF


!
!
*IF, SINGLEHOLD, EQ, 0, THEN
*IF,mrat,eq,0,and,comp_hold,gt,tens_hold,THEN ! See Rule #2
peak_displ=displ_min
valley_displ=displ_max
*ENDIF
*ENDIF
!
*IF,mrat,eq,-1,THEN    ! See Rule #3 (only in Z-to-C case)
peak_displ=displ_min
valley_displ=displ_max
half_cycle=half_cycle*2
peak_temp=tmca
valley_temp=tmt
temp_init=tmt
*IF,dwelltype,EQ,0,THEN
peak_hold=holdtime
valley_hold=1.01e-2/3600
*ENDIF
*IF,dwelltype,EQ,1,THEN
peak_hold=1.01e-2/3600
valley_hold=holdtime
*ENDIF
*ENDIF
!
*IF,mrat,eq,1,THEN     ! See Rule #4 (only in Z-to-T case)
peak_displ=displ_max
valley_displ=displ_min
half_cycle=half_cycle*2
peak_temp=tmt
valley_temp=tmca
temp_init=tmca
*IF,dwelltype,EQ,1,THEN
peak_hold=holdtime
valley_hold=1.01e-2/3600
*ENDIF
*IF,dwelltype,EQ,0,THEN
peak_hold=1.01e-2/3600
valley_hold=holdtime
*ENDIF
*ENDIF
```

```
!
!*IF,mrat,eq,-1,THEN ! See Rule #5
!init_period_hr=half_cycle*peak_displ/displ_range  ! Period of Step 1 cycle
[hr]
!displ_init=0                                  !  Initial  displacement  for
Step 0 [mm]
!*ENDIF
!
!!!!!!!!!!!!!!!!!!!!!!!!!!!!!!!!!!!!!!!!!!!!!!!!!!!!!!!!!!!!!!!!!!!!!!!!!!!
!!!!!!!!!!!!!!!!!!!!!!!!!!!!!!!!!!!!!!!!!!!!!!!!!!!!!!!!!!!!!!!!!!!!!!!!!!!

! For hold only at max temp
*IF, SINGLEHOLD, EQ, 1, THEN

*IF,mrat,eq,0,and,tmca,gt,tmt,THEN ! See Rule #2
peak_displ=displ_min
valley_displ=displ_max
peak_temp=tmca
valley_temp=tmt
*ENDIF

*IF, peak_temp, GT, valley_temp, THEN
peak_hold=holdtime
valley_hold=1.01e-2/3600
*ENDIF

*IF, peak_temp, LT, valley_temp, THEN
peak_hold=1.01e-2/3600
valley_hold=holdtime
*ENDIF

!*IF, peak_temp, EQ, valley_temp, THEN
!peak_hold=holdtime
!valley_hold=holdtime
!*ENDIF



*ENDIF

!!!!!!!!!!!!!!!!!!!!!!!!!!!!!!!!!!!!!!!!!!!!!!!!!!!!!!!!!!!!!!!!!!!!!!!!!!!
!!!!!!!!!!!!!!!!!!!!!!!!!!!!!!!!!!!!!!!!!!!!!!!!!!!!!!!!!!!!!!!!!!!!!!!!!!!

! Fixing the substep times

load_init_dwell_time_peak = 1.0E-2/3600.0
load_init_dwell_time_valley = 1.0E-2/3600.0
load_init_dwell_time_first = 1.0E-2/3600.0

*IF, first_hold, GT, 2.0E-2/3600, THEN
```

```
load_init_dwell_time_first = first_hold/20
*ENDIF

*IF, peak_hold, GT, 2.0E-2/3600, THEN
load_init_dwell_time_peak = peak_hold/20
*ENDIF

*IF, valley_hold, GT, 2.0E-2/3600, THEN
load_init_dwell_time_valley = valley_hold/20
*ENDIF


!!!!!!!!!!!!!!!!!!!!!!!!!!!!!!!!!!!!!!!!!!!!!!!!!!!!!!!!!!!!!!!!!!!!!!!!!!!

!Fixing first hold


*IF, firstholdon, EQ, 0, THEN
first_hold=peak_hold
*ENDIF


!TUNIF,70

!tref,temp_init        !ignore CTE for single element case

FINISH                           ! Finish pre-processing
!!!!!!!!!!!!!!!!!!!!!!!!!!!!!!!!!!!!!!!!!!!!!!!!!!!!!!!!!!!!!!!!!!!!!!!!!!!

!!!!!!!!!!!!!!!!!!!!!!!!!!!!!!!!!!!!!!!!!!!!!!!!!!!!!!!!!!!!!!!!!!!!!!!!!!!
!
!switch back to the global system to define boundry conditions
!local,12,0,0,0,0,0,-ang,0,,          ! trying to get reference frame back
to global
!rsys,0
!
!!!!!!!!!!!!!!!!!!!!!!!!!!!!!!!!!!!!!!!!!!!!!!!!!!!!!!!!!!!!!!!!!!!!!!!!!!!

!!!!!!!!!!!!!!!!!!!!!!!!!!!!!!!!!!!!!!!!!!!!!!!!!!!!!!!!!!!!!!!!!!!!!!!!!!!
!
! Begin Initial Solution Stage
/CONFIG,NRES,500000
/NERR,5000000,5000000,,0
/SOLU
ALLSEL
!
! Step 1                                  ! renamed step
total_time = abs(load_ramp_time)              ! Total time [s]
Antype, trans                                 !  ANTYPE,  Antype,  Status,
LDSTEP, SUBSTEP, Action
```

```
nropt,auto                                  ! Uses Newton-Raphson
lnsrch,auto                                 ! Auto line searching for NR
NLGEOM,auto                                       ! Non-linear geometry
Solcontrol, 1                                   !     Optimizes     nonlinear
solutions
Cnvtol,F,3
Time, total_time                            ! Time at end of step
NSUBST,5,1000,5                             ! Specifies substeps
!Deltim, load_init_time, load_mini_time, load_maxi_time  !  DELTIM,  DTIME,
DTMIN, DTMAX, Carry
Autots, 1                                   ! Auto Time Stepping
!D, TOP , UZ , displ_init                                          !   modified
displacement
!NSEL,ALL
BF,ALL,TEMP,temp_init                           ! Nodal body force load
Outres, All, data_freq                          ! Outputs data to be read by
ESOL
Crplim, 20, 1                                   !   CRPLIM,   CRCR,   Option,
!Creep Ratio Limit
Rate, 0                                         ! Activates Creep for step
Kbc, 0                                          ! Specifies stepped or ramped
load, 1=stepped
Solve

! Step 2:
total_time = abs(half_cycle)+total_time
Antype, trans
nropt,auto
lnsrch,auto
NLGEOM,auto
Solcontrol, 1
Cnvtol,F,3
Time, total_time
NSUBST,30,100,30 !NSUBST,70,100,70

!Deltim, load_init_time, load_mini_time, load_maxi_time

Autots, 1
D, TOP , UZ , peak_displ                                          !   modified
displacement
!NSEL,ALL
BF,ALL,TEMP,peak_temp
Outres, All, data_freq
Crplim, 20, 1
Rate, 1
Kbc, 0
Solve

!!!!!!!!!!!!!!!!!!!!!!!!!!!!!!!!!!!!!!!!!!!!!!!!!!!!!!!!!!!!!!!!!!!!!!!!!!!!
```

```
!!!!!!!!!!!!!!!!!!!!!!!!!!!!!!!!!!!!!!!!!!!!!!!!!!!!!!!!!!!!!!!!!!!!!!!!!!!!!!!

! Continue Solution Stage with Subsequent Cycling
total_cycles=num_cycles                                          !    Number    of
cycles
*do,cycle,1,total_cycles,1                    !   Do   cycles   from   1   to
total_cycles with increment 1

! Step 3:
*GET, LOADNUM,ACTIVE,0,SOLU, NCMLS
*IF, LOADNUM, EQ, 2, THEN                     ! Equal to 2 because the 3rd
load step hasn't started yet
total_time = abs(first_hold) + total_time
*ELSE
total_time = abs(peak_hold) + total_time
*ENDIF
Antype, trans
nropt,auto
lnsrch,auto
NLGEOM,auto                       ! Non-linear geometry
Solcontrol, 1
Cnvtol,F,3
Time, total_time
NSUBST,30,100,30
!*IF, LOADNUM, EQ, 2, THEN
!Deltim,         load_init_dwell_time_first,         load_mini_dwell_time,
load_maxi_dwell_time
!*ELSE
!Deltim,          load_init_dwell_time_peak,         load_mini_dwell_time,
load_maxi_dwell_time
!*ENDIF
Autots, 1
D, TOP , UZ , peak_displ                                          !   modified
displacement
NSEL,ALL
BF,ALL,TEMP,peak_temp
Outres, All, data_freq
Crplim, 20, 1
Rate, 1
Kbc, 0
Solve

! Step 4:
total_time = abs(full_cycle) + total_time
Antype, trans
nropt,auto
lnsrch,auto
NLGEOM,auto                       ! Non-linear geometry
Solcontrol, 1
Cnvtol,F,3
```

```
Time, total_time
NSUBST,30,100,30
!Deltim, load_init_time, load_mini_time, load_maxi_time
Autots, 1
D, TOP , UZ , valley_displ                                          !   modified
displacement
NSEL,ALL
BF,ALL,TEMP,valley_temp
Outres, All, data_freq
Crplim, 20, 1
Rate, 1
Kbc, 0
Solve

! Step 5:
total_time = abs(valley_hold) + total_time
Antype, trans
nropt,auto
lnsrch,auto
NLGEOM,auto                        ! Non-linear geometry
Solcontrol, 1
Cnvtol,F,3
Time, total_time
NSUBST,30,100,30
!Deltim,         load_init_dwell_time_valley,         load_mini_dwell_time,
load_maxi_dwell_time
Autots, 1
D, TOP , UZ , valley_displ                                          !   modified
displacement
NSEL,ALL
BF,ALL,TEMP,valley_temp
Outres, all, data_freq
Crplim, 20, 1
Rate, 1
Kbc, 0
Solve

! Step 6:
total_time = abs(full_cycle) + total_time
Antype, trans
nropt,auto
lnsrch,auto
NLGEOM,auto                        ! Non-linear geometry
Solcontrol, 1
Cnvtol,F,3
Time, total_time
NSUBST,30,100,30
!Deltim, load_init_time, load_mini_time, load_maxi_time
Autots, 1
```

```
D, TOP , UZ , peak_displ                                          !  modified
displacement
NSEL,ALL
BF,ALL,TEMP,peak_temp
Outres, all, data_freq
Crplim, 20, 1
Rate, 1
Kbc, 0
Solve
*enddo
FINISH

!!!!!!!!!!!!!!!!!!!!!!!!!!!!!!!!!!!!!!!!!!!!!!!!!!!!!!!!!!!!!!!!!!!!!!!!!!!

/Post1
/OUTPUT, FEA_Junk3,txt
ALLSEL
RSYS,0                      ! global
*GET,LSTSET, ACTIVE, 0, SET, NSET
*GET,RFTSET, ACTIVE, 0, SET, NSET,LAST,8

!TOTARRAYSTEPS=LSTSET-RFTSET+1
TOTARRAYSTEPS=LSTSET


*dim,atime,array,TOTARRAYSTEPS
*dim,acurlo,array,TOTARRAYSTEPS
*dim,acursb,array,TOTARRAYSTEPS
*dim,atemp,array,TOTARRAYSTEPS
*dim,aestrn,array,TOTARRAYSTEPS
*dim,apstrn,array,TOTARRAYSTEPS
*dim,acstrn,array,TOTARRAYSTEPS
*dim,atstrn,array,TOTARRAYSTEPS
*dim,astrss,array,TOTARRAYSTEPS


!t=1
!*DO,tttt,RFTSET,LSTSET,1
*DO,t,1,LSTSET,1
!SET,,,,,,,tttt
SET,,,,,,,t

*GET,acurlo(t), ACTIVE, 0, SET, LSTP
*GET,acursb(t), ACTIVE, 0, SET, SBST                    !get  the  current
sub step
*GET,atime(t), ACTIVE,0, SET, TIME

ETABLE, ESTRVALN, EPEL, Z                    ! Make an element table for
other stresses and strains
ETABLE, PSTRVALN, EPPL, Z
```

```
ETABLE, CSTRVALN, EPCR, Z
ETABLE, TSTRVALN, EPTT, Z
ETABLE, STRSVALN, S, Z
ETABLE, TEMPVAL, BFE, TEMP


*get,aestrn(t),elem,1,etab,ESTRVALN
*get,apstrn(t),elem,1,etab,PSTRVALN
*get,acstrn(t),elem,1,etab,CSTRVALN
*get,atstrn(t),elem,1,etab,TSTRVALN
*get,astrss(t),elem,1,etab,STRSVALN
*get,atemp(t),elem,1,etab,TEMPVAL



!t=t+1
*ENDDO

mxstrn=atstrn(RFTSET)
mnstrn=atstrn(LSTSET)
mxstrs=astrss(RFTSET)
mnstrs=astrss(LSTSET)
mxtem=atemp(RFTSET)
mxrate=strain_rate

! Hysteresis File

*CFOPEN,
FEA_N_%tmc%_%tmt%_%sr%_%mrat%_%strain_rate%_%holdtime%_%dwelltype%,data,,
*VWRITE, atime(1),acurlo(1), acursb(1), atemp(1), aestrn(1), apstrn(1),
acstrn(1), atstrn(1), astrss(1)   ! If using an array and put (1), will
write all rows, which saves processing time
(E11.5,6X F10.2,6X F10.2,6X F10.2,6X E11.5,6X E11.5,6X E11.5,6X E11.5,6X
F10.3)
*CFCLOS

! Index File

*CFOPEN, FEA_Index_N,txt,,append
JOB_NAME1='FEA_N_%tmc%_%tmt%_%sr%_'
JOB_NAME2='%mrat%_%strain_rate%_%holdtime%_%dwelltype%'
*VWRITE, JOB_NAME1,JOB_NAME2
%C%C


*CFOPEN, FEA_SUM, txt,,append
*vwrite, mxtem, mxrate, mxstrn, mxstrs, mnstrn, mnstrs
(F10.2, 6x E11.5, 6x E11.5, 6x F10.2, 6x E11.5, 6x F10.2)

/OUTPUT, FEA_Junk22,txt
```

```
!!!!!!!!!!!!!!!!!!!!!!!!!!!!!!!!!!!!!!!!!!!!!!!!!!!!!!!!!!!!!!!!!!!!!!!!!!!
! Parametric Simulation Termination
!
I=I+1
J=J+1
K=K+1
L=L+1
M=M+1
FINISH
*ENDDO
*ENDDO
!*ENDDO
*ENDDO
!*ENDDO
!*ENDDO



Finish
/clear
/POST1

/inquire,numind,lines,FEA_Index_N,txt
*DIM,indfil,array,numind

*SREAD,indfil,FEA_Index_N,txt,,,

*DIM,nuln,array,numind

*DO,xx, 1, numind

/inquire,nuln(xx),lines,indfil(1,xx),data

*DIM,arr%xx%,array,nuln(xx),9

*VREAD,arr%xx%(1,1),indfil(1,xx),data,,JIK,9,nuln(xx)
(E11.5,6X F10.2,6X F10.2,6X F10.2,6X E11.5,6X E11.5,6X E11.5,6X E11.5,6X
F10.3)

*ENDDO

*vscfun,numfr,max,nuln
numfc=10*numind

*DIM,fortrx,array,numfr,numfc

*DO,zz,1,numind

colnum=10*(zz-1)+1
```

```
blankcol=10*zz

*mfun,fortrx(1,colnum),copy,arr%zz%(1,1)

fortrx(1,blankcol)=0

ntimes=numind-1
*ENDDO

*CFOPEN, tempinput,txt,,
texline1='*mwrite,fortrx,combineddata,csv,,,'
texline2='(E11.5,"," F10.2,"," F1'
texline3='0.2,"," F10.2,","'
texline4='" E11.5,"," E11.5,"," E1'
texline5='1.5,"," E'
texline6='11.5,"," F10.3,"," F'
texline7='1.0, %ntimes%(","'
texline8='" E11.5,"," F10.2,","'
texline9='" F10.2,"," F10.'
texline10='2,"," E11.5,"," E1'
texline11='1.5,"," E11.5,'
texline12='"," E11.5,"," F10.3,"'
texline13=',"  F1.0))'

*VWRITE,
texline1,texline2,texline3,texline4,texline5,texline6,texline7,texline8,te
xline9,texline10,texline11,texline12,texline13
%C%/%C%C%C%C%C%C%C%C%C%C%C%C
*CFCLOS

/input,tempinput,txt

FINISH
!!!!!!!!!!!!!!!!!!!!!!!!!!!!!!!!!!!!!!!!!!!!!!!!!!!!!!!!!!!!!!!!!!!!!!!!!!
```

APPENDIX C: RELATED PUBLICATIONS

- Irmak, F., Gordon, A.P., Medelin, D., Bouchenot, T., Felemban,B. “Life Prediction of a Low Alloy Steel under Uniaxial loading with Creep-Fatigue” , Internation Journal of Fatigue (In-Progress), 2017.
- Irmak, F., Gordon, A.P., Bouchenot, T., and Felemban,B. “A Reduced Order Life Prediction Modeling Approach for Materials under Thermomechanical Fatigue” AIAA Science and Technology Forum (In-Progress), Kissimmee, FL, January 8^{th} – 12^{th} ,2018.
- Gordon, A.P., Irmak, F., Medelin, D., Bouchenot, T., and Felemban,B. “Application of Non-Interactive Constitutive Model for Life Prediction of 2.25Cr-1Mo under Creep-Fatigue” ASME International Mechanical Engineering Congress and Exposition, Tampa, FL, November 3^{rd}-9^{th} , 2017.
- Irmak, F. and Gordon, A.P. “A Framework For Life Prediction of 2.25Cr-1Mo Under Creep and Thermomechanical Fatigue” ASME Turbomachinery Technical Conference & Exposition, Oslo, Norway, June 11^{th} – 15^{th}, 2018.
- Irmak, F. and Gordon, A.P. “A Life Predicition Approach For Low Alloy Steels Under Creep and Thermomechanical Fatigue” 12^{th} International Fatigue Congress, Poitiers Futuroscope, France, May 27^{th}-June 1^{st} , 2018. (Accepted)

REFERENCES

[1] Cai, C., Liaw, P. K., Ye, M., and Yu, J. (1999) "Recent Developments in the Thermomechanical Fatigue Life Prediction of Superalloys" *Journal of Materials,* 51(4).

[2] Zhuang, W. Z., and Swansson, N. S. (1998) "Thermo-Mechanical Fatigue Life Prediction: A Critical Review" DSTO Aeronautical and Maritime Research Laboratory, Melbourne, Australia.

[3] Cailletaud, G., Nouailhas, D., Grattier, J., Levaillant, C., Mottot, M., Tortel, J., Escavarage, C., Heliot, J., and Kang, S. (1984) "A Review of Creep-Fatigue Life Prediction Methods: Identification and Extrapolation to Long Term and Low Strain Cyclic Loading," *Nuclear Engineering and Design,* 83: 267-278.

[4] ASTM, A542/A542M-13 "Standard Specification for Pressure Vessel Plates, Alloy Steel, Quenched-and-Tempered, Chromium-Molybdenum, and Chromium-Molybdenum-Vanadium" *ASTM Book of Standards* Volume 01.04, ASTM International, West Conshohocken, PA, 2013.

[5] Bynum, J. E., Ellis, F. V., and Roberts, B. W. (1976) "Tensile and Creep Properties for an Annealed versus Normalized and Tempered 2-1/4 Cr – 1 Mo Steel Plate" Chrome Moly Steel in 1976, *Winter Annual Meeting of the ASME,* New York, December 5th-10th.

[6] Polak, J., Helesic, J., and Klesnil, M., (1988) "Effect of Elevated Temperatures on the Low Cycle Fatigue of 2.2SCr-1Mo Steel-Part I: Constant Amplitude Straining," Low Cycle

Fatigue, ASTM STP 942, H. D. Solomon, G. R. Halford, L. R. Kaisand, and B. N. Leis, Eds., American Society for Testing and Materials, Philadelphia, 1988, pp. 43-57.

[7] NIMS Fatigue Data Sheet No. 94, "Data sheet on long-term, high temperature low-cycle fatigue properties of SCMV4 (2.25Cr–1Mo) steel plate for boilers and pressure vessels," National Institute for Materials Science (NIMS), Tukuba, 2004.

[8] NRIM Fatigue Data Sheet No. 62, "Data sheet on elevated-temperature, time-dependent low-cycle fatigue properties of SCMV4 (2.25Cr–1Mo) steel plate for pressure vessels," National Research Institute for Materials (NRIM), Tokyo, 1989

[9] NRIM Fatigue Data Sheet No. 7, "Data sheet on elevated-temperature, low-cycle fatigue properties of SCMV4 (2.25Cr–1Mo) steel plate for pressure vessels," National Research Institute for Materials (NRIM), Tokyo, 1978.

[10] Tian, Y., Yu, D., Zhao, Z., Chen, G., and Chen, X. (2016) "Low cycle fatigue and creep-fatigue interaction behavior of 2.25Cr1MoV steel at elevated temperature" Materials at High Temperatures.

[11] Kushima, H., Watanabe, T., Murata, M., Kamihira, K., Tanaka, H., and Kimura, K. (2005) "Metallographic Atlas for 2.25Cr-1Mo Steels and Degradation due to Long-term Service at the Elevated Temperatures," *ECCC Creep Conference*, London, September 12th-14th.

[12] dos Reis Sobrihno, J. F. and de Oliveira Bueno, L. (2014) "Hot Tensile and Creep Rupture Data Extrapolation on 2.25Cr-1Mo Steel Using the CDM Penny-Kachanov Methodology" *Materials Research*, 17(2): 518-526.

[13] Zhang, J., Yu, D., Zhao, Z., Zhang, Z., Chen, G., and Chen, X. (2016) "Low Cycle Fatigue of 2.25Cr1Mo Steel with Tensile and Compressed Hold" *Materials Science & Engineering*

A, 667:251-260.

[14] Iwasaki, Y., Hiroe, T. Igari, T., (1987) "Application of the Viscoplasticity Theory to the Inelastic Analysis at Elevated Temperature (On the Deformation and Lifetime Analysis Under Time-Varying Temperature)," *Nippon Kikai Gakkai Ronbunshu*, A Hen/Transactions of the Japan Society of Mechanical Engineers, Part A, 53: 1838-1843.

[15] Saltsman, J. F., and Halford, G. R. (1994) "Ability of the Total Strain Version of Strainrange Partitioning to Characterize Thermomechanical Fatigue Behavior" *NASA Technical Memorandum 4556*, Lewis Research Center.

[16] Bueno, L., O. and Marino, L. (2001) "High-Temperature Oxidation Behavior of 2 ¼-Cr-1Mo Steel in Air-Part 2: Scale Growth, Metal Loss Kinetics, and Stress Enhancement Factors During Creep Testing," *Journal of Pressure Vessel Technology*, 123: 97-104.

[17] Sumida, T., Ikuno, T., Otsuka, N., and Saburi, T. (1995) "High Temperature Oxidation Behavior of 2.25%Cr-1%Mo Steel Boiler Tubes in Long-Term Exposure to Superheated Steam," *Materials Transactions, JIM*, 36(11): 1372-1378.

[18] Bouchenot, T., Gordon, A. P., Shinde, S., and Gravett, P. (2014) "An Analytical Stress-Strain Hysteresis Model for a Directionally-Solidified Superalloy Under Thermomechanical Fatigue," *ASME Turbo Expo 2014: Turbine Technical Conference and Exposition*, Düsseldorf, Germany.

[19] Bouchenot, T., Gordon, A. P., Shinde, S., and Gravett, P. "Approach for Stabilized Peak/Valley Stress Modeling of Non-Isothermal Fatigue of a DS Ni-Base Superalloy," *Materials Performance and Characterization*, 3.

[20] Bouchenot, T., Gordon, A. P., Holycross, C., and Penmetsa, R. C. (2017) "Application

of Non-Interaction Constitutive Models for Deformation of IN617 under Elevated Temperature Fatigue" *Fatigue and Fracture of Engineering Materials & Structures* (under review).

[21] Bouchenot, T., Felemban, B., Mejia, C., and Gordon, A. P. (2016) "Application of Ramberg-Osgood Plasticity to Determine Cycle Hardening Parameters" *ASME Power Conference*, Charlotte, NC, Jun 26th-30th.

[22] Gordon, A. P., (2012) *Dictionary of Experiments of Mechanics of Materials*, Creative Printing and Publishing, Sanford, FL

[23] Ramberg, W., and Osgood, W. R., (1943) "Description of Stress-Strain Curves by Three Parameters" Technical Note No. 902, National Advisory Committee for Aeronautics.

[24] Masing, G., (1926) "Eigenspannungen und Verfestigung beim Messing (Self Stretching and Hardening for Brass)," *Proceedings of the Second International Congress for Applied Mechanics*, Zurich, Switzerland, pp. 332-335.

[25] Armstrong, P. J., and Frederick, C.O., (1966) "A Mathematical Representation of the Multiaxial Bauschinger Effect", CEGB Report, RD/B/N731, Berkeley Nuclear Laboratories.

[26] May, D.L., Gordon, A. P., and Segletes, D. S., (2013) "The application of the Norton-Bailey law for creep prediction through power law regression," *ASME Turbo Expo 2013: Turbine Technical Conference and Exposition*, San Antonio, TX.

[27] Garofalo, F., (1965) *Fundamentals of creep and creep rupture in metals*, MacMillan, Inc., New York.

[28] Rieiro, I., Carsi, M., and Ruano, O. A., (2009) "New numerical method for the fit of Garofalo equation and its application for predicting hot workability of a (V-N) microalloyed steel," *Materials Science and Technology*, 25: 995-1002.

[29] Parker, J. D., (1985) “Prediction of Creep Deformation and Failure for 1/2 Cr-1/2 Mo-1/4V and 2-1/4 Cr-1 Mo Steel,”

Pressure Vessel and Piping, 98: 109-115.

[30] Robinson, E. L. (1952) “Effect of Temperature Variation on the Long- Time Rupture Strength of Steels,” *Transactions of the ASME*, 74: 777-781.

[31] Felemban, B., Bouchenot, T., Irmak, F., and Gordon, A. P. (2017) 2.25Cr-1Mo steel under Multiaxial Loading with Creeep and Plasticity,” *Materials at High Temperature* (under review).

[32] Inoue, T., Kawai, M., Yoshida, F., Niitsu, Y., Ohno, N., and Imatani, S. (1989) “Plasticity-Creep Behavior of 2-1/4Cr-1Mo Steel at 600°C,” *ASME Pressure Vessel & Piping Conference*: 101-107.

[33] Inoue, T., Yoshida, F., Niitsu, Y., Ohno, N., Uno, T., and Suzuki, A. (1994) “Inelastic stress-strain response of 2¼Cr-1Mo steel under combined tension-torsion at 600°C” *Nuclear Engineering and Design*, 150: 107-118.

[34] ISO 6892-1: "Metallic materials. Tensile testing. Method of test at ambient temperature" (2009)

[35] ASTM E8/E8M-13: "Standard Test Methods for Tension Testing of Metallic Materials" (2013)